



**Politecnico
di Torino**

Master course in

MECHANICAL ENGINEERING

Academic year 2024/2025

Master's thesis

Algorithms for Damage-detection in Rolling Bearing Elements

Supervisor

Prof. Fasana Alessandro

Candidate

Devaraja R

Abstract

Rolling bearing elements are critical components in mechanical industries, and their failure can result in significant operational downtime and maintenance costs. Ensuring reliability through early damage detection is essential to prevent catastrophic failures. This thesis reviews and compares various algorithms for damage detection in rolling bearing elements. The study covers traditional techniques such as time-domain, frequency-domain, and time-frequency domain methods, alongside advanced signal processing techniques. A special emphasis is placed on envelope analysis, which excels in extracting fault-related modulations from noisy environments, making it particularly effective for detecting early-stage defects in complex or non-stationary signals. Key performance metrics, including fault detection accuracy, sensitivity, computational efficiency, and robustness under diverse operating conditions, are evaluated. The findings offer detailed insights into selecting the most effective diagnostic algorithms, contributing to the development of reliable, real-time damage detection systems for predictive maintenance in rolling bearing systems.

Acknowledgement

First and foremost, I would like to express my heartfelt thanks to my supervisor, **Fasana Alessandro**, for his invaluable guidance, encouragement, and constructive feedback, which have been instrumental in shaping this work. Whenever I faced difficulties in progressing with my thesis, his door was always open, offering timely advice and support.

I am also profoundly grateful to **Politecnico di Torino** for providing the necessary resources and a conducive environment for my research. Their support has been integral to the successful completion of this thesis.

I sincerely thank my family for their unwavering support since my childhood, which has been a source of constant motivation and encouragement throughout my academic and professional journey.

I would also like to acknowledge my dear friends **Aakash T S**, **Bharath K** and **Venkatesh K** for their consistent encouragement and support, which helped me stay focused during challenging times.

Last but not least, I would like to express my deepest gratitude to my beloved brother, **Sathishkumar M**, and his family for their unwavering support and encouragement. Their steadfast motivation has guided me toward achieving my goals and reaching where I aspire to be in life. He has always been my greatest source of inspiration—without him, my life would be incomplete.

Table of Contents

1. Introduction	1
1.1 REB.....	2
1.2 Defect Frequency	3
1.2.1 Inner Race Damage.....	4
1.2.2 Outer Race Damage	5
1.2.3 Cage Damage	5
1.2.4 Roller Damage	5
1.3 Methodology.....	5
1.4 Techniques	6
1.5 Other techniques for damage detection.....	6
1.5.1 Acoustic Emission (AE)	6
1.5.2 Infrared Thermography	6
1.5.3 Ultrasonic Testing.....	7
1.6 Damage-detection by traditional methods and its challenges.....	8
2. Vibration Signal Analysis Techniques	10
2.1 Enhancement of Bearing Signals	12
2.2 Envelope analysis.....	12
2.3 Spectral Kurtosis and Kurtogram.....	14
2.3.1 Spectral Kurtosis.....	14
2.3.2 Kurtogram	15
2.3.3 Fast Computation of the Kurtogram	16
2.4 Cyclostationarity	17
2.5 The Autogram and the fast-Autogram	18
2.6 Cyclic Spectral Analysis and Spectral Correlation	20
2.7 Spectral Amplitude Modulation (SAM).....	21
2.8 Cyclic Modulation Spectrum	23
2.9 Spectral Correlation (SC).....	24
3. Experimental Analysis	31
3.1 Experimental setup.....	31
3.2 Diagnostic Methods	32
3.2.1 Method 1: Envelope Analysis of the raw signal	32
3.2.2 Method 2: Cepstrum Pre-whitening.....	32
3.2.3 Method 3: Benchmark Method	32

3.3 Comparison of various fault's diameter	33
3.3.1 Damage Quantification and Comparative Analysis of Diagnostic Methods	33
3.3.2 Error Analysis method	34
3.3.3 Inner race damage: [12K_Drive-End_Bearing_Fault_Data]	35
3.3.4 Outer race damage: [12K_Drive-End_Bearing_Fault_Data]	42
3.3.5 Ball damage: [12K_Drive-End_Bearing_Fault_Data]	49
3.4 Summary of Comparison	56
4. Results & Discussions	61
4.1 Data records	61
4.2 Characterisation of all data sets	61
4.3 Summary of Results	61
4.4 Verification of Algorithms with Politecnico test rig.....	67
4.4.1 Description of the tests	67
4.4.2 Experimental results.....	68
4.5 Conclusion	81
References	83

1. Introduction

Rolling Element Bearings (REBs) are a critical component in rotating machinery, which is mainly designed for supporting and guiding the rotation or oscillation of shafts with minimal friction. REB's failure is the most important factor for the machinery breakdowns. Therefore, it is very essential to detect and diagnose faults to prevent catastrophic damage to both the equipment and personnel before the completion of bearing failure.

When a localized defect develops on an inner race, outer race, or roller part of a bearing, it generates impacts each time the defect passes through the load zone. These impacts excite both the bearing and the machine structure, particularly at their resonance frequencies. Consequently, the vibration signal produced will contain multiple harmonics, which repeat almost periodically based on the bearing's geometry.

Detecting these vibration patterns and analyzing them for abnormalities can help in identifying potential bearing faults at an early stage. Vibration signal analysis is a cornerstone in predictive maintenance strategies for rolling element bearings. It enables the early detection of bearing faults, such as surface wear, defects in the inner and outer races, cage, and degradation of rolling elements. By analyzing vibration signals, maintenance can be performed proactively, minimizing downtime, and extending the life of machinery.

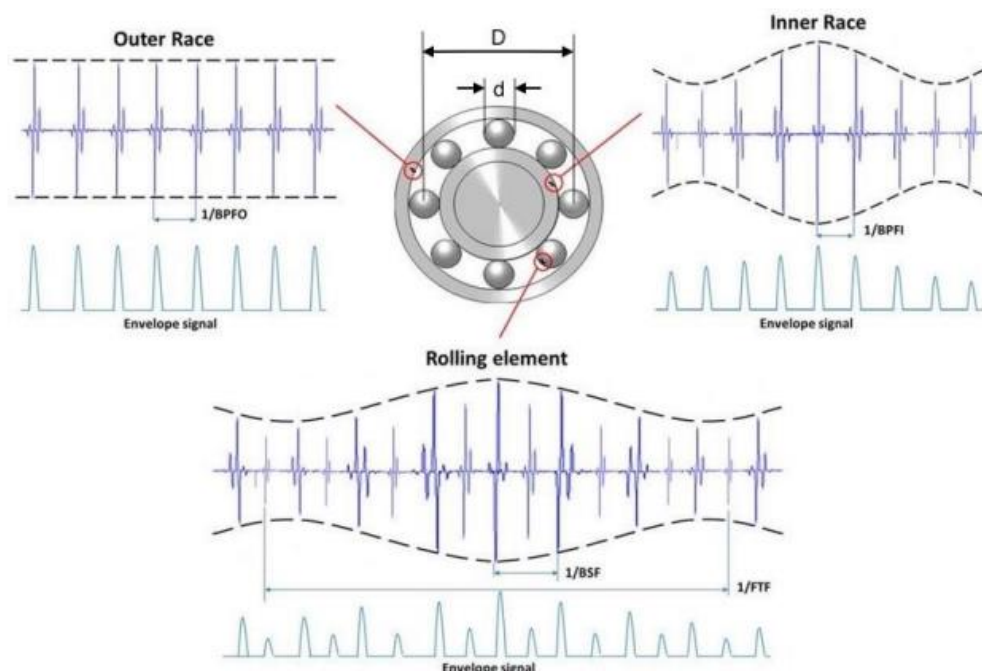


Fig 1. Typical signals and envelope signals from local faults in rolling element bearings from Ref. [2]

Fig 1. shows the typical acceleration signals produced by localized faults in the various components of a rolling element bearing and the corresponding envelope signals produced by amplitude demodulation. The analysis of envelope signals provides more diagnostic information than the analysis of the raw signals.

As explained in [2], the series of broadband bursts excited by the shocks could be modulated in amplitude by two factors:

1. The strength of the bursts depends on the load borne by the rolling element(s), and this is normally modulated by the rate at which the fault is passing through the load zone.
2. When the fault is moving, the transfer function of the transmission path varies concerning the fixed positions of response transducers.

Nomenclature

REB	Rolling Element Bearings
d	Rolling Element Diameter
D	Bearing Pitch Diameter
BPFI	Ball Pass Frequency Inner race
BPFO	Ball Pass Frequency Outer race
FTF	Fundamental Train Frequency
BSF	Ball Spin Frequency
DE	Drive-End Acceleration
FE	Fan-End Acceleration
BA	Base Plate Acceleration
Y1, Y2	Successful Diagnoses
P1, P2	Partially Successful Diagnoses
N1, N2	Unsuccessful Diagnoses

1.1 REB

A REB is well-defined in Wikipedia, as it says that a rolling-element bearing is a bearing that carries a load by placing rolling elements (such as balls or rollers) between two concentric, grooved rings called races. The relative motion of the races causes the rolling elements to roll with little rolling resistance and sliding.

Rolling-element bearings often work well also in non-ideal conditions, but sometimes minor problems cause bearings to fail quickly and mysteriously. For example, with a stationary (non-rotating) load, small vibrations can gradually press out the lubricant between the races and rollers or balls (false brinelling). Without lubricant, the bearing fails, even though it is not rotating and thus is not being used. For these reasons, much of the bearing design is about failure analysis. Vibration-based analysis can be used for fault identification of bearings.

1.2 Defect Frequency

To diagnose faults in rolling-element bearings, fault frequencies are derived from the bearing's geometry and the rotational speed. These frequencies help in identifying specific types of defects such as outer race, inner race, rolling elements, and the cage.

The formula for the various frequencies associated with bearing faults (shown in Fig 1.) is given below,

Ball pass frequency, inner race:

$$BPFI = \frac{n \cdot fr}{2} \left\{ 1 + \frac{d}{D} \cos \phi \right\}$$

Ball pass frequency, outer race:

$$BPFO = \frac{n \cdot fr}{2} \left\{ 1 - \frac{d}{D} \cos \phi \right\}$$

Fundamental train frequency (cage speed):

$$FTF = \frac{fr}{2} \left(1 - \frac{d}{D} \cos \phi \right)$$

Ball (roller) spin frequency:

$$BSF = \frac{D}{2d} \left\{ 1 - \left(\frac{d}{D} \cos \phi \right)^2 \right\} \cdot fr$$

where,

fr - shaft speed, n - number of rolling elements, ϕ - angle of the load from the radial plane

Table 1. Envelope spectrum for various fault types Ref [42]

Fault type	Expected components in envelope spectrum
Inner race	BPFI and harmonics, sidebands spaced at fr. Harmonics of fr.
Outer race	BPFO and harmonics, no sidebands
Rolling element (ball)	BSF and harmonics (even harmonics often dominant), sidebands spaced at FTF. Harmonics of FTF

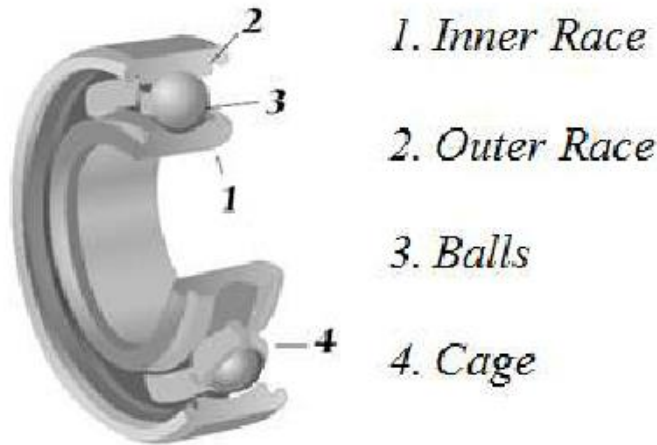


Fig 2. Fundamental components of a rolling bearing

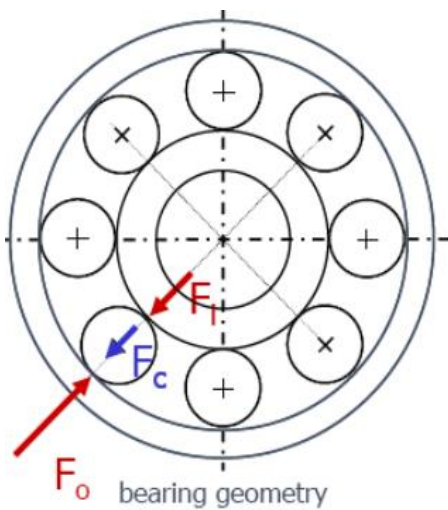


Fig 3. Bearing Geometry

F_i = Inner race force

F_c = Circumferential force on balls

F_o = Outer race force

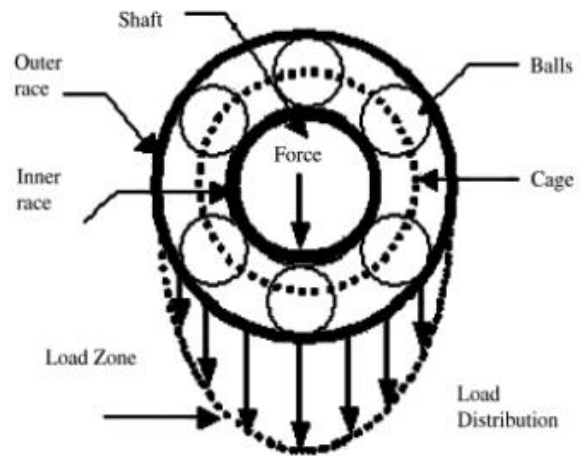


Fig 4. Load distribution of a bearing under a unidirectional vertical load

1.2.1 Inner Race Damage

Inner race damage in rolling bearings occurs due to several factors. Firstly, Fatigue spalling is one common cause, where overloading, cyclic stresses, poor lubrication, and contamination lead to repeated stress cycles that weaken the material, causing surface flaking. Secondly, Wear is another major issue, resulting from inadequate lubrication, contamination, and misalignment, which cause abrasive wear and material loss over time. Finally, Creep occurs when there is insufficient interference fit, thermal expansion, or improper mounting, leading to the relative movement between the inner race and the shaft or housing, causing wear and deformation. This understanding helps in diagnosing issues earlier and the lifespan of the bearing is extended by implementing preventive measures.

1.2.2 Outer Race Damage

The outer race plays a critical role in supporting loads, transmitting forces, and ensuring smooth operation. It transmits and distributes the applied loads from the shaft to the housing or vice versa, depending on the bearing type. Outer races are made from hardened steel alloys, such as chrome steel (AISI 52100) or stainless steel, due to their high strength, wear resistance, and compatibility with lubricants. The main cause of outer race damage is when the repeated stress cycles happen due to overloading, misalignment, inadequate lubrication, or contamination leading to surface fatigue and the formation of pits or flakes. Another is when the external impacts or shock loads exceeding the bearing's capacity can cause deformation, cracking, or denting of the outer race.

1.2.3 Cage Damage

Cages or retainers are responsible for maintaining the appropriate relative positions of the rolling elements which helps to prevent them from colliding. Inadequate lubrication is the most common fault in cages, which causes them to wear and deform. Additionally, using improper tools or incorrect mounting can cause severe damage.

Unlike more massive bearing components, defects in cages are often less visible and can be challenging to detect until they significantly impact bearing performance. However, early detection can be achieved by monitoring the vibration spectrum, which can help identify irregular patterns associated with cage faults.

1.2.4 Roller Damage

Rollers are designed for distributing and supporting heavy loads efficiently. Their cylindrical shape and rolling action enable them to carry substantial weight while minimizing frictional resistance. Rollers operate with lower friction compared to sliding contact mechanisms. The rolling action between the roller and its mating surface minimizes wear and energy loss, contributing to higher operational efficiency and reduced maintenance requirements. Rollers are made from durable materials such as steel, stainless steel, or polymers, depending on the application requirements, which offer high strength, wear resistance, and corrosion resistance, ensuring long-term reliability and extended service life in demanding environments.

1.3 Methodology

The methodology of vibration analysis for rolling element bearings encompasses data acquisition, signal processing, and fault diagnosis. The vibration signals are generated by mounting accelerometers or velocity sensors on bearing housings. Fast Fourier Transform (FFT), Wavelet Transform, and Envelope Analysis are the most efficient Signal processing techniques applied to extract characteristic features from noise-dominated signals.

1.4 Techniques

For diagnosing bearing faults advanced signal processing techniques are used to detect and classify various types of bearing damage. Among these, the Autogram, Fast Kurtogram, Fast Autogram, Spectral Amplitude Modulation, and Spectral Correlation stand out for their effectiveness in identifying bearing defects.

1.5 Other techniques for damage detection

For detecting damages in rolling bearing elements, apart from vibration analysis, there are several other techniques which can be seen below. These methods enhance various symptoms and causes of bearing damage, providing a comprehensive approach to maintenance and diagnosis.

1.5.1 Acoustic Emission (AE)

Acoustic Emission is the non-destructive testing method that detects the transient elastic waves generated by the rapid release of energy from localized sources within a material. AE is highly sensitive and capable of detecting minute defects & irregularities within REB. AE sensors are typically mounted on the bearing housing to detect the high-frequency stress waves produced when a material undergoes deformation. These waves are generated by several sources such as Crack formation and propagation, Frictional contacts between surfaces, Plastic deformation & Material dislocations.

When a defect or irregularity, such as a crack or spall, develops in the bearing, it emits stress waves. The AE sensors can capture these waves and possibly convert them into electrical signals, which are then analyzed to determine the presence and severity of defects.

Ref [40] aimed to detect early seizure in high-speed sliding bearings by measuring the high-frequency components of Acoustic Emission signals. High-frequency AE sensors were deployed to capture signals above 1 MHz. Their ability to detect changes in AE signals before catastrophic failure provides valuable time for maintenance and intervention. AE signals indicate distinct changes when the lubricating film gets ruptured. This was characterized by an increase in the amplitude and specific frequency components of the AE signals. Also, this study shows that the progression from lubrication film rupture to wear and seizure could be tracked accurately to provide insights into the lifetime assessment of sliding bearings. The experiment was carried out in a test rig which is designed to simulate real machine conditions, allowing them for the examination of friction and wear in a controlled environment.

1.5.2 Infrared Thermography

According to Wikipedia, Infrared thermography is a non-contact & non-destructive technique to detect temperature variations on the surface of objects by using infrared imaging. In a Thermography system, an infrared camera was used to capture infrared radiation and convert it into a thermographic image. For the easy detection of hot spots and abnormal thermal patterns, the thermogram shows temperature variations in different colors. In the case of Thermographic analysis, the Temperature Gradient was used to measure the rate of temperature

change across the material. The major advantage is that the Thermography does not require physical contact for the measurement, it measures moving or rotating objects, even if the objects have a very high temperature.

According to Ref [51], a passive thermographic experiment was performed to monitor the fault on deep-grooved ball bearing. The temperature characteristics such as excessive friction, lubrication failure, or wear of the ball bearing under dynamic loading conditions were analyzed. For bearing damage detection, an infrared thermography method was used to identify abnormal temperature patterns that indicate potential issues. The thermography detects high friction which is mainly due to the inadequate lubrication or misalignment generated by heat. Localized hot spots could be identified due to increased friction when the bearing runs without adequate lubrication. Due to overheating, the bearing tends to work beyond its optimal temperature range, indicating potential problems.

Ref [52] discusses the use of Prognostics and Health Management (PHM) and State Assessment (SA) for classifying the health state of physical asset through signal processing from selected sensors. However, there is a noted gap in the literature regarding the use of Infrared Thermography (IRT) for the SA of rolling bearings. To address this issue, the study explores the potential of indicators obtained via passive thermography to classify the severity of failures in the outer race of rolling bearings. Single point defects were introduced in the bearing outer-race using electrical discharge machining, followed by the acquisition of thermal images during bearing operation. Indicators of both transient and steady-state behavior were calculated to classify different health states. Four indicators demonstrated a monotonic trend relative to defect size, showing promise for the SA of rolling bearings. The study suggests that, given IRT's effectiveness in other areas, this research could promote further investigation into the use of IRT in the PHM of rolling bearings.

1.5.3 Ultrasonic Testing

Ref [49] states that, ultrasonic testing (UT) is a non-destructive testing (NDT) technique that uses high-frequency sound waves to detect internal and surface defects in materials. Ultrasonic testing can detect cracks, voids, and other irregularities that could not be detected through other methods for rolling element bearings. Ultrasonic testing mainly involves the transmission of high-frequency sound waves into the bearing material. These sound waves travel through the material and reflect from any discontinuities, such as cracks or inclusions. Reflected waves are captured by a transducer and converted into electrical signals, then analyzed to determine the presence and defects characteristics. A pulser/receiver is an electronic device that can produce high voltage electrical pulse. The transducer driven by the pulser generates high frequency ultrasonic energy. The main component of Ultrasonic Testing was a couplant, wherein a particular medium a gel or liquid, was applied between the transducer and the bearing surface to facilitate the transmission of sound waves.

According to Ref [48], ultrasonic probes provide a reliable method for monitoring the condition of bearings. Early warning signs of incipient problems can be detected, allowing them to be dealt with before they lead to failure. The deformation occurs mainly due to the fatigue that produce irregular surfaces which will cause an increase in the emission of ultrasonic sound

waves. An incipient bearing failure is indicated by change in amplitude from the original reading (when exceeds 12 decibels).

Ref [50] states that, ultrasonic signal is used for early failure detection in tapered roller bearings. The ultrasonic signal analysis is performed using time domain parameters i.e. kurtosis and RMS, and in the frequency domain using the power spectral density obtained by the Welch periodogram. Among the parameters studied, the RMS parameter demonstrated superior performance in fault location extraction and monitoring, allowing for the identification of faulty conditions and qualitative evaluation of fault severity.

1.6 Damage-detection by traditional methods and its challenges

As discussed in section 1.5, Traditional methods such as vibration analysis often rely on amplitude and frequency spectrum analysis to detect changes in vibration patterns that indicate faults. However, damage can sometimes be subtle in the raw frequency spectrum, especially when the signal is measured at the fan-end while the damage is at the drive-end.

1. Inner Race Defect

Traditional Detection: Vibration analysis can detect inner race defects by identifying high-frequency vibration signals at the Ball Pass Frequency of the Inner race (BPFI) and its harmonics. However, the effectiveness depends on the sensor placement and noise levels, as inner race damage produces less prominent signals when measured far from the drive-end.

Challenges: Traditional methods might miss or inaccurately quantify inner race damage because sideband frequencies around BPFI are often subtle and can be masked by other frequencies in the spectrum. Additionally, if the damage is on the drive-end but measured on the fan-end, the signal is weaker.

Advanced Benefits: Envelope analysis can more effectively identify sidebands, a crucial indicator of inner race damage, by demodulating the signal and enhancing these sideband frequencies, which indicate fault modulation and confirm damage presence.

2. Outer Race Defect

Traditional Detection: Outer race defects can be detected at the Ball Pass Frequency of the Outer race (BPFO) and its harmonics in a vibration spectrum. Traditional methods are more effective for outer race defects than inner race defects because they generate clearer signals that are less sensitive to sensor placement.

Challenges: Although more detectable, traditional methods may still fail to capture sideband frequencies or low-level outer race defects, especially when the damage is on the non-load zone of the bearing, making the signal weaker.

Advanced Benefits: Advanced spectral analysis or demodulation techniques (like envelope analysis) amplify these sideband frequencies around BPFO, enabling a more precise detection, particularly for early-stage or minor outer race damage.

3. Cage Defect (Retainer Damage)

Traditional Detection: Cage defects are harder to detect using traditional vibration methods because the cage typically rotates at a lower frequency (the Fundamental Train Frequency, or FTF). This low-frequency signal is often overshadowed by other noise or operational vibrations.

Challenges: Traditional methods may overlook cage defects as they create low-amplitude, low-frequency vibrations that blend into the general operational noise, particularly in high-speed machinery.

Advanced Benefits: Advanced signal processing, like high-resolution spectral analysis or time-domain averaging, can enhance FTF detection, highlighting subtle vibrations related to cage damage. SAM can also amplify low-frequency signals, making it more effective at detecting early cage faults.

4. Ball Defect

Traditional Detection: Ball defects often produce vibrations at the Ball Spin Frequency (BSF), which can sometimes be detected in a vibration spectrum using traditional analysis. However, the signals may appear intermittent or inconsistent because balls rotate and contact races at varying points.

Challenges: Traditional methods may miss or under-detect ball defects due to the irregular and modulated nature of the ball vibration signature. Also, these signals may vary in amplitude, making detection difficult without more advanced filtering.

Advanced Benefits: Techniques such as envelope analysis or time-domain demodulation can isolate BSF and associated sidebands, effectively capturing the intermittency in ball defect signals. Advanced methods can therefore detect even minor pitting or deformation in ball bearings by emphasizing these unique vibration patterns.

2. Vibration Signal Analysis Techniques

As discussed in the previous chapter, bearing damage can be detected by analyzing the acceleration signals generated by specific components. The vibration signals produced by faults have been widely studied and diagnosed through advanced signal processing techniques as mentioned in section 1.4. These techniques can generally be classified into time domain, frequency domain, time-frequency domain approaches, and envelope analysis.

Time Domain Approach: This method involves analyzing the raw vibration signals as functions of time. Key parameters such as root mean square (RMS), peak value, crest factor, and kurtosis are used to identify anomalies. Time domain analysis is straightforward and provides initial insights into the condition of the bearings.

Frequency Domain Approach: In this approach, the vibration signal is transformed from the time domain to the frequency domain using techniques like the Fast Fourier Transform (FFT). This helps in identifying periodic frequency components related to the fundamental movements of machine parts. By examining these frequency components, it is possible to pinpoint the sources of undesirable vibrations. This method is particularly effective for identifying specific types of bearing faults, such as inner race, outer race, and rolling element defects.

Time-Frequency Domain Approach: Techniques such as Short-Time Fourier Transform (STFT) and Wavelet Transform are used to analyze signals whose frequency characteristics change over time. This approach provides a detailed representation of the signal, revealing transient features and non-stationary components that might be missed in pure time or frequency domain analyses. It is useful for detecting and diagnosing complex and intermittent bearing faults.

Envelope Analysis: This technique involves demodulating the vibration signal to extract the envelope of the high-frequency resonance. Envelope analysis is particularly effective for detecting early-stage faults in bearings. It enhances the signal-to-noise ratio, making it easier to identify the characteristic frequencies of bearing defects.

When analyzing machine vibrations in the frequency domain, a number of prominent periodic frequency components related to the machine's fundamental movements can be discovered. Frequency analysis enables trending the source of undesirable vibrations. There are also tutorials that cover the separation of bearing signals from discrete frequency noise and the enhancement of bearing signals.

This chapter will list several universal techniques and focus on unique information extraction towards the end. The last three methods time-frequency domain approach, frequency domain approach, and envelope analysis will be applied to analyze the bearing simulation signal in the coming chapters.

Nomenclature

RMS	Root Mean Square
FFT	Fast Fourier Transform
STFT	Short-Time Fourier Transform
IR	Impulse Response
MED	Minimum Entropy Deconvolution
SK	Spectral Kurtosis
AC	Unbiased Autocorrelation
MODWPT	Maximal Overlap Discrete Wavelet Packet Transform
WPT	Wavelet Packet Transform
SNR	Signal-to-Noise Ratio
MFB	Multirate Filter-Bank
CSA	Cyclic Spectral Analysis
CMS	Cyclic Modulation Spectrum
LES	Log-Envelope Spectrum
LSES	Logarithm-Squared Envelope Signal
FT	Fourier Transform
Fast-SC	Fast Spectral Correlation
ACP	Averaged Cyclic Periodogram
EES	Enhanced Envelope Spectrum
SES	Squared Envelope Spectrum
SC	Spectral Correlation

2.1 Enhancement of Bearing Signals

Ref [1] describes that, when the discrete frequency “noise” is even removed, the bearing signal will often be masked in many frequency bands by other noise and if the individual fault pulses are modified by passage through a transmission path with a long impulse response (IR) may also be rendered less impulsive than at the source. This is the most common case with high-speed bearings, where the bearing fault frequencies are so high, and corresponding spacings so short, that the IR is of the same length as the intervals between them. A method called ‘minimum entropy deconvolution’ (MED) removes the effect of the transmission path, which is first discussed, and then several methods are presented to enhance the bearing signal for residual background noise.

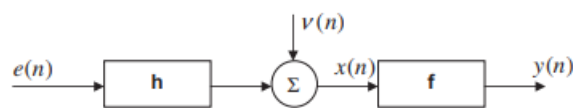


Fig 5. Inverse filtering (deconvolution) process for MED

Fig 5. illustrates the basic idea that the forcing signal $e(n)$ passes through the structural filter h whose output is mixed with noise $v(n)$ to give the measured output $x(n)$. The inverse (MED) filter f produces output $y(n)$, which has to be as close as possible to the original input $e(n)$. Of course, the input $e(n)$ is unknown, but is assumed to be as impulsive as possible.

2.2 Envelope analysis

In the year 1974, envelope analysis was originally developed and has been recognized as the benchmark method for bearing diagnostics. Robert B. Randall and Jérôme Antoni [1] demonstrated the spectrum of the raw signal which typically lacks appropriate diagnostic information concerning bearing faults. Envelope analysis involves bandpass filtering the signal mainly due to its structural characteristics within a high-frequency range to the fault impulses. Subsequently, the envelope signal is generated by the amplitude modulation. When the fault passes through the load zone or moves relatively to its reference point the modulation occurs. The envelope spectrum contains the diagnostic information with its repetition frequency (such as ball pass frequency or ball spin frequency). These frequency components within the envelope spectrum were used effectively to analyze its characteristics correlated with bearing faults, which facilitates maintenance and accurate machinery conditions.

Generally, envelope analysis techniques used analogue techniques with inherent limitations. The Amplitude demodulation used Hilbert transform techniques particularly to have substantial benefits by adopting digital methods, where a one-sided spectrum (positive frequencies only) is inversely transformed to the time domain. This yields a complex time signal called ‘analytic signal’ whose imaginary part is the Hilbert transform of the real part. This methodology extracts the spectrum to be demodulated by an ideal filter which can be separated from adjacent components, and it is not always possible with analogue filters and real-time digital filters as

they suffer from same restrictions on filter characteristic. The application to envelope analysis is shown in Fig 6.

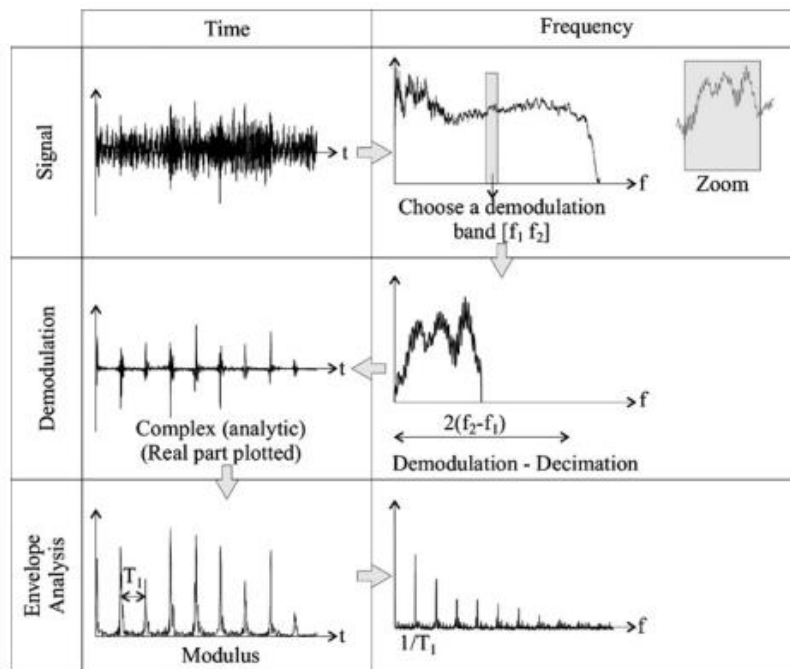


Fig 6. Procedure for envelope analysis using the “Hilbert transform” method

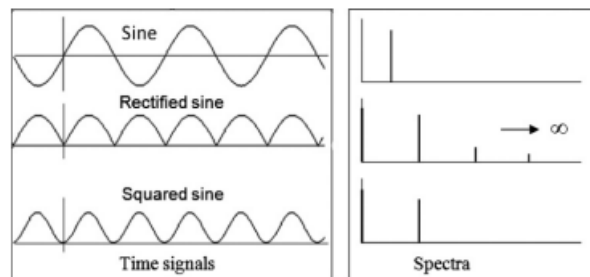


Figure 7. Potential aliasing given by squaring and rectifying a sinusoidal signal. With just squaring, but not rectification, aliasing can be avoided by doubling the sampling frequency before squaring

D. Ho and R.B. Randall [17], suggest that the squared envelope signal is more advantageous than analyzing the envelope itself. The reason behind this was clearly explained in Figure 7 which compares the spectra of a rectified signal and a squared sinusoid. Likewise, a rectified signal is the square root of the squared signal, and it should be noted that the envelope of a signal is the square root of the squared envelope mathematically. These issues occur due to the square root operation which introduces additional components that are not present in the original squared signal.

Figure 7 demonstrates that a rectified signal exhibits sharp cusps, requiring harmonics to extend infinitely to reproduce them accurately. Until now, the operation has been done digitally then it is not possible to remove these high harmonics by lowpass filtration (as it leads to an analogue

rectifier). To avoid loss of high-frequency components the sampling frequency should ideally be doubled for managing when digitally squaring or rectifying a signal. This concept aligned with the zero-padding illustrated in Figure 6 during the processing of the analytic signal.

The convolution performs only when the resultant spectrum reveals different frequencies, such as sideband spacings, which carry crucial modulation information relevant to diagnostics. Contrastingly, for a real-valued signal $x(t)$, the spectrum of its squared value simply convolves $X(f)$ (the spectrum of $x(t)$) within itself. Both difference frequencies and sum frequencies (the addition of positive and negative frequencies) are generated by convolution, where the latter components do not contribute diagnostic information and instead mask the desired results.

Interference can be circumvented with a real-valued signal by introducing frequency shifting to create zero padding around zero frequency and the Nyquist frequency. It requires doubling the sampling frequency for the same demodulation band and imposing larger transform sizes for equivalent problem scenarios.

Ref. [17] showed that despite potential noise masking (random/discrete frequency) up to three times the power of the bearing signal within the demodulation band, analyzing the squared envelope remained advantageous. Using spectral kurtosis, it is possible to identify a spectrum band where the signal-to-noise ratio of the bearing signal is significantly higher.

2.3 Spectral Kurtosis and Kurtogram

2.3.1 Spectral Kurtosis

Ref. [1] states that finding the most suitable band for demodulation is very difficult from the earliest days of envelope analysis. But this problem has been solved by using Spectral kurtosis (SK) and Kurtogram which helps to identify impulsive or non-Gaussian characteristics (after removal of discrete frequency masking). Spectral Kurtosis has proven to be determining the frequency bands by containing the maximum impulsivity of signals. Spectral kurtosis (SK) is a higher-order statistical measure used to analyze the frequency content of a signal. Unlike traditional kurtosis, which measures the peakedness of a signal's time-domain amplitude distribution, spectral kurtosis assesses how the shape of a signal's power spectrum varies across different frequencies. It evaluates the degree to which a signal's power distribution deviates from a Gaussian (normal) distribution. This method specifies frequency bands where signals exhibit asserted impulsiveness or non-Gaussian behavior, which often correlates with the presence of transient events or machinery faults. Kurtosis had been used for measuring the severity of machine faults, proposed by Stewart et al. in the 1970s Ref. [34].

Kurtosis is computed using Short Time Fourier Transform (STFT) coefficients for different window lengths, thus leading to the 3D representation coined Kurtogram. However, the original algorithm used for estimating the “full” Kurtogram had a prohibitive computational cost and hence offered limited industrial potential. By interpreting higher SK values, could be able to identify critical frequency ranges that require closer inspection for fault-related vibrations, enhancing the accuracy and efficiency of machinery condition monitoring and diagnostic information. The application of SK, along with the Kurtogram helps to visualize spectral kurtosis across frequency bands, enabling effectively prioritizing and investigating

potential faults based on the distinctive characteristics of vibration signals in different frequency domains.

$$\text{Kurtosis} = \frac{\sum_{i=1}^N (x(ti) - \mu_x)^4}{[\sum_{i=1}^N (x(ti) - \mu_x)^2]^2}$$

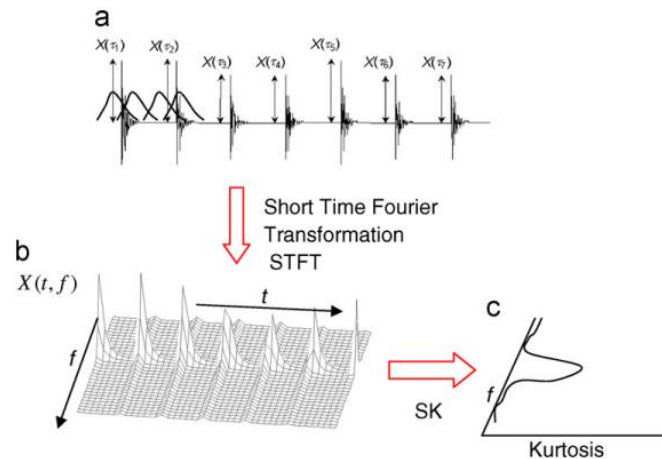


Fig 8. Calculation of SK from the STFT for a simulated bearing fault signal: (a) simulated time signal, (b) STFT, and (c) SK as a function of frequency

Key points:

- **Fault Detection:** SK is highly effective in detecting faults in rolling element bearings, gears, and other rotating machinery.
- **Frequency Domain Analysis:** By analyzing the kurtosis of the frequency spectrum, it helps pinpoint frequencies where transient or impulsive events occur.
- **Non-Gaussian Signal Identification:** It excels in identifying non-Gaussian noise or irregularities within the signal, which standard spectral analysis might miss.

2.3.2 Kurtogram

The Kurtogram is a visual representation of spectral kurtosis across different frequency bands and scales. It is used to determine the optimal frequency band for demodulating the signal to detect faults more clearly. The Kurtogram helps in identifying the specific band where the kurtosis value is maximized, indicating the presence of a fault with greater clarity.

Key points:

- **Optimal Band Selection:** The Kurtogram aids in selecting the optimal frequency band for demodulation, enhancing the fault detection process.

- **Enhanced Diagnostic Accuracy:** Focusing on the most informative frequency bands, improves the accuracy and reliability of fault diagnosis.
- **Visual Analysis Tool:** Provides a clear, visual method to identify and isolate fault frequencies, making it easier to interpret complex signals.

2.3.3 Fast Computation of the Kurtogram

Ref. [3] In the realm of signal analysis, the Kurtogram serves as a powerful tool for investigating non-stationary signals. However, fully exploring the entire (frequency, scale) plane (represented as f and Δf) can be computationally intensive and impractical for real-time industrial applications. Therefore, an efficient algorithm is designed to compute the Kurtogram swiftly over a dyadic grid in the (frequency, scale) plane, with computational complexity scaled to $O(N \log N)$.

The primary objective of this fast algorithm is to provide balanced computational efficiency with robust exploratory capabilities. By utilizing a dyadic grid, the algorithm optimizes the exploration process, focusing computational efforts where they are most informative for identifying signal characteristics associated with bearing faults and other mechanical anomalies.

Algorithm

The proposed algorithm builds upon an arborescent Multirate filter-bank structure, incorporating unique characteristics derived from the application of quasi-analytic filters. Initially designed with a binary tree structure, the algorithm has been further developed to encompass a more complex 1/3-binary tree configuration, enhancing its analytical capabilities.

The key principle revolves around utilizing a hierarchical filter-bank approach, where signals are processed through multiple stages of filtering and down-sampling. This structure allows for efficient decomposition of signals into frequency bands, facilitating detailed analysis across different scales. The incorporation of quasi-analytic filters introduces additional sophistication by enabling the computation of analytic signals, which are crucial for envelope analysis and other diagnostic techniques in signal processing.

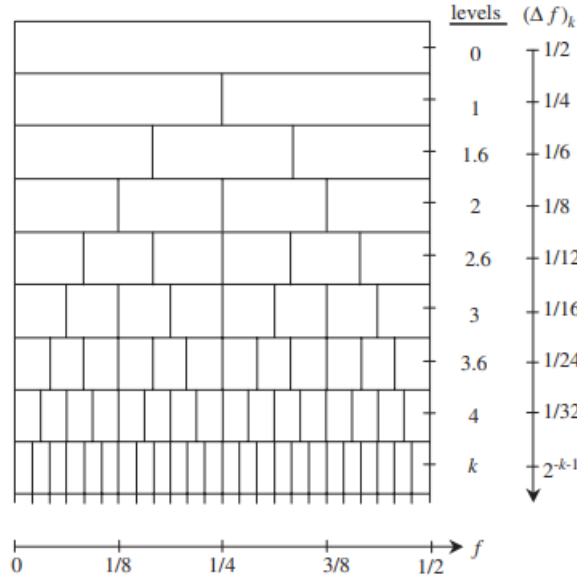


Fig 9. Paving of the (frequency/frequency resolution) plane in the case of the 1/3-binary tree Kurtogram estimator

The proposed FastKurtogram is a vital alternative to the original “full” Kurtogram of Ref. [35] which was estimated using several STFTs. It is also superior to the Discrete wavelet transform (DWT) and Discrete wavelet packet transform (DWPT) approaches. WT is much better adapted to the detection of transients than the Fourier transform and (DWT) are considered particularly for fast decomposition algorithms. The discrete WPT (DWPT) also enjoys a fast algorithm with complexity $O(N \log N)$ as it theoretically offers the same detection capabilities of WT, but with increased frequency selectivity since it is not restricted to constant-percentage bandwidth analysis filters. And, contrary to the continuous wavelet transform (WT) approach, the proposed FastKurtogram offers a more comprehensive exploration of the (f and Δf) plane whilst still enjoying a fast decomposition algorithm. Finally, it is worth mentioning that achieving an orthogonal decomposition is not a property of interest for the Kurtogram - as opposed to the DWT and DWPT - for it is essentially an analysis tool.

2.4 Cyclostationarity

Cyclostationarity is a fundamental concept in signal processing, characterized by the periodic variation of statistical properties of a signal over time. Unlike stationary signals, whose statistical measures remain constant, cyclostationary signals exhibit periodicity in their mean, variance, and autocorrelation functions. This property is particularly prevalent in signals generated by mechanical systems with rotating components like rolling element bearings.

Randall et al. [36] investigated the bearing signal characteristic in the presence of localized faults. The inner race, outer race, and rolling elements defects are the most frequent bearing faults. The vibrations produced by the localized faults are a sequence of impulses dominated by the high resonance frequencies of the structure. Slippage of rolling elements and cage introduces some level of randomness [3,20] in the spacing of the impacts and, although it is not larger than a few percent of the rate of burst repetition, the resulting signals cannot be

categorized as a periodic process. Ref. [36] pointed out that a bearing localized fault signal may be modeled as a 2nd order cyclostationary process. A second-order cyclostationarity determines processes with a periodic autocovariance function in time.

Autocovariance is a function of not only the time lag τ but also the instantaneous time t_i and it should not be confused with the stationary autocorrelation function calculated as the time average.

A localized fault is not truly cyclostationary and the signals are strictly speaking pseudo-cyclostationary as they seem to be cyclostationary but are not. However, they can be treated as cyclostationary in a first approximation as the departure from cyclostationarity may essentially be small.

2.5 The Autogram and the fast-Autogram

The Autogram methodology is rooted in the concept of cyclostationarity, particularly in the context of signals from damaged bearings that exhibit pseudo-cyclostationary characteristics of order 2. This means that their second-order statistics, such as the autocovariance, are approximately periodic. This periodicity manifests as a periodic envelope signal, which is a key feature used for fault detection.

To enhance this periodicity and filter out uncorrelated signal components (like noise and random impulses unrelated to bearing faults), the Autogram utilizes the unbiased autocorrelation (AC) of the squared envelope signal. This approach ensures robustness against both Gaussian and non-Gaussian noise types.

The Autogram methodology can be summarized into three main steps [4]:

- a) Frequency Band Splitting:** The signal is decomposed into frequency bands using a dyadic tree structure, typically achieved through the Maximal Overlap (undecimated) Discrete Wavelet Packet Transform (MODWPT). This method avoids down-sampling and preserves frequency resolution.
- b) Unbiased Autocorrelation (AC):** For each frequency band obtained from the wavelet transform, the unbiased autocorrelation of the squared envelope signal is computed. This step enhances the periodicity of the signal and suppresses noise components.
- c) Utility Function (Kurtosis of ACs):** The kurtosis of the autocorrelations across different frequency bands is calculated to generate a colormap. This colormap visually highlights frequency bands that exhibit maximum kurtosis, indicating potential bearing faults.

After identifying these informative frequency bands, further analysis involves utilizing the Fourier transform of the squared envelope signal (SES).

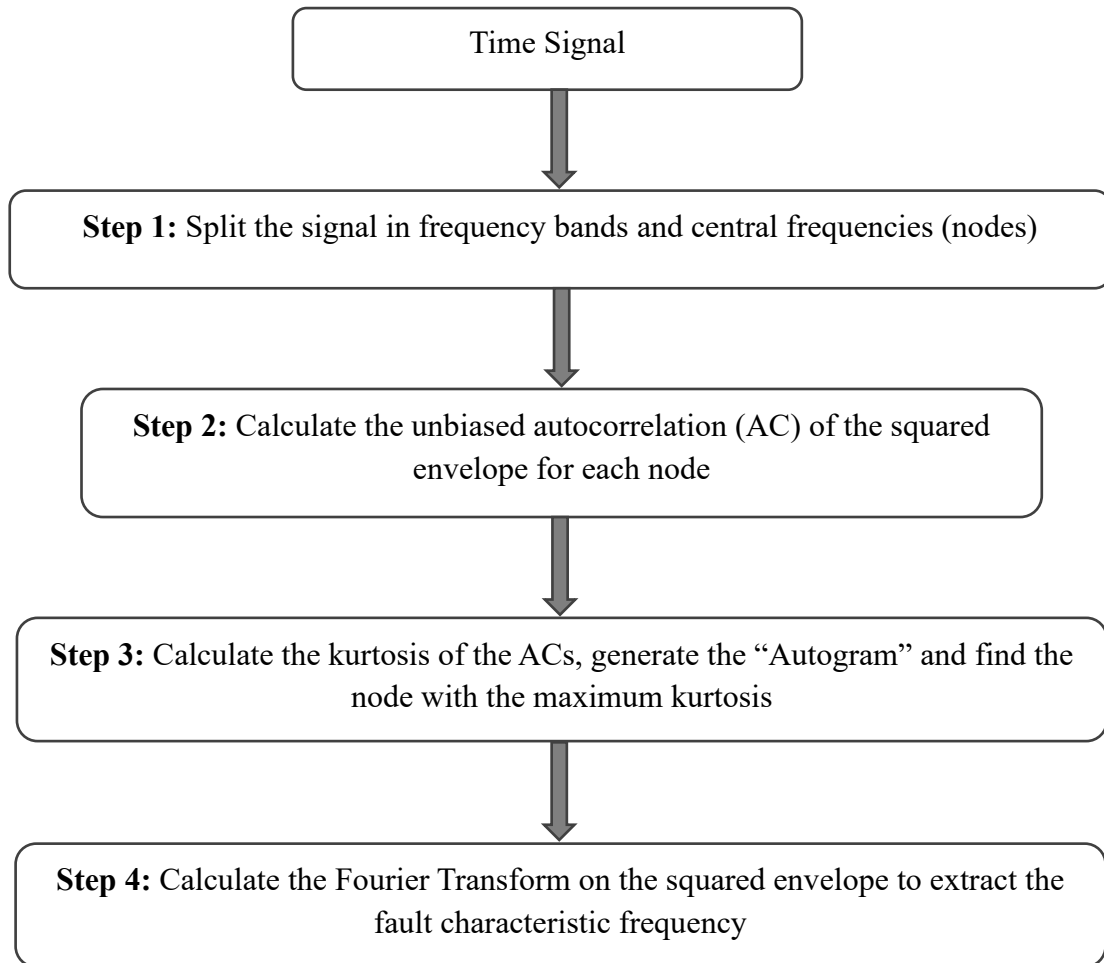


Fig 10. Flowchart of the Autogram

The Fast-Autogram

To optimize the computational efficiency of the algorithm, replacing the Maximal Overlap Discrete Wavelet Packet Transform (MODWPT) with the Multirate Filter-Bank (MFB) structure from the Fast-Kurtogram algorithm [3] is proposed. This substitution offers significant advantages. Firstly, it reduces the computational complexity of the signal decomposition to $O(N \log N)$, making it more suitable for processing large datasets and real-time applications. The MFB structure also enhances the coverage of the (frequency, scale) plane, known as $(f, \Delta f)$, crucial for accurately pinpointing frequency components within the signal spectrum related to bearing faults. Unlike the Discrete Wavelet Packet Transform (DWPT), which is limited to binary subdivisions, the MFB can implement a more flexible binary-ternary paving. This capability improves frequency localization, particularly beneficial for identifying specific fault signatures. Moreover, while DWPT's frequency localization diminishes with deeper decomposition levels due to spectral aliasing, the MFB maintains superior performance throughout, ensuring precise detection of fault-related frequencies. Overall, integrating the MFB structure enhances both the efficiency and accuracy of the algorithm in analyzing vibration signals for bearing fault diagnostics, advancing its capability in complex signal processing tasks.

The fundamental steps of the improved algorithm using the Multirate Filter-Bank (MFB) structure can be summarized as follows:

a) Signal Splitting: Employ a dyadic-ternary tree structure via the Multirate Filter-Bank (MFB) as proposed in [3] to divide the signal into frequency bands. This approach enhances computational efficiency with a complexity of $O(N \log N)$ and provides better coverage of the (frequency, scale) plane compared to traditional methods.

b) Compute Unbiased Autocorrelation (AC): Calculate the unbiased autocorrelation of the squared envelope for each frequency band obtained from step (a). This step improves the periodicity of the signal and removes uncorrelated components such as noise, essential for robust bearing fault detection.

c) Utility Function Calculation: Compute the kurtosis of the autocorrelations across all frequency bands to generate a colormap. This colormap visually highlights bands with maximum utility, indicating potential bearing faults based on their cyclostationary properties.

Subsequently, analyze the Squared Envelope Spectrum (SES) of the frequency band exhibiting the highest kurtosis in the autocorrelation analysis. This step focuses on identifying characteristic spectral lines associated with bearing damage.

2.6 Cyclic Spectral Analysis and Spectral Correlation

Methods like FastKurtogram and Autogram have been developed to overcome the challenge of finding the effective frequency for demodulation. It is done by selecting frequency bands in which the filtered time signal, Squared Envelope Spectrum (SES) of the filtered signal, and autocorrelation of the filtered time signal's envelope have the highest kurtosis respectively. The main disadvantage of these techniques is selecting a single frequency band for demodulation. Especially, the problem arises when multiple defects are present in different frequency bands because in this case only one defect is detected, and the others are overlooked. To solve this problem combined squared envelope spectrum (CSES) has been proposed [4].

Cyclic Spectral Analysis (CSA) [9] is another approach for condition monitoring of rotating machinery. This is a powerful method that separates and describes different 2nd-order cyclostationary components in terms of the spectral (carrier) frequency and the cyclic (modulation) frequency variables.

Spectral Correlation (SC) is one of the main tools to define the two-dimensional Fourier Transform (FT) of the instantaneous autocovariance function of machine signals. To estimate the SC, various proposed methods have been discussed by [10]. High computational cost is the main drawback of these methods which hindered their application for condition monitoring of rotary machinery. [11] includes a new approach called 'Cyclic Modulation Spectrum (CMS)', it serves as a fast alternative to Spectral Correlation (SC) by providing a cascade of envelope spectra across all possible frequency bands. CMS is unified in the form of cyclostationary estimators, making it an efficient estimator of SC. A major drawback of the Cyclic Modulation Spectrum (CMS) is its inability to detect cyclic frequencies that exceed the frequency

resolution of the Short-Time Fourier Transform (STFT). Recently, Spectral Correlation (SC) has been computed using a fast algorithm to enhance its computational efficiency. This method also overcomes the limitation faced by CMS. The techniques mentioned above are considered as the linear transformations. An alternative nonlinear transformation is Cepstral analysis which was proposed by Ref. [13] and it has been used for several purposes such as speech analysis, modal analysis, and REBs diagnosis [14]. This method becomes more advanced in detecting periodicities in the spectrum of a signal by reducing a whole family of harmonics into a single cepstral line. Randall and Swahili [15]. By leveraging the features of cepstral analysis, Borghesani et al. [16] have proposed two approaches: cepstrum editing and cepstrum pre-whitening. These techniques are used to separate periodic and random components and to pre-whiten a signal, respectively.

2.7 Spectral Amplitude Modulation (SAM)

In this section, a generalized version of Cepstrum Pre-Whitening is developed. CPW is an effective approach for achieving the desired results of REB diagnosis [6] but it suffers from two major drawbacks. Firstly, the magnitude of a signal in the whole frequency domain is set to one, the signal-to-noise ratio (SNR) for the reconstructed signal is decreased hopefully and the frequency components of noise have the same magnitude as the frequencies linked to the defect signals (carrier frequencies). Secondly, assuming bearing defect signals exhibit 2nd order cyclostationarity leads to the conclusion that the peaks related to damages do not have considerable amplitude in the real cepstrum [16]. In many cases, this assumption is not precise and always acceptable because the random slippage is not high, and the discrete components related to defects can be detected in both frequency and quefrequency domains.

In addition, a new envelope spectrum, namely the Log-Envelope Spectrum (LES), has been proposed by [18] to investigate 2nd order cyclostationary signals contaminated by highly non-Gaussian and impulsive background noise. In the presence of sizable and non-periodic impulses, LES can be employed as a more robust alternative to SES for the computation of modified signals' envelopes spectra. The only drawback of LES is related to the lower SNR. Therefore, it is recommended to use this indicator whenever impulsive noise exists in the signals. In this paper, rather than LES, the Fourier transform of the logarithm of the squared envelope signal is computed and it is called "LSES".

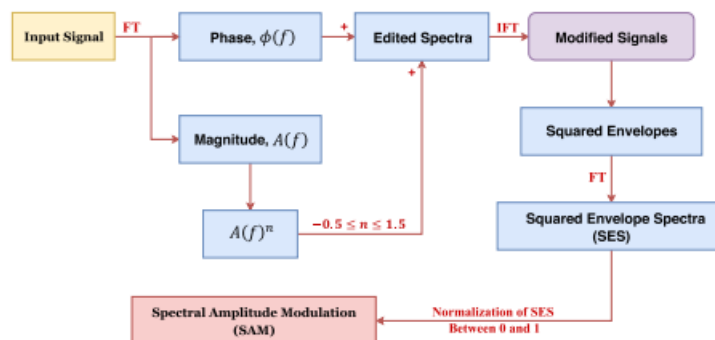


Fig 11. Flowchart of SAM

Moshrefzadeh et. al [54] introduced a new empirical method for bearing fault diagnosis named spectral amplitude modulation (SAM). First, the magnitude and phase of a signal are calculated using Fourier transform (FT). Subsequently, different weights called magnitude order (MO) are given to the magnitude of the original signal and obtain edited amplitude, which is then combined with the actual phase to reconstruct a series of modified signals using inverse Fourier transform (iFT). Afterwards, the squared envelope spectrum (SES) of each modified signal is computed to extract fault characteristics. SAM can be performed without any additional input parameters and is proved to be an efficient, convenient and effective method. Moshrefzadeh employed SAM in condition monitoring and intelligent diagnosis to extract signal components with different energy levels.

To implement and apply SAM, the last step requires to selection of the limits of MO. Thus, there is no theoretical restriction for choosing the upper limit of MO. a and b are two arbitrary numbers while $a \leq n \leq b$ hereafter, the variable n is referred to as Magnitude Order (MO). However, it is reasonable to avoid very high values of b , since in that case only a few large peaks, mostly not linked to REB signals, will then dominate the magnitude spectrum and mask other components of the signal. On the other hand, new false components will be added to the SESs of modified signals for very low and negative values of MOs. In this condition, very low amplitude components in the magnitude spectrum of raw signal dominate the magnitude spectra of modified signals. In SAM, the magnitude calculated by Fourier transform is a global representation of the time process. Moreover, since MSES is constructed by viewing along the MO-axis, which deals with the invalid components under different weights.

For practical reasons and to keep the approach as general as possible for REB diagnosis, the values of -0.2 and 1.5 for a and b are suggested and their validity will be examined with practical examples in the following section. Additionally, a simple yet effective approach is proposed to find the lowest acceptable value of MO which is called critical point since false peaks in the SESs of modified signals begin to appear for lower values than this. As all the SESs are normalized between 0 and 1 , it can be deduced that the mean value of normalized SES of a signal related to noise will be very high. The reason is that many components in the normalized SES of noise are equal to one or have very high values. In contrast, a few peaks in a normalized SES will reduce its mean value. As the value of MO decreases, the effect of noise will gradually grow and, at the critical point, the modified signal will be completely noisy and therefore with the highest mean. For lower MO than the critical point, false peaks start to emerge in the SESs and the mean value of normalized SESs decreases subsequently. This characteristic of normalized SESs could be used to find the minimum acceptable value of negative MOs. The critical point is revealed as a maximum in a mean-MO plot.

Ref [53] proposed Time-frequency spectral amplitude modulation (TFSAM) method, its main motive is to settle the above drawbacks and improve the SAM method. The proposed method is more robust than SAM since more detailed information of the amplitude is obtained in the time-frequency domain. In TFSAM, the amplitude and phase in the time-frequency domain are computed using short-time Fourier transform (STFT), by which means more accurate results can be obtained since the amplitude is not calculated as an average value over the whole-time

process. Furthermore, an indicator is proposed to select the optimal value of MO adaptively in order to acquire more evident fault characteristic frequencies in rolling bearing fault diagnosis.

2.8 Cyclic Modulation Spectrum

The CMS has been proposed by [11] as an estimator of the SC. Although the CMS proves to be a valid diagnostic tool in many situations, it has limited performance in general being constrained to the uncertainty principle: it cannot detect periodic patterns other than in the form of modulations whose frequencies are necessarily lower than the frequency resolution. As mentioned below in this paper, the CMS is also not properly calibrated to quantify modulation depth. Besides, computationally efficient algorithms for the estimation of the SC have been proposed early in the ninetens in Refs. [38,39], of which the FFT Accumulation Method (FAM) is the fastest. As far as the authors tell the FAM is still recognized as the most computationally efficient algorithm in the specialized literature. Unfortunately, its computational advantage comes at the price of a degradation of the statistical performance of the estimator. The cyclic frequency resolution and variance are non-uniform, meaning that estimation errors can be locally very high. This is probably unacceptable in the kind of applications targeted by this paper[11].

The CMS takes a different look at cyclostationary signals. It intends to track periodic flows of energy in frequency bands by evaluating the Fourier transform of the squared envelope at the output of a filter bank [11]. It is thus interpreted as a waterfall of envelope spectra. The CMS is efficiently computed as the Discrete Fourier Transform (DFT) of the spectrogram.

2.9 Spectral Correlation (SC)

The SC is defined as the double discrete Fourier transform of the instantaneous autocorrelation function (a Fourier series in time t and a Fourier transform in time-lag τ when continuous time is considered). In the case of a second-order cyclostationary signal, the SC displays a characteristic signature continuous in frequency f and discrete in cyclic frequency α . The SC may therefore be understood as a decomposition of the signal for the “modulation frequency” α and the “carrier frequency” f . A popular estimator of the SC is obtained from the so-called “time-smoothed cyclic periodogram” [10,37] or, equivalently, the Averaged Cyclic Periodogram (ACP) [9] which is an extension of Welch’s method (also known in spectral analysis as the “Weighted-Overlapped-Segment-Averaging” method) to cyclostationary signals.

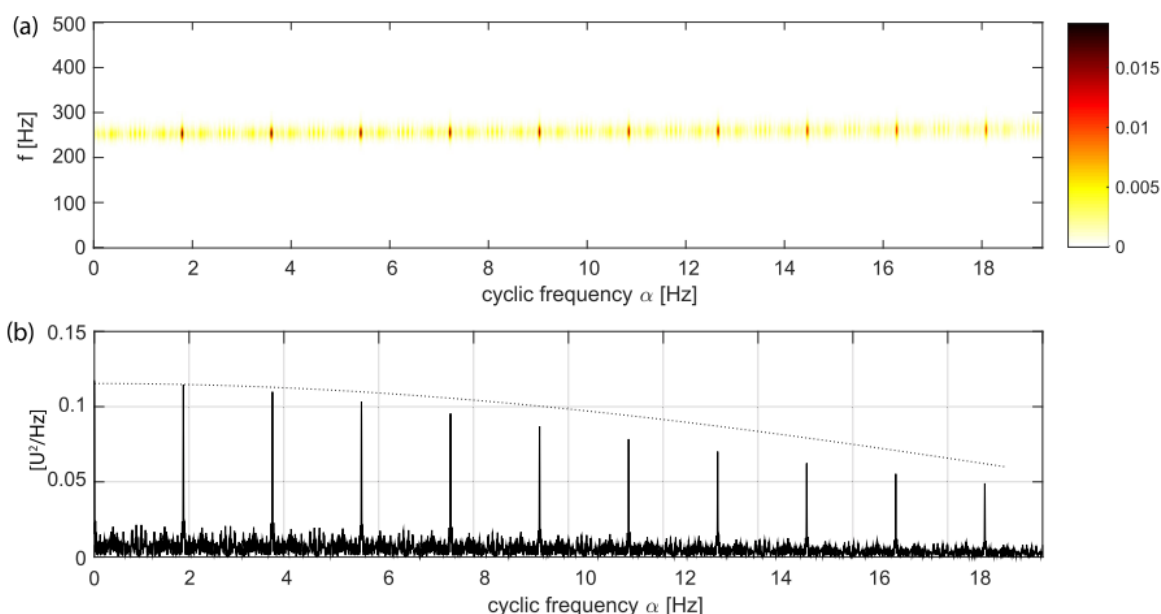


Fig 12. (a) Spectral correlation estimated from the Averaged Cyclic Periodogram, $S_x^{ACP}(\alpha, f)$, with $N_w = 2^8$ ($\Delta f = 4$ Hz; $\Delta\alpha = 0:01$ Hz) and (b) its evaluation at $f = 250$ Hz together with the theoretical envelope of the peaks (dotted line) as obtained from a square modulation

Fig 12. (a) displays the estimated SC as a colormap. It is seen that the vertical lines are correctly identified at α_0 and its multiples in a frequency band around the resonance at 250 Hz. The SC evaluated at the resonance frequency, $S_x^{ACP}(\alpha, f_0)$, was displayed in Fig 12. (b): it is expected to show the Fourier spectrum of the square modulation whose theoretical envelope (the cardinal sine function) was indicated by the black dotted line.

Ref [13] introduces a fast algorithm to estimate the SC, the “Fast Spectral Correlation” (Fast-SC), which essentially proceeds from the Short-Time Fourier Transform (STFT). It may be seen as a correction of the CMS such as to make it approach the ideal SC. Most of the computational effort is required for the calculation of the STFT, which makes many efficient implementations now exist in commercial software. This makes the proposed algorithm weakly

intrusive and of low complexity. For all these reasons, the approach proposed by Jérôme Antoni et. al should participate in making the SC a more widely spread tool in condition monitoring. Another contribution is to maintain a simple vision of cyclostationarity. While the CMS is simply interpreted as the detection of periodic flows of energy in frequency bands, the Fast-SC extends it to the detection of periodic flows across different frequency bands. This should help to make cyclostationarity easier to interpret while not sacrificing the usage of its most performant tools.

The central tool for the “cyclic spectral analysis” of machine signals is the Spectral Correlation (SC) which displays at once, in the form of a bi-spectral map shown below, the whole structure of modulations and carriers in a signal.

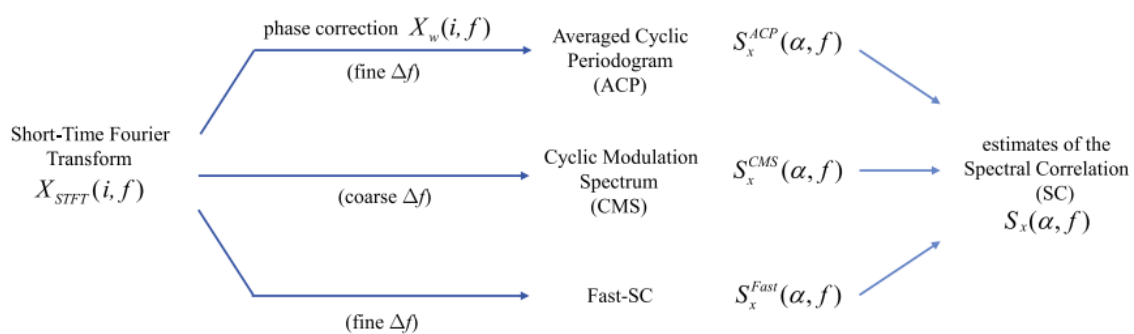


Fig 13. Connections between the spectral quantities

Fig 13. represents the estimation of Spectral Correlation (SC) from a signal involves several steps, each leveraging different aspects of the Short-Time Fourier Transform (STFT). The process can be described as follows:

1. Short-Time Fourier Transform (STFT) Calculation:

The signal is first subjected to a Short-Time Fourier Transform, denoted as $X_{STFT}(i, f)$, where i represents the time index and f the frequency.

2. Branching into Different Analysis Paths:

After computing the STFT, the process branches into three distinct paths depending on the required resolution and computational efficiency:

Path 1: Phase Correction with Fine Frequency Resolution (Δf):

- The STFT undergoes phase correction, resulting in $X_w(i, f)$.
- This corrected signal is then used to compute the Averaged Cyclic Periodogram (ACP), producing $S_x^{ACP}(\alpha, f)$.
- The ACP method provides an estimate of the Spectral Correlation, denoted as $S_x(\alpha, f)$.

Path 2: Coarse Frequency Resolution (Δf):

- Without phase correction, the STFT directly leads to the computation of the Cyclic Modulation Spectrum (CMS), resulting in $S_x^{CMS}(\alpha, f)$.
- The CMS method offers another estimate of the Spectral Correlation, $S_x(\alpha, f)$.

Path 3: Fine Frequency Resolution (Δf) with Fast-SC Method:

- A variant of the STFT is applied to quickly compute the Spectral Correlation using the Fast-SC method, yielding $S_x^{Fast}(\alpha, f)$.
- The Fast-SC method provides an efficient estimate of the Spectral Correlation, $S_x(\alpha, f)$.

3. Resulting Estimates of Spectral Correlation:

Each of these methods ACP, CMS, and Fast-SC provides estimates of the Spectral Correlation, $S_x(\alpha, f)$, which can be utilized for various signal analysis purposes. These methods differ in their computational requirements and the resolution of the resulting SC estimates, offering flexibility depending on the specific needs of the analysis.

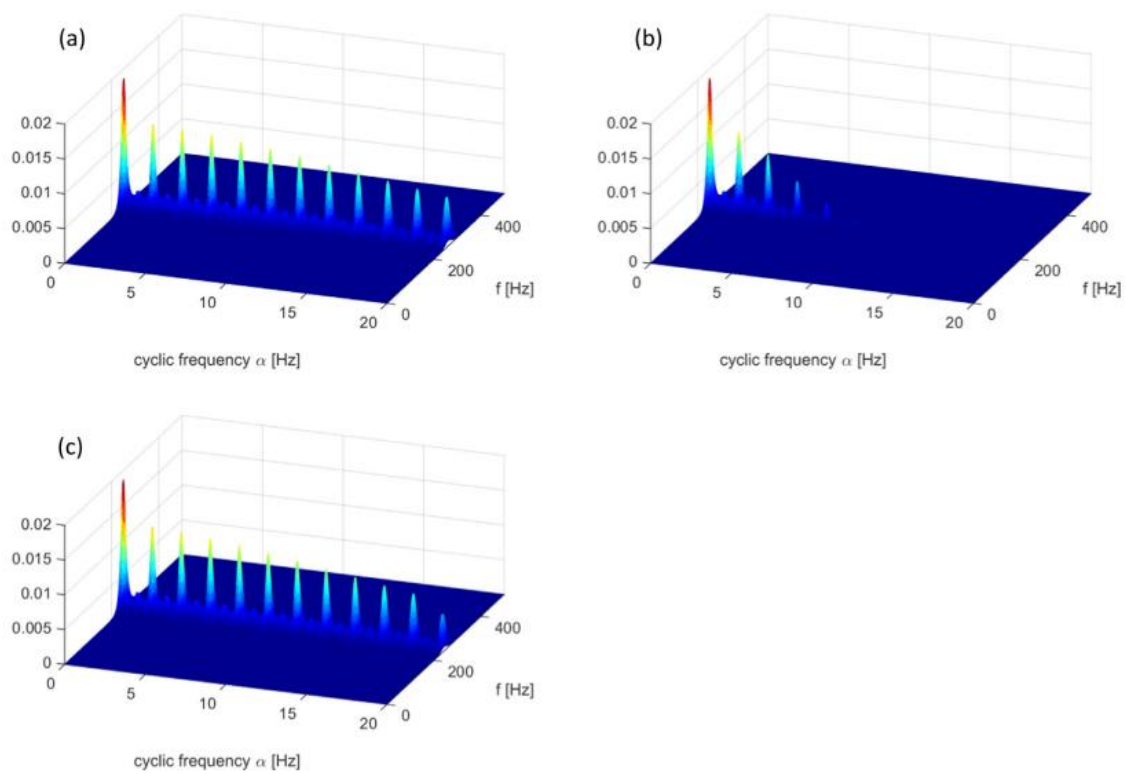


Fig 14. 3D comparison of estimates of the SC obtained from (a) the ACP, (b) the CMS and (c) the Fast-SC

The section describes the application of the Fast-SC (Fast Spectral Correlation) method in various experiments, particularly for diagnostics related to bearing signatures in small fans (first tested fan, second tested fan) & signature of the outer race in rolling element bearings. It notes that some of the signals in these experiments are too long for analysis using ACP within a reasonable time frame. This limitation necessitates the use of more efficient techniques, specifically CMS (Cyclic Modulation Spectrum) and Fast-SC.

Methods:

1. **Outer Race Signature:** The outer race of a rolling element bearing is a critical component in diagnostics. Vibration patterns from defects in this area are of particular concern.
2. **Signal Length:** Some signals collected during these experiments are too long for traditional analysis methods like ACP, as they require excessive computation time.
3. **Use of CMS and Fast-SC:** In cases where ACP is impractical, CMS and Fast-SC are the preferred techniques. These methods are more efficient and better suited for handling long signals, allowing for the timely analysis of bearing diagnostics.

The magnitude and the number of harmonics linked to the incriminated cyclic frequency may serve as an indicator of severity of the fault. As advocated in Ref. [11], the Spectral Coherence is computed instead of the SC. The Spectral Coherence is a normalized version of the SC with magnitude normalized within 0 and 1. It may be directly interpreted as the “depth” of a modulation with frequency α and carrier f . The Spectral Coherence may also be interpreted as the SC of the whitened signal, which tends to equalize regions with very different energy levels and thus to magnify weak cyclostationary signals. In the following, the Spectral Coherence will serve as a basis to define the Squared Envelope Spectrum (SES) measured in a given frequency band $[f_1;f_2]$ and, a newly proposed spectral quantity, the “Enhanced Envelope Spectrum” (EES).

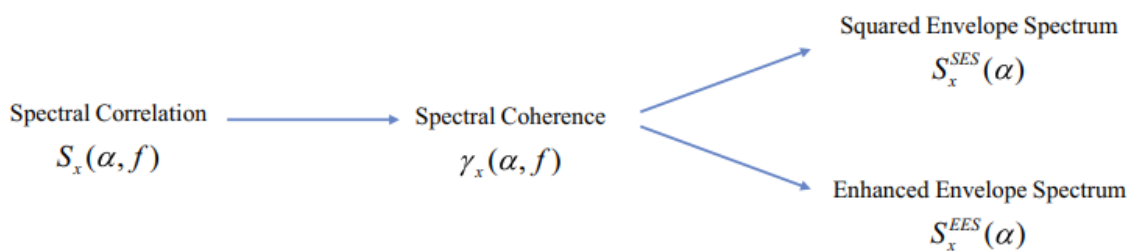


Fig 15. Connection between the Spectral Correlation and the envelope spectra

The process of obtaining the Squared Envelope Spectrum (SES) and Enhanced Envelope Spectrum (EES) from a signal involves a series of well-defined steps, beginning with Spectral Correlation (SC) and continuing through Spectral Coherence calculations. Each step reveals important features of the signal's behavior, particularly in relation to cyclic frequencies and envelope characteristics.

The steps are outlined as follows:

1. Spectral Correlation ($S_x(\alpha, f)$):

- The first stage involves calculating the Spectral Correlation (SC) of the signal, denoted as $S_x(\alpha, f)$ where:
 - α represents the cyclic frequency (related to periodic components).
 - f represents the spectral frequency (related to the frequency content of the signal).
- Spectral Correlation quantifies the periodic correlation between different frequency components within the signal. It captures how frequency components relate to each other over time.

2. Spectral Coherence ($\gamma_x(\alpha, f)$):

- After calculating the Spectral Correlation, the next step is to compute the Spectral Coherence $\gamma_x(\alpha, f)$, which measures the degree of linear relationship between two frequency components at specific cyclic and spectral frequencies.
- Spectral Coherence is essentially a normalized measure, allowing us to evaluate how strongly the frequency components are related at each cyclic frequency α .

3. Derivation of Envelope Spectra:

Based on the Spectral Coherence, two distinct envelope spectra can be derived:

a. Squared Envelope Spectrum (SES):

- The Squared Envelope Spectrum is denoted as $S_x^{SES}(\alpha)$.
- The SES represents the power of the signal's envelope at different cyclic frequencies α .
- It is useful for analyzing how much power is associated with the signal's periodic components, making it an essential tool in diagnostics.

b. Enhanced Envelope Spectrum (EES):

- The Enhanced Envelope Spectrum is represented as $S_x^{EES}(\alpha)$.
- The EES provides an enhanced view of the signal's envelope characteristics, offering more refined details than the SES. It is typically employed for deeper analysis where subtle signal features are critical.

4. Resulting Envelope Spectra:

Both the SES and EES offer valuable insights into the signal's envelope behavior:

- SES focuses primarily on the power aspects of the signal's envelope.
- EES emphasizes enhanced details for a more comprehensive analysis.

These envelope spectra are important tools in signal processing, particularly for diagnosing faults in mechanical systems like bearings, where envelope modulation patterns often contain critical information.

The process and connection between SC, Spectral Coherence, SES, and EES can be visualized in the referenced fig. 15, highlighting the relationships among these key signal analysis components.

Therefore, the combination of Spectral Correlation, Spectral Coherence, SES, and EES provides a comprehensive framework for understanding and diagnosing the periodic behavior and envelope characteristics of signals, particularly in rotating machinery and similar applications.

The upcoming section shows the development of diagnostic algorithms for the Rolling Bearing Elements. Over the years, the Case Western Reserve University (CWRU) bearing data center [41] has been recognized as a benchmark dataset for bearing diagnostics. Therefore, the performance of the advanced signal processing techniques (which is mentioned in section 1.4) is discussed in this chapter. The comparative analysis uses 5 the diagnostic algorithms to determine the most effective diagnostic approach among them.

Nomenclature

CWRU	Case Western Reserve University
DE	Drive-End Acceleration
FE	Fan-End Acceleration
BA	Base Plate Acceleration
FK	FastKurtogram
FA	FastAutogram
SAM	Spectral Amplitude Modulation
SC	Spectral Coherence
M1-3	Methods 1-3

3. Experimental Analysis

3.1 Experimental setup

The Case Western Research University (CWRU) test rig consists of a 2 hp Reliance Electric motor driving a shaft on which a torque transducer and encoder are mounted, as shown in Fig. 15. Torque is applied to the shaft via a dynamometer and electronic control system.

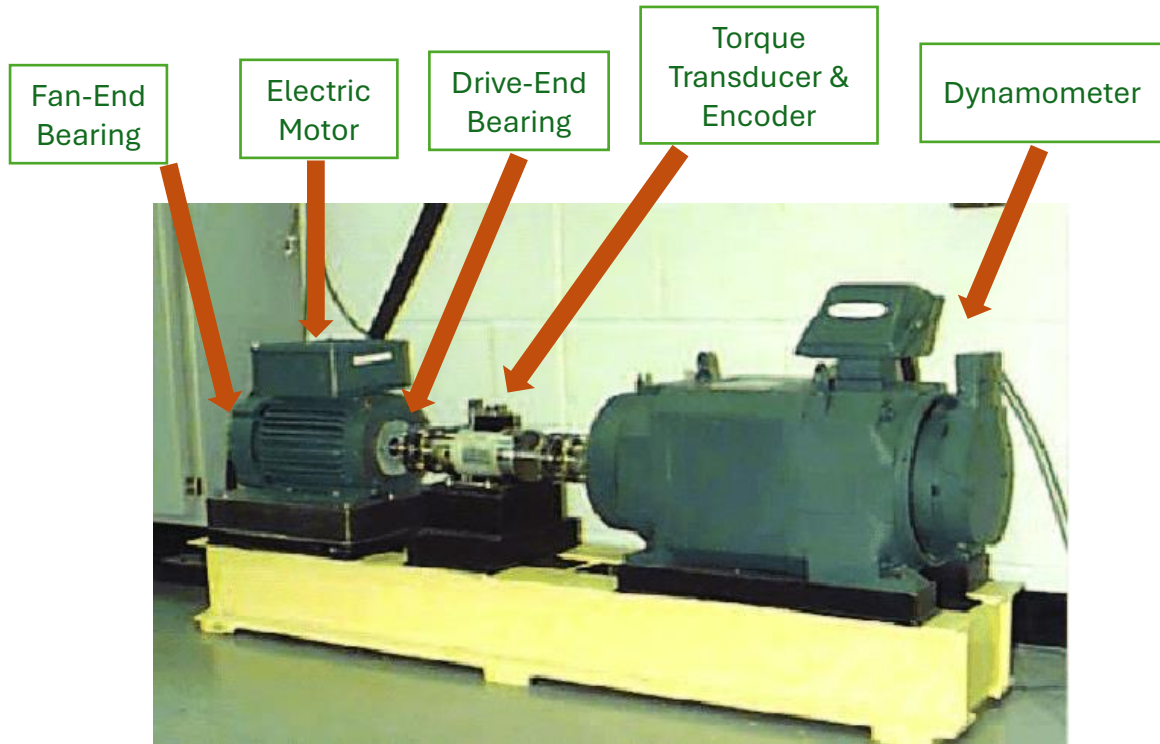


Fig 16. CWRU bearing test rig

Faults ranging in diameter from 0.007 to 0.028 inches (0.18 to 0.71 mm) were seeded on the rolling elements of the inner and outer races of the drive-end and fan-end bearings (described in Table 1) of the motor using electro-discharge machining (EDM). Acceleration was always measured in the vertical direction on the housing of the drive-end bearing (DE), and sometimes also in the vertical direction on the fan-end bearing housing (FE) and on the motor supporting base plate (BA). The sample rates used were 12 kHz for some tests and 48 kHz for others. The machine was then run at a constant speed for motor loads of 0 to 3 HP (approximate motor speeds of 1797 to 1720 rpm).

Table 1. Bearing Information

Drive end bearing: 6205-2RS JEM SKF, Deep groove ball bearing

Defect frequencies: (multiple of running speed in Hz)			
BPMI	BPFO	FTF	BSF
5.4152	3.5848	0.39828	4.7135

Fan end bearing: 6203-2RS JEM SKF, Deep groove ball bearing

Defect frequencies: (multiple of running speed in Hz)			
BPFI	BPFO	FTF	BSF
4.9469	3.0530	0.3817	3.9874

3.2 Diagnostic Methods

These data sets utilize three diagnostic methods. As the final diagnostic tool, all these methods use the squared envelope spectrum. However, to obtain the envelope signal different preprocessing steps were carried out as an initial step.

For all data sets, first Method 1 – envelope analysis of the raw signal was applied. When Method 1 proved unsuccessful Methods 2 and 3 were applied accordingly. This study primarily aims to test the diagnostic algorithms, which is why complex methods were applied to data that could not be diagnosed using Method 1.

3.2.1 Method 1: Envelope Analysis of the raw signal

The raw vibration signal from a machine is directly analyzed without complex preprocessing or filtering steps. This full bandwidth signal retains all the information, including noise and other potential disturbances. In envelope analysis, the amplitude modulation of the signal is extracted. This is particularly effective when fault-related frequencies are modulated onto higher-frequency carrier waves. To obtain the envelope, the raw signal is typically rectified (squared) to smooth out the high-frequency components and leave the modulated envelope signal. The spectrum of this envelope is then computed to detect bearing fault frequencies.

3.2.2 Method 2: Cepstrum Pre-whitening

This method consists of the following steps:

1. Cepstrum pre-whitening to set all frequency components to the same magnitude
2. Envelope analysis (squared envelope spectrum) of the full bandwidth signal

Ref [43] proposed this method and it has been applied to variable speed applications in [16]. The basis of its functionality is that since all spectral bands have the same power spectral density, those with more impulsivity will tend to dominate the time records and show impulsive responses that are typical of bearing faults. Resonances are also removed, but this can mean that resonances at frequencies that do not carry bearing fault information are less likely to mask those that do.

3.2.3 Method 3: Benchmark Method

This method is a streamlined version of the benchmark method proposed in [1], which was based on the semi-automated bearing diagnostics procedure suggested in [44], and consisted of the following steps:

1. Discrete/random separation (DRS) to remove deterministic (discrete frequency) components
2. Spectral kurtosis to determine the most impulsive band, followed by bandpass filtering
3. Envelope analysis (squared envelope spectrum) of the bandpass-filtered signal

The separation of random and deterministic components was achieved using discrete/random separation (DRS) [45], based on the transfer function between the signal and a delayed version of itself. Ideally, such a function would be unity at the frequencies of discrete components, since they remain correlated regardless of time lag. Random components become less correlated with increasing delay, so, provided the delay time is well chosen, the transfer function would be close to zero for these frequencies. This transfer function, obtained directly in the frequency domain (using transform size N), is then applied to the signal as a discrete/random separation filter. The DRS settings used in this paper – filter length N and delay Δ (in number of samples) – were established by trial and error on a small number of data sets, with $N = 16384$ and $\Delta = 500$ chosen for the 12k data and $N = 8192$ and $\Delta = 500$ used for the 48k data.

3.3 Comparison of various fault's diameter

As mentioned in Chapter 1, the four defects (Inner race, Outer race, Cage & Ball) in Rolling Bearing Elements are discussed in detail. Among the motor loads ranging from 0 to 3 HP in the bearing data center files. The 2 HP case was selected. Fault diameters ranging in small(0.007 inches), medium(0.014 inches), and high(0.021 inches) were considered.

3.3.1 Damage Quantification and Comparative Analysis of Diagnostic Methods:

This section details a methodical process for assessing and comparing the diagnostic techniques' ability to identify and quantify damage in the system. By performing a structured frequency analysis and filtering approach, this method isolates damage-related frequencies and calculates a standardized metric to evaluate each technique. The steps are as follows:

1. Identification of Closest Frequency Match

Each harmonic frequency is matched to the closest frequency f in the signal spectrum that corresponds to the target damage frequency f_d . This step considers both the central damage frequency and any predefined sidebands, ensuring that relevant frequency components associated with each harmonic are captured. Identifying the nearest frequency provides a reliable foundation for peak analysis, which is crucial for assessing the presence of damage indicators in the frequency spectrum.

2. Peak Spectrum Value Determination

Around each damage frequency f_d , a specific range is defined to locate the maximum peak value in the spectrum S . This peak value represents the highest spectral response near the damage frequency and is a critical indicator of potential damage severity. Ensuring that the peak within this range is accurately captured highlights the primary spectral components linked to damage.

3. Spectrum Filtering and New Spectrum Creation

To enhance the analysis, significant peaks identified in S are removed to produce a new spectrum S_{new} , that reflects the baseline spectral content. By excluding dominant peaks, S_{new} enables a cleaner view of the underlying signal, free from interference from major damage-related frequencies. This filtered spectrum is critical for establishing a baseline for measuring normalized damage and ensuring that comparisons are not biased by dominant peaks.

4. Calculation of Normalized Damage Metric

The final damage value for each method is determined by dividing the cumulative damage by the root-mean-square (RMS) of S_{new} . This step yields a normalized damage metric, which standardizes the damage calculation across different diagnostic techniques, facilitating direct comparisons. This metric reflects each method's sensitivity and precision in detecting and representing system damage, providing a consistent measure for determining the most effective diagnostic approach.

This process results in a damage metric that offers insight into each method's accuracy and reliability, guiding the selection of the most suitable diagnostic technique. By standardizing damage calculations, this method ensures a robust comparative analysis, accounting for each method's performance based on its peak response and overall effectiveness in analyzing the underlying spectrum. This structured framework aids in objectively identifying the optimal diagnostic method based on quantitative evaluation criteria.

3.3.2 Error Analysis method:

The error analysis method is designed to quantitatively evaluate each diagnostic approach's accuracy by measuring how closely detected frequencies align with expected damage frequencies. This method provides an objective comparison, grounded in measurable results, by defining an acceptable tolerance around expected damage frequencies and classifying error on a scale of 0 to 1:

Tolerance Definition:

A tolerance band of $\pm 0.3\%$ around the expected damage frequencies, namely the Ball Pass Frequency of Inner Race (BPFI) and its harmonic ($2 \times \text{BPFI}$), along with their sidebands, is established. Frequencies detected within this range are considered accurate detections, indicating correct frequency identification by the diagnostic method.

Error Value Scale:

The error metric ranges from 0 to 1:

Error = 1: Indicates that damage frequencies are present and accurately detected.

Error = 0: Indicates failure to identify significant peaks at damage frequencies, suggesting the method's limitations in detection accuracy.

This approach enables a quantitative evaluation of each technique’s precision, allowing for fair and objective comparison based on how effectively each diagnostic method detects damage frequencies within the specified tolerance range.

3.3.3 Inner race damage: [12K_Drive-End_Bearing_Fault_Data]

Here, the acceleration signal is measured on the fan-end, while the damage is in the drive-end bearing.

For the Inner race, the figures given below show the results of the raw time signal with the red dash-dot line indicating the expected damage frequency of the first two -harmonics (BPFI & 2*BPFI), and their respective sidebands frequencies. The presence of sidebands is often a strong indicator of modulation related to damage, further confirming fault presence.

IR_007 (107FE) (small fault)

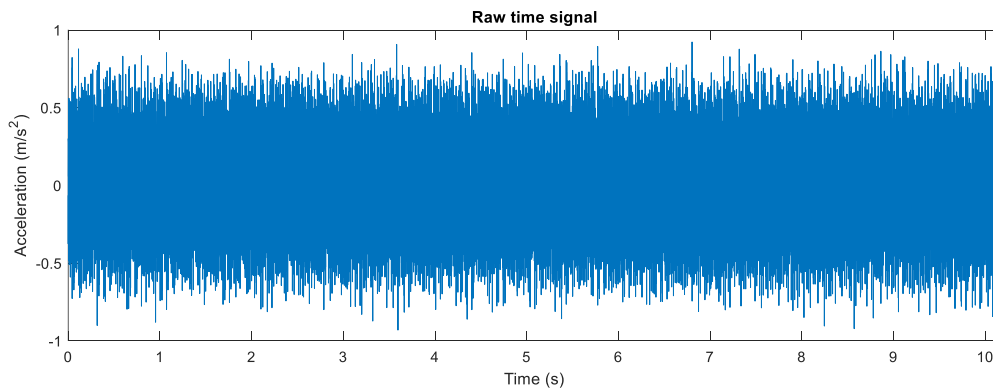


Fig 17. Raw Signal

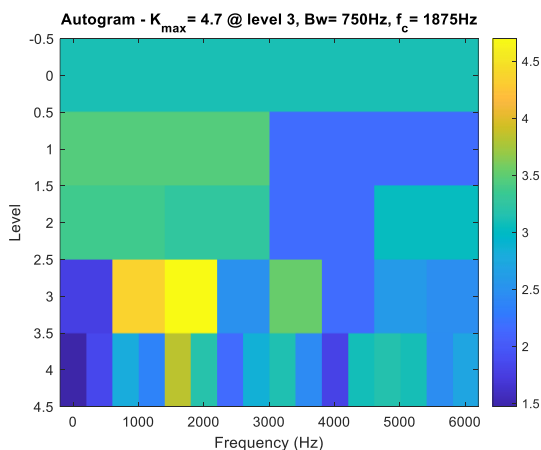


Fig 18. Autogram

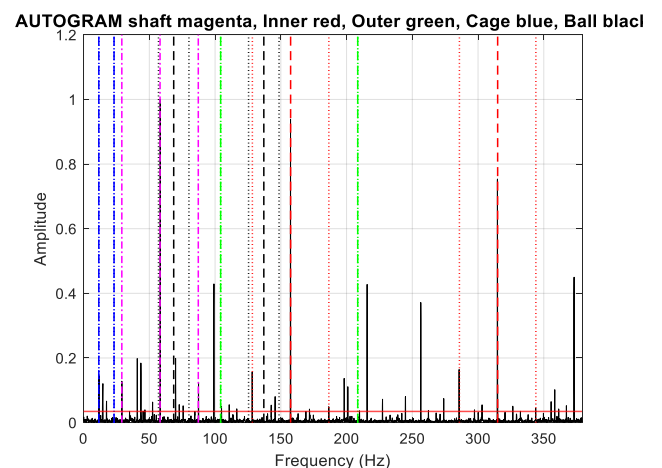


Fig 19. Autogram, Normalized SES

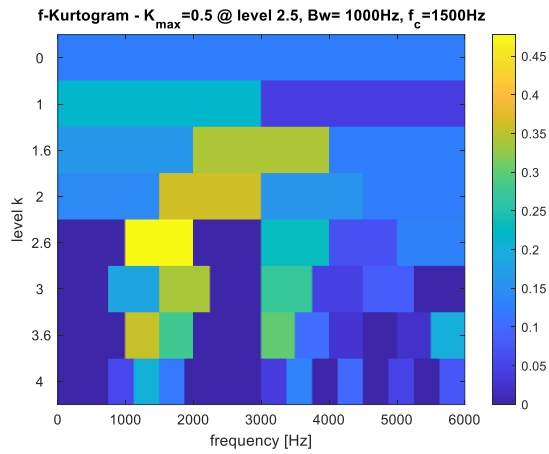


Fig 20. FastKurtogram

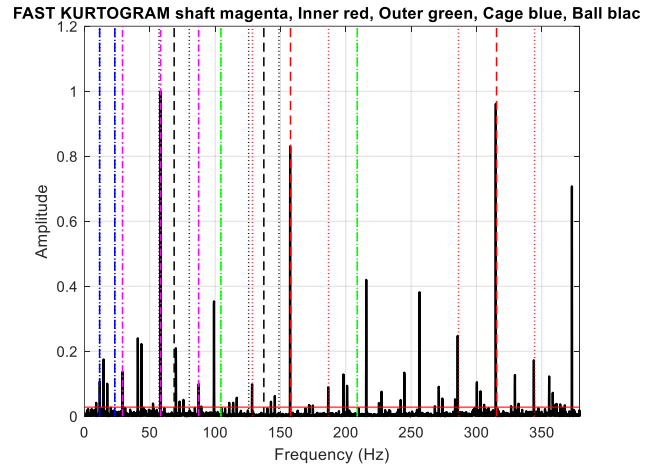


Fig 21. FastKurtogram, Normalized SES

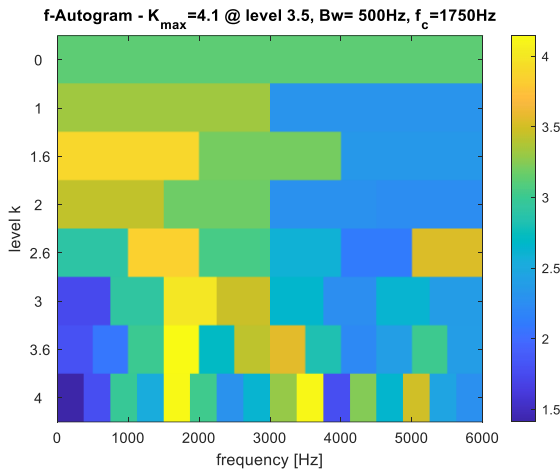


Fig 22. FastAutogram

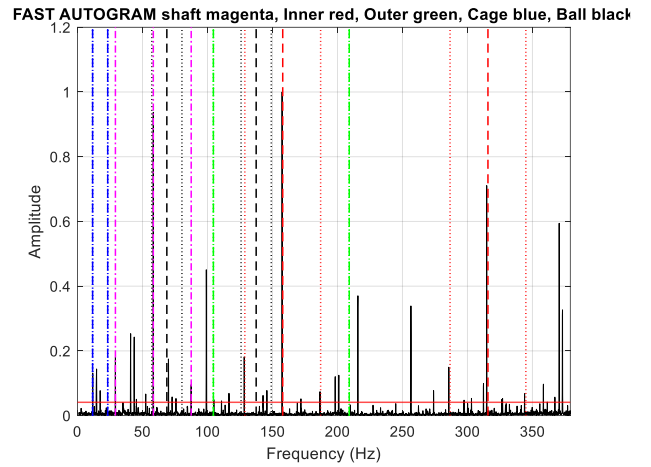


Fig 23. FastAutogram, Normalized SES

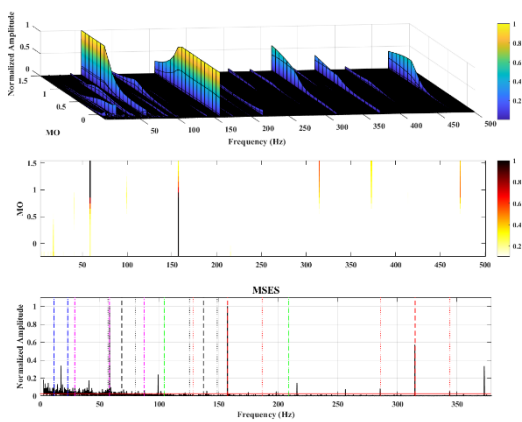


Fig 24. SAM, Normalized MSES

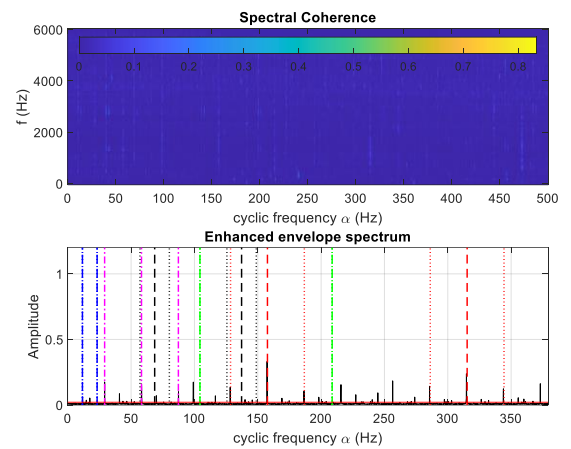


Fig 25. SC, Normalized EES

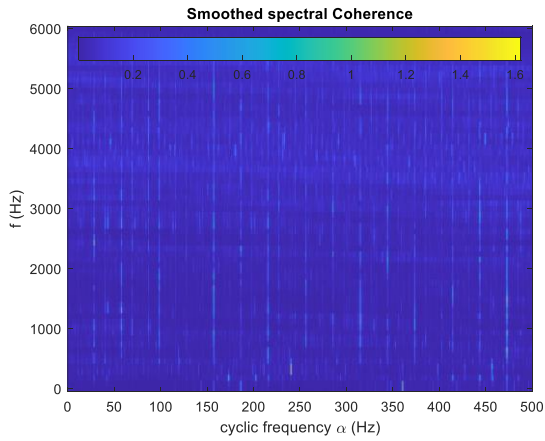


Fig 26. Smoothed SC

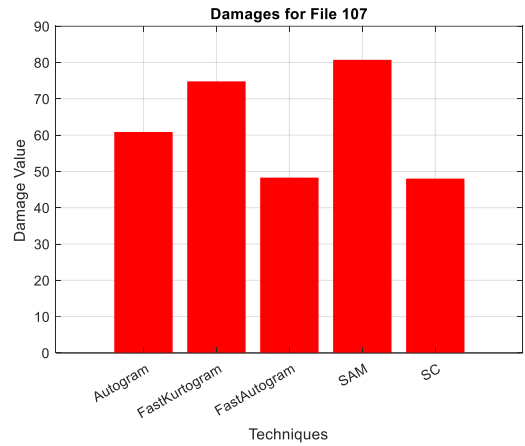


Fig 27. Damage value for file 107FE

In the analysis of the 107FE data file, SAM proved to be the most effective diagnostic approach for both identifying and quantifying the damage. The quantification method described in Section 3.3.1 yielded a damage value of 80.7334, which is marginally higher than those obtained from other techniques, suggesting a more sensitive detection. Furthermore, the error analysis method outlined in Section 3.3.2 resulted in an error value of 0.9045, reinforcing the detection accuracy. This low error value indicates a strong alignment between the detected damage frequencies and the anticipated damage patterns, supporting the conclusion that damage is indeed present in the system.

IR_014 (171FE) (medium fault)

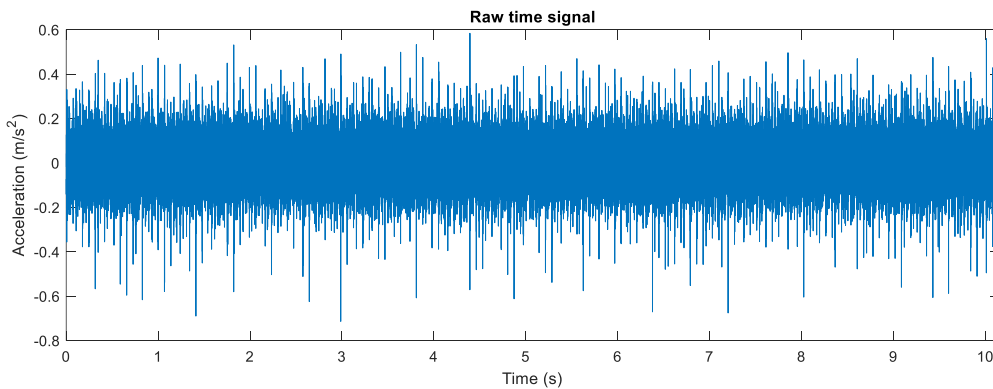


Fig 28. Raw Signal

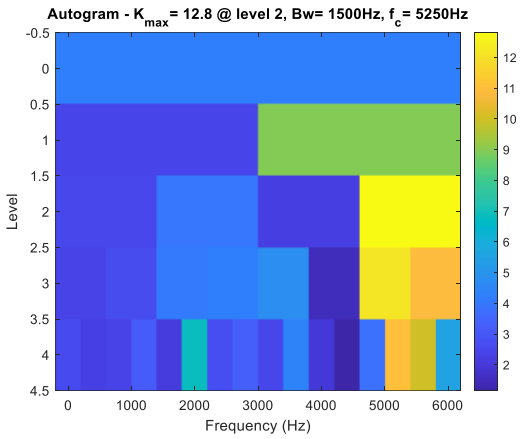


Fig 29. Autogram

AUTOGRAM shaft magenta, Inner red, Outer green, Cage blue, Ball black

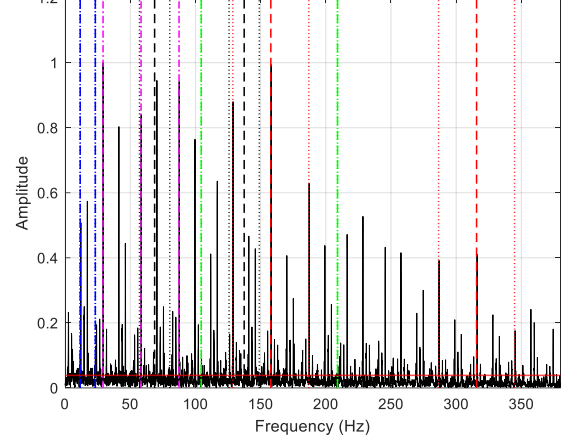


Fig 30. Autogram, Normalized SES

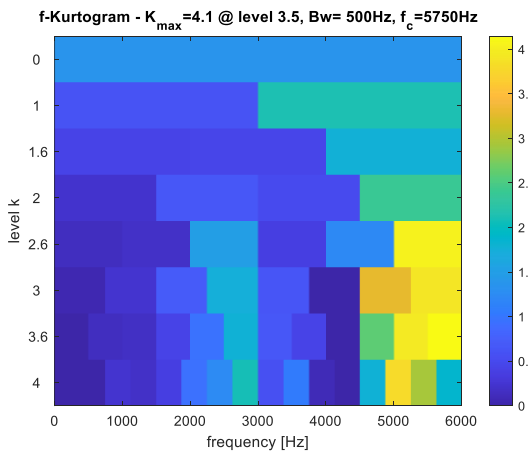


Fig 31. FastKurtogram

FAST KURTOGRAM shaft magenta, Inner red, Outer green, Cage blue, Ball black

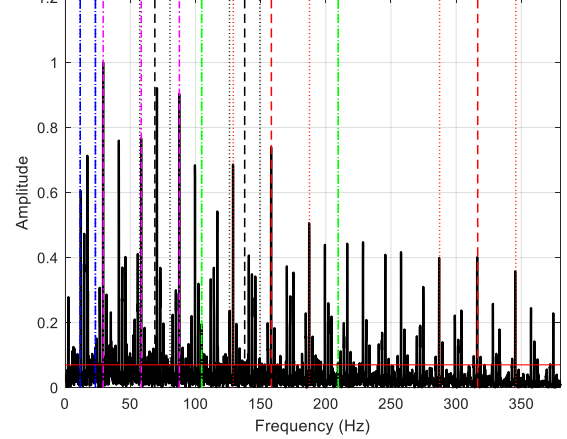


Fig 32. FastKurtogram, Normalized SES

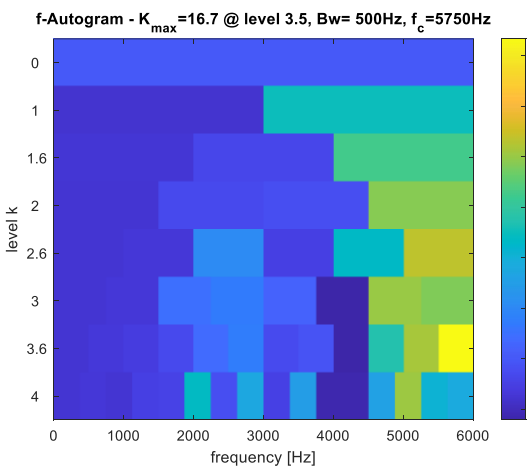


Fig 33. FastAutogram

FAST AUTOGRAM shaft magenta, Inner red, Outer green, Cage blue, Ball black

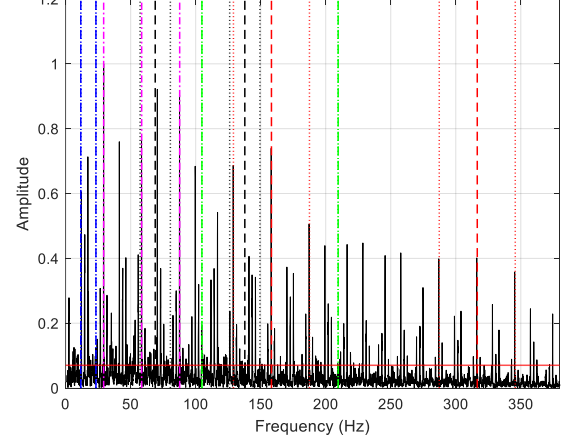


Fig 34. FastAutogram, Normalized SES

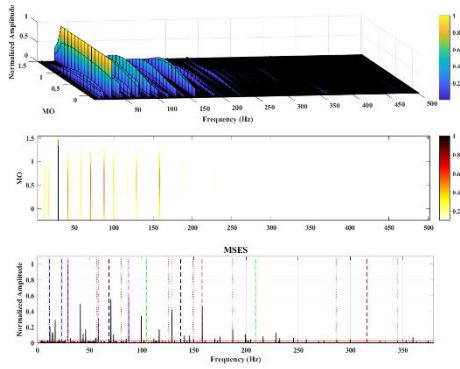


Fig 35. SAM, Normalized MSES

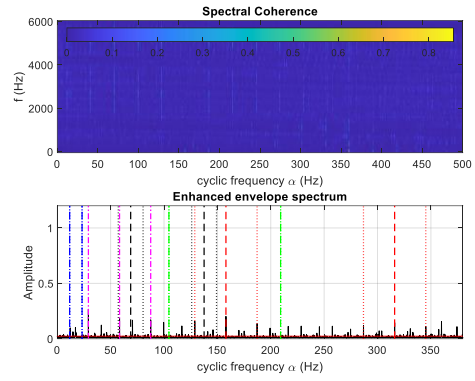


Fig 36. SC, Normalized EES

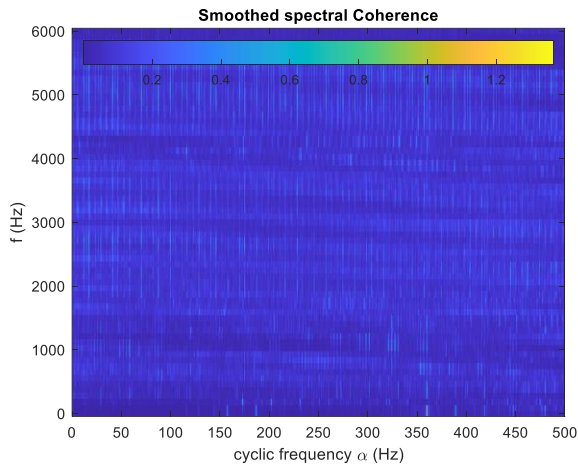


Fig 37. Smoothed SC

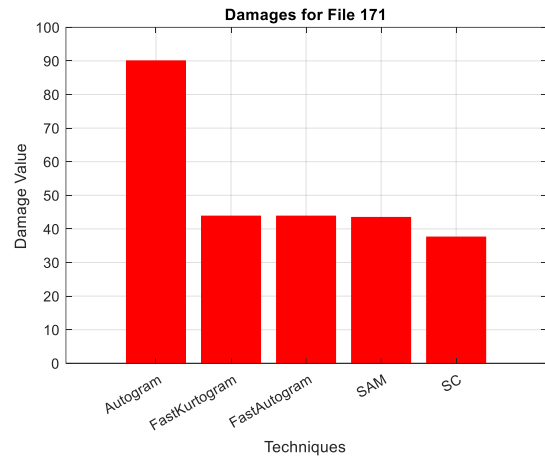


Fig 38. Damage value for file 171FE

In the analysis of the 171FE data file, Autogram proved to be the most effective diagnostic approach for both identifying and quantifying the damage. The quantification method described in Section 3.3.1 yielded a damage value of 90.1652, which is marginally higher than those obtained from other techniques, suggesting a more sensitive detection. Furthermore, the error analysis method outlined in Section 3.3.2 resulted in an error value of 0.9502, reinforcing the detection accuracy. This low error value indicates a strong alignment between the detected damage frequencies and the anticipated damage patterns, supporting the conclusion that damage is indeed present in the system.

IR_021 (211FE) (high fault)

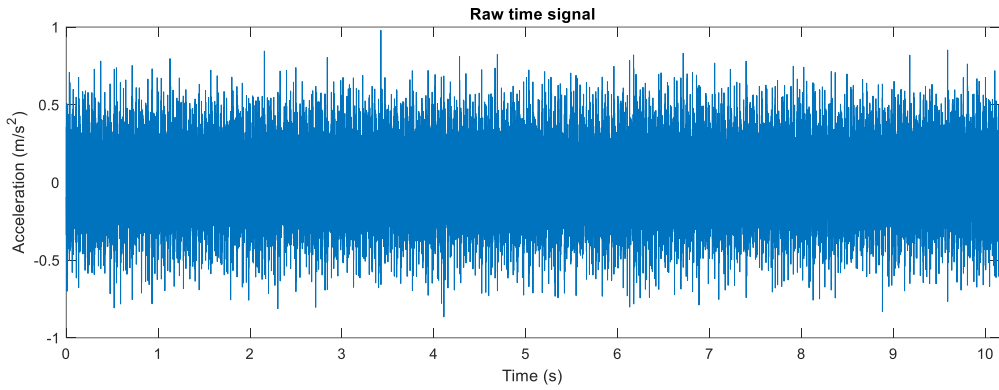


Fig 39. Raw Signal

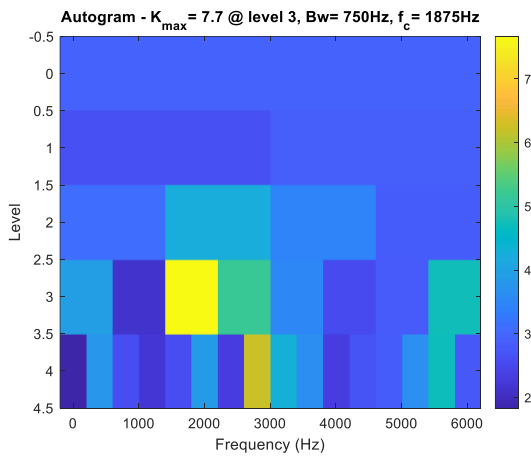


Fig 40. Autogram

AUTOGRAM shaft magenta, Inner red, Outer green, Cage blue, Ball black

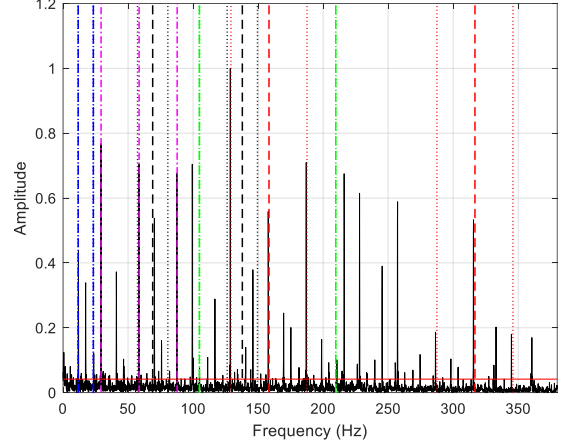


Fig 41. Autogram, Normalized SES

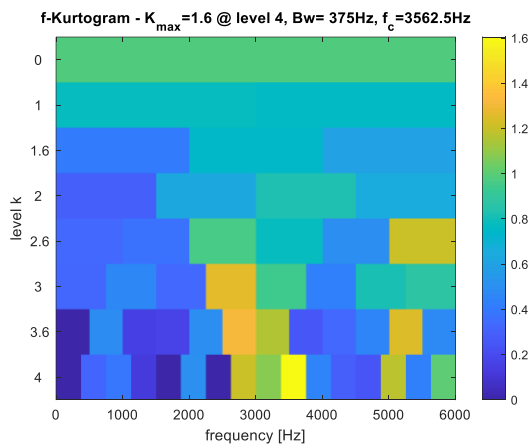


Fig 42. FastKurtogram

FAST KURTOGRAM shaft magenta, Inner red, Outer green, Cage blue, Ball black

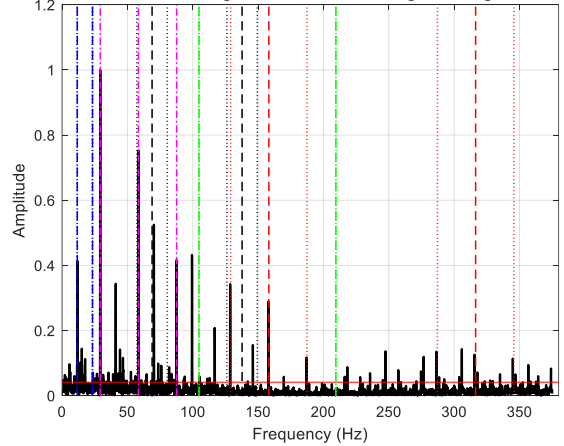


Fig 43. FastKurtogram, Normalized SES

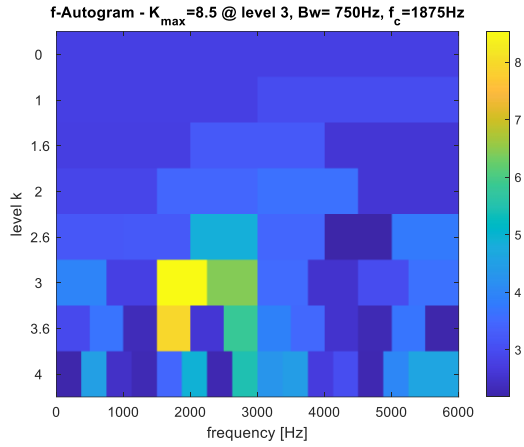


Fig 44. FastAutogram

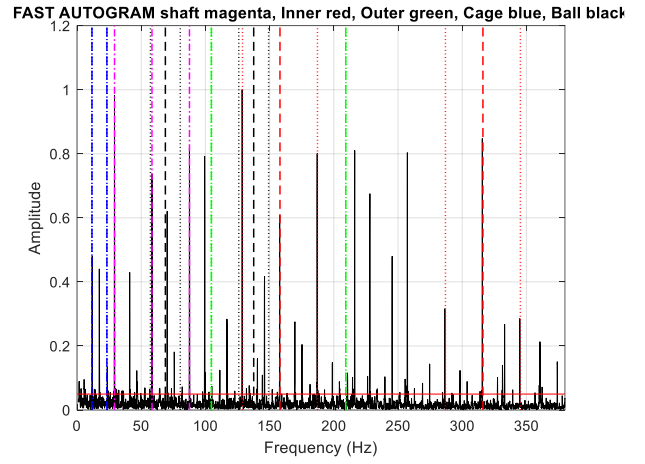


Fig 45. FastAutogram, Normalized SES

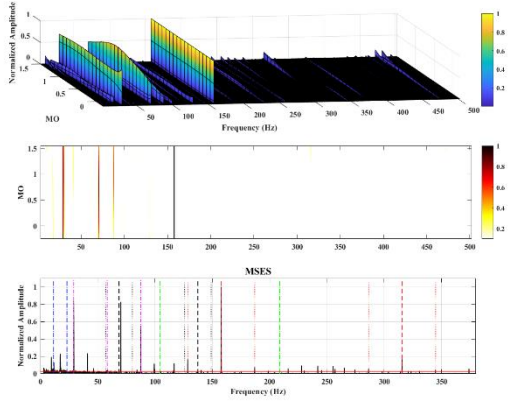


Fig 46. SAM, Normalized MSES

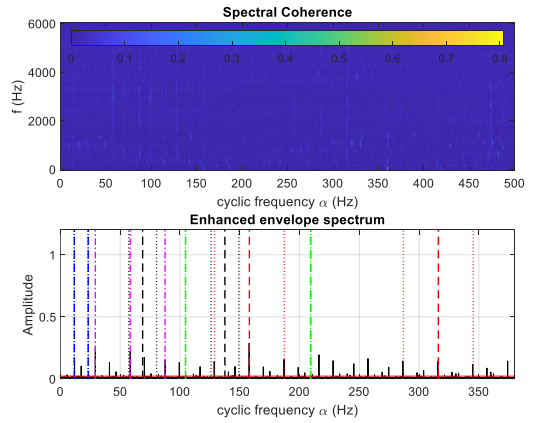


Fig 47. SC, Normalized EES

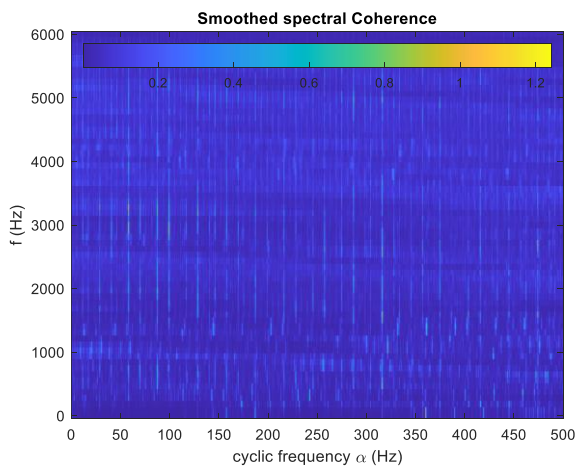


Fig 48. Smoothed SC

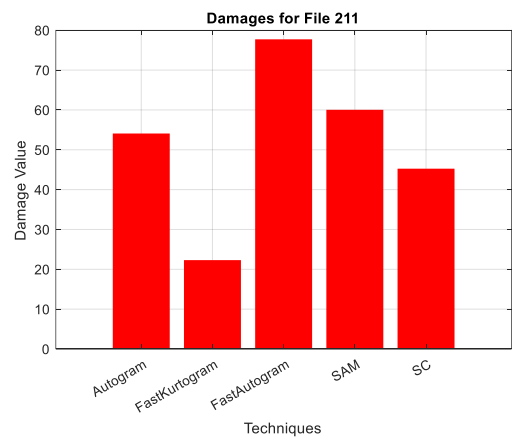


Fig 49. Damage value for file 211FE

In the analysis of the 211FE data file, FastAutogram proved to be the most effective diagnostic approach for both identifying and quantifying the damage. The quantification method described in Section 3.3.1 yielded a damage value of 77.7228, which is marginally higher than those obtained from other techniques, suggesting a more sensitive detection. Furthermore, the error analysis method outlined in Section 3.3.2 resulted in an error value of 0.9692, reinforcing the detection accuracy. This low error value indicates a strong alignment between the detected damage frequencies and the anticipated damage patterns, supporting the conclusion that damage is indeed present in the system.

3.3.4 Outer race damage: [12K_Drive-End_Bearing_Fault_Data]

Here, the acceleration signal is measured on the fan-end, while the damage is in the drive-end bearing.

For the Outer race, the figures given below show the results of the raw time signal with the green dash-dot line indicating the expected damage frequency of the first two -harmonics (BPFO & 2*BPFO), and no sideband frequencies are present (as mentioned in Table 1). The significant peaks are identified at the damage frequencies to analyze the frequency spectrum for each technique. Finally, a bar plot was shown to find the most effective diagnostic approach. The effectiveness is quantified by a damage value, which presumably measures the prominence of the damage frequencies.

OR_007 (132FE) (small fault)

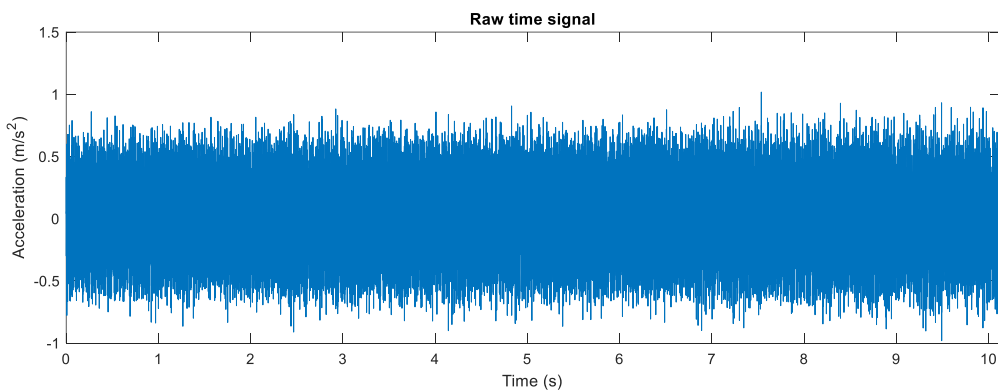


Fig 50. Raw Signal

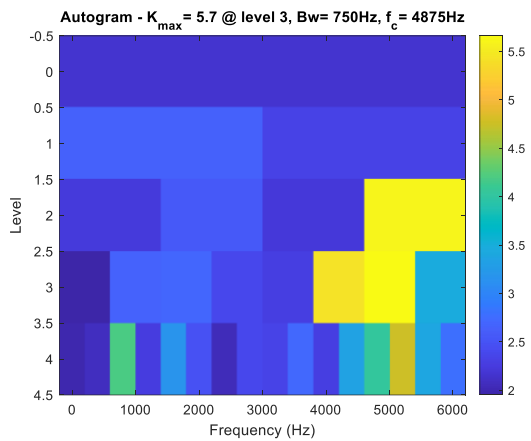


Fig 51. Autogram

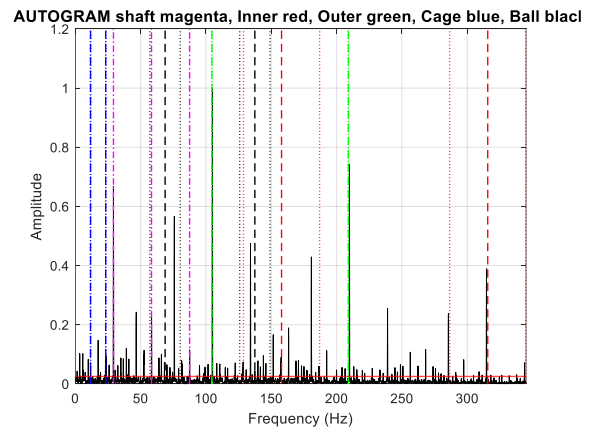


Fig 52. Autogram, Normalized SES

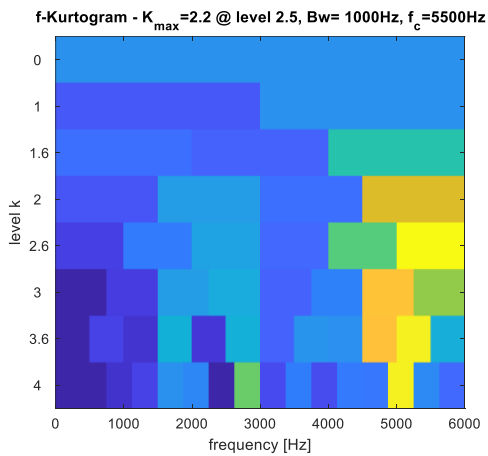


Fig 53. FastKurtogram

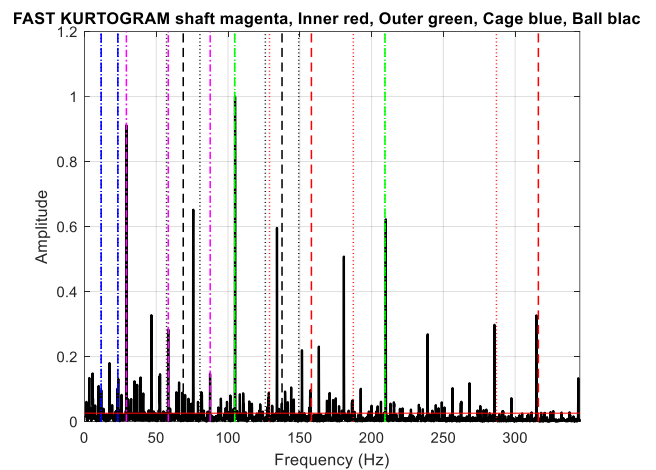


Fig 54. FastKurtogram, Normalized SES

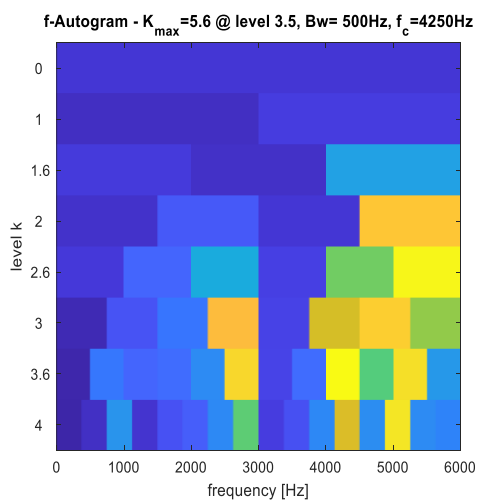


Fig 55. FastAutogram

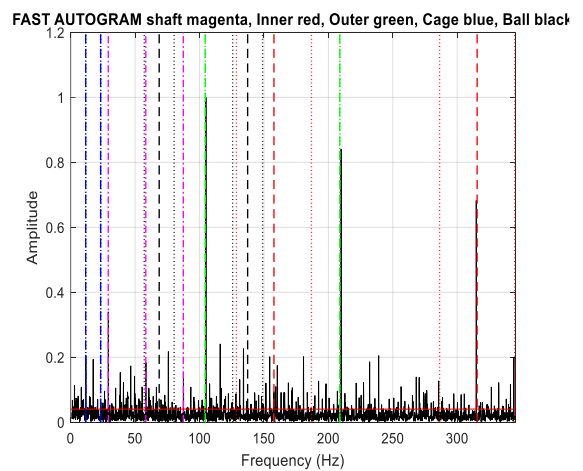


Fig 56. FastAutogram, Normalized SES

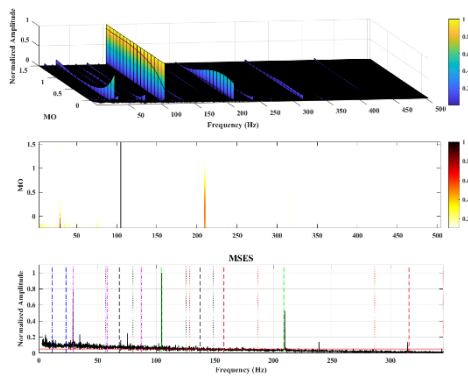


Fig 57. SAM, Normalized MSES

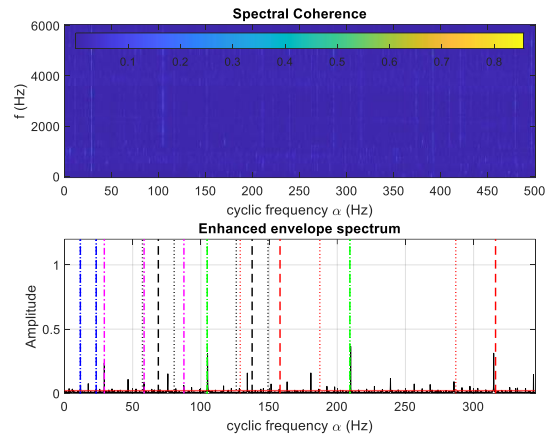


Fig 58. SC, Normalized EES

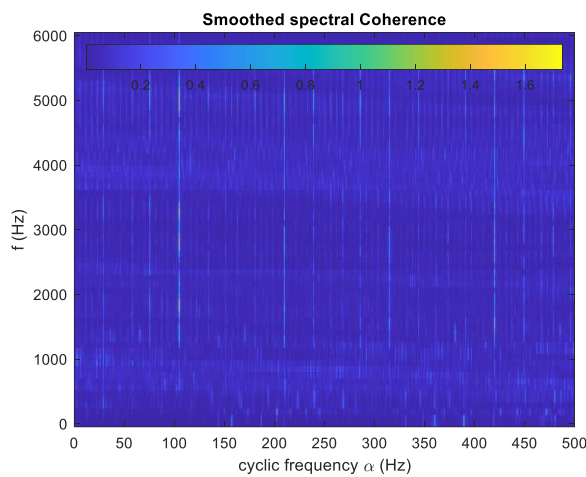


Fig 59. Smoothed SC

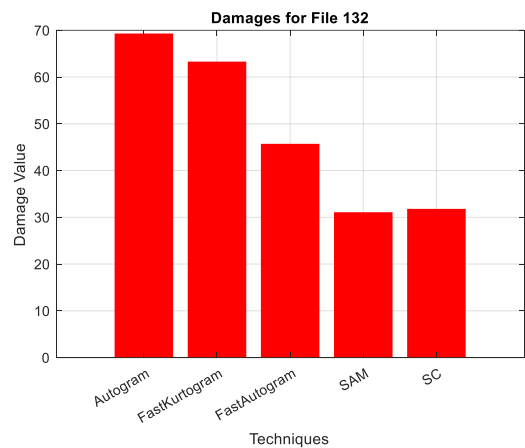


Fig 60. Damage value for file 132FE

In the analysis of the 132FE data file, Autogram proved to be the most effective diagnostic approach for both identifying and quantifying the damage. The quantification method described in Section 3.3.1 yielded a damage value of 69.3021, which is marginally higher than those obtained from other techniques, suggesting a more sensitive detection. Furthermore, the error analysis method outlined in Section 3.3.2 resulted in an error value of 0.9878, reinforcing the detection accuracy. This low error value indicates a strong alignment between the detected damage frequencies and the anticipated damage patterns, supporting the conclusion that damage is indeed present in the system.

OR_014 (199FE) (medium fault)

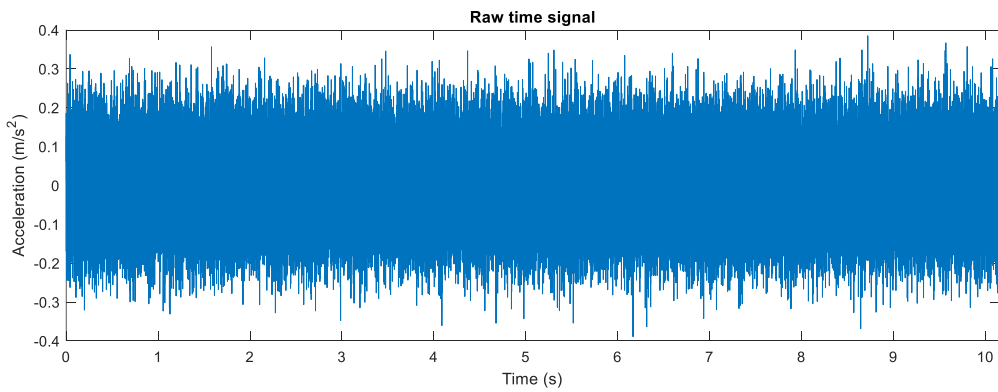


Fig 61. Raw Signal

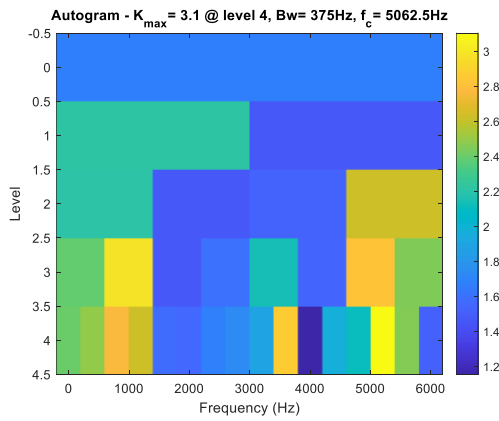


Fig 62. Autogram

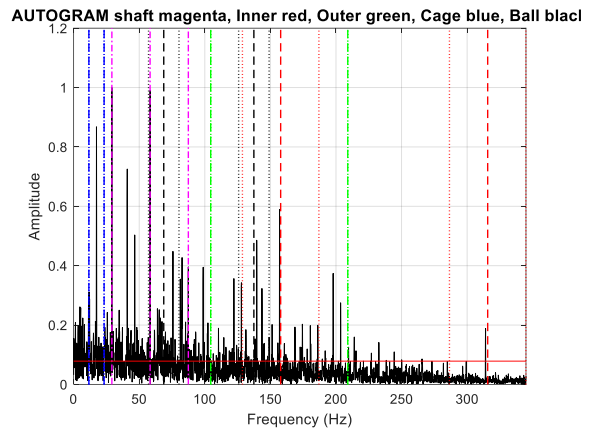


Fig 63. Autogram, Normalized SES

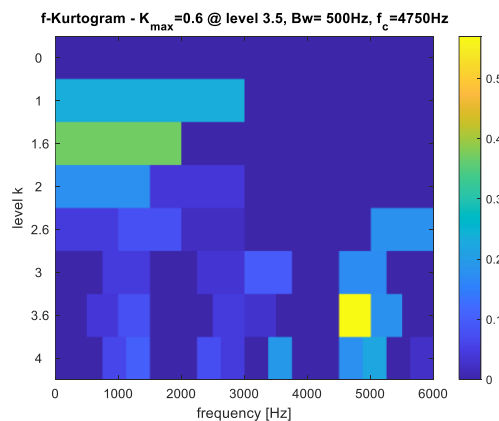


Fig 64. FastKurtogram

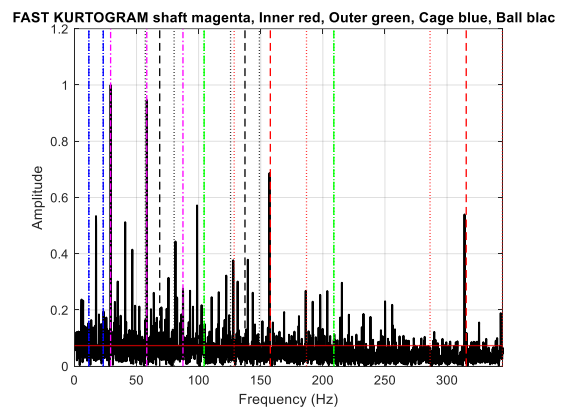


Fig 65. FastKurtogram, Normalized SES

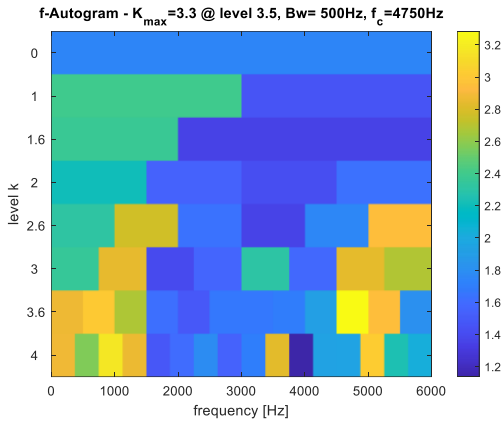


Fig 66. FastAutogram

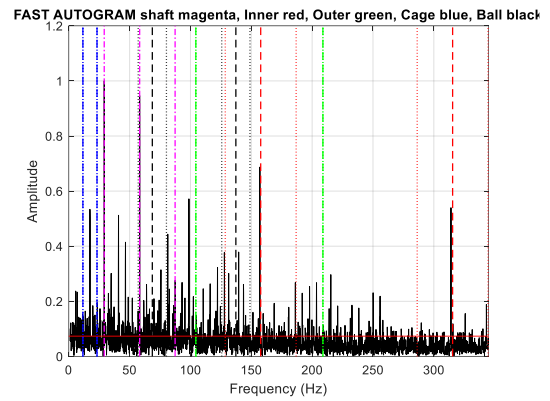


Fig 67. FastAutogram, Normalized SES

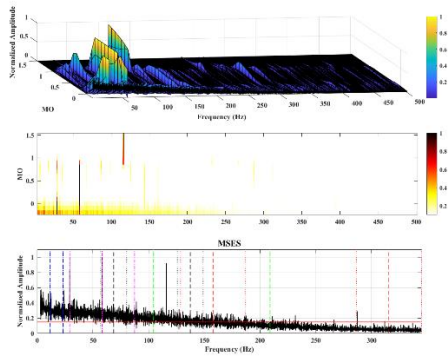


Fig 68. SAM, Normalized MSES

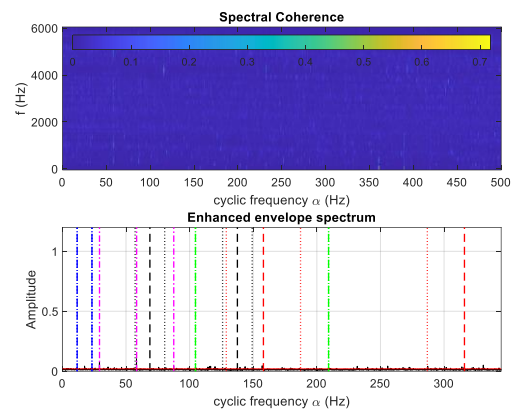


Fig 69. SC, Normalized EES

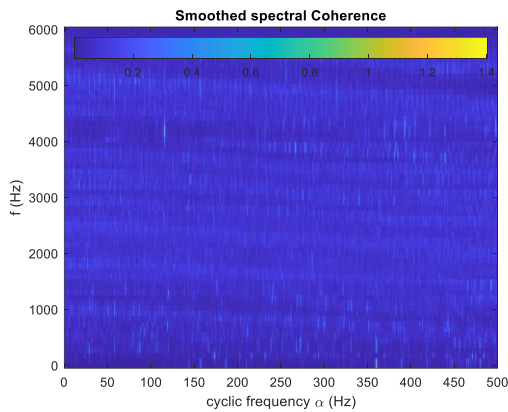


Fig 70. Smoothed SC

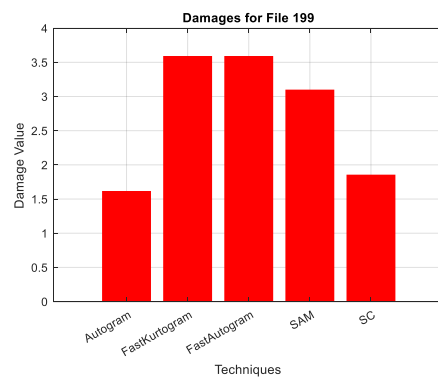


Fig 71. Damage value for file 199FE

In the analysis of the 199FE data file, it was concluded that no damage is present. Using the quantification method outlined in Section 3.3.1, the approach yielded a damage value of 3.5926, which, although slightly higher than other techniques, suggests this method may have greater sensitivity in detecting even minor anomalies. The error analysis in Section 3.3.2 produced an error value of 0.5523, highlighting the method's accuracy in this case. This relatively low error indicates an alignment with expected non-damage frequencies, confirming

that no significant damage patterns were detected, thus supporting the conclusion of no damage in the system.

OR_021 (236FE) (high fault)

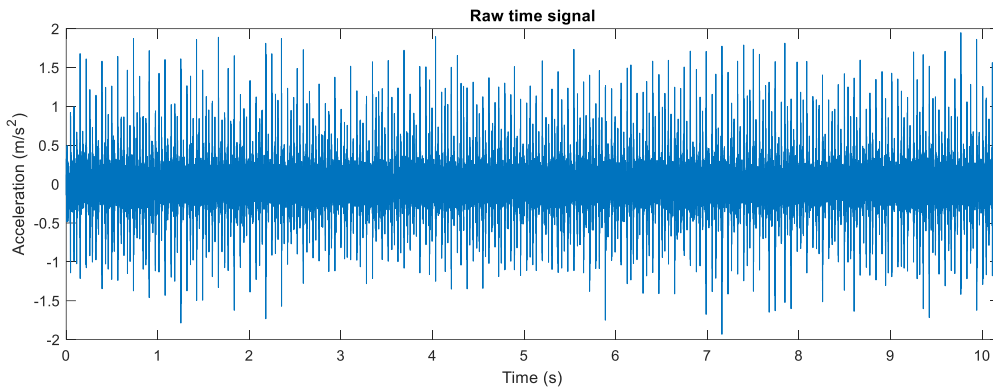


Fig 72. Raw Signal

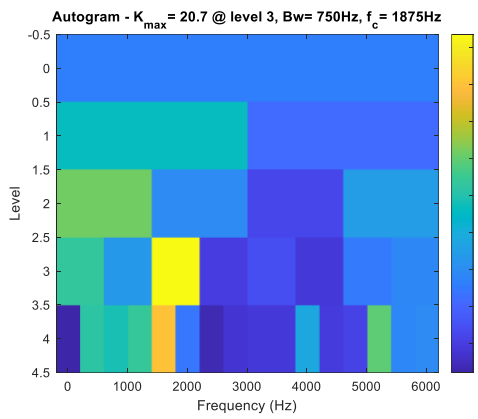


Fig 73. Autogram

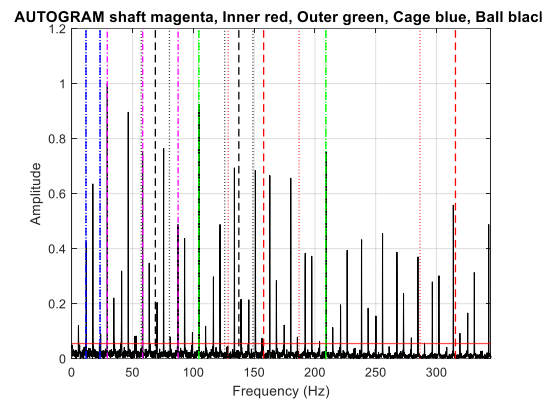


Fig 74. Autogram, Normalized SES

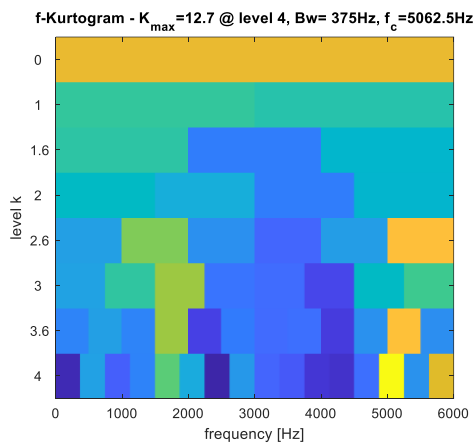


Fig 75. FastKurtogram

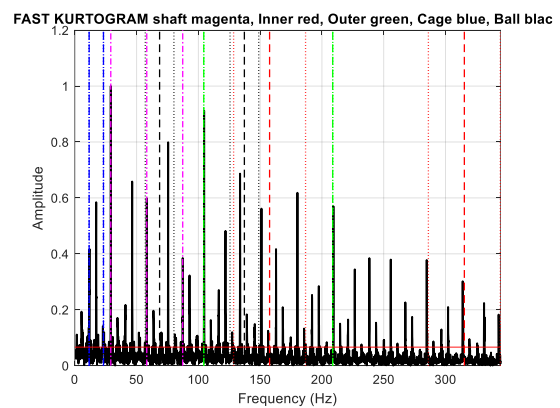


Fig 76. FastKurtogram, Normalized SES

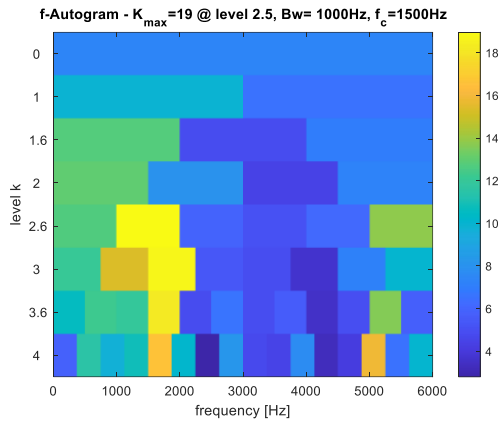


Fig 77. FastAutogram

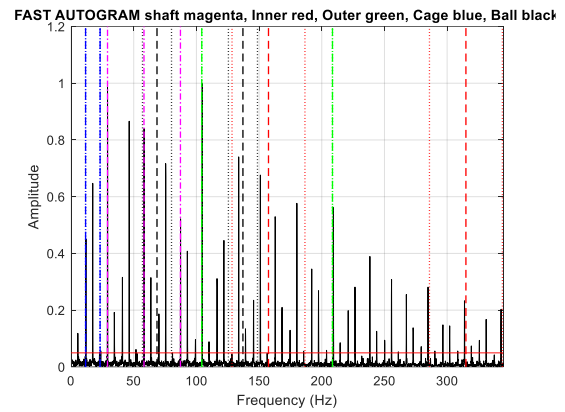


Fig 78. FastAutogram, Normalized SES

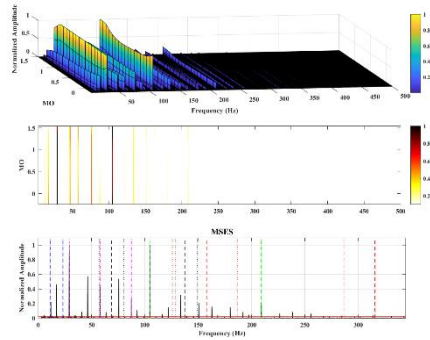


Fig 79. SAM, Normalized MSES

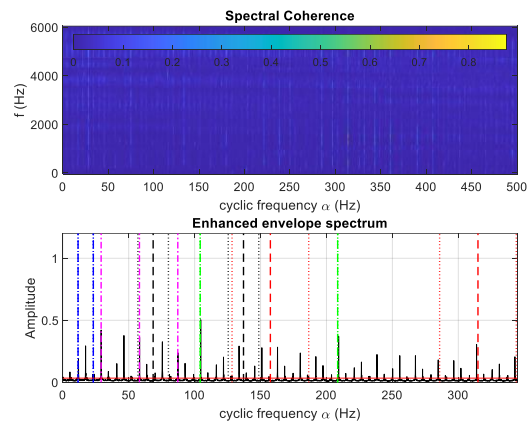


Fig 80. SC, Normalized EES

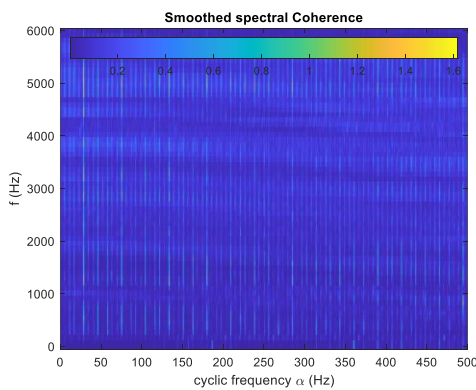


Fig 81. Smoothed SC

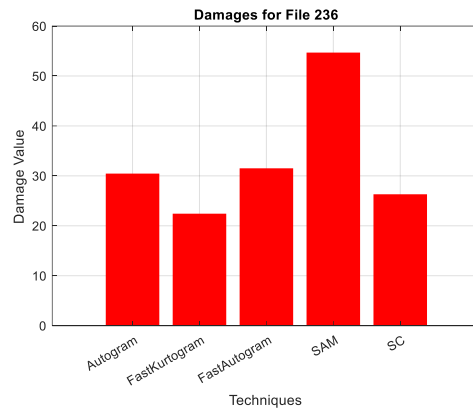


Fig 82. Damage value for file 236FE

In the analysis of the 236FE data file, SAM proved to be the most effective diagnostic approach for both identifying and quantifying the damage. The quantification method described in Section 3.3.1 yielded a damage value of 54.6891, which is marginally higher than those obtained from other techniques, suggesting a more sensitive detection. Furthermore, the error analysis method outlined in Section 3.3.2 resulted in an error value of 0.9957, reinforcing the detection accuracy. This low error value indicates a strong alignment between the detected

damage frequencies and the anticipated damage patterns, supporting the conclusion that damage is indeed present in the system.

3.3.5 Ball damage: [12K_Drive-End_Bearing_Fault_Data]

Here, the acceleration signal is measured on the fan-end, while the damage is in the drive-end bearing.

For the Ball, the figures given below show the results of the raw time signal with the black dash-dot line indicating the expected damage frequency of the first two -harmonics (BPFI & 2*BPFI), and their respective sidebands frequencies. The presence of sidebands is often a strong indicator of modulation related to damage, further confirming fault presence.

B_007 (120FE) (small fault)

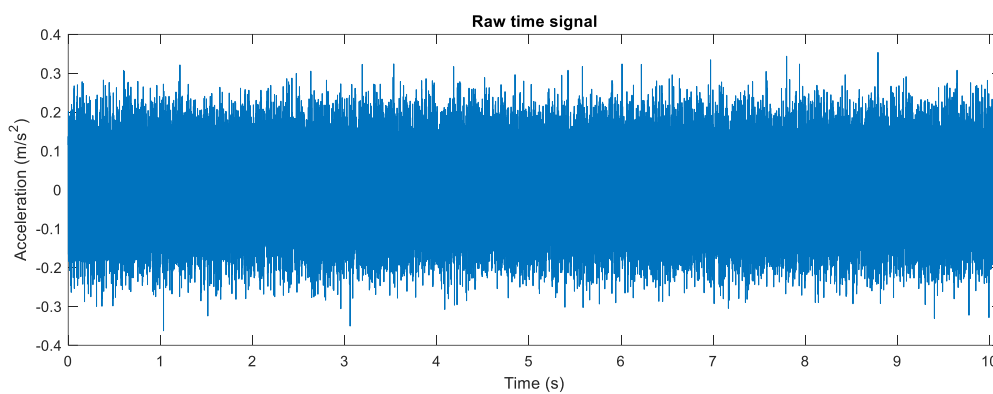


Fig 83. Raw Signal

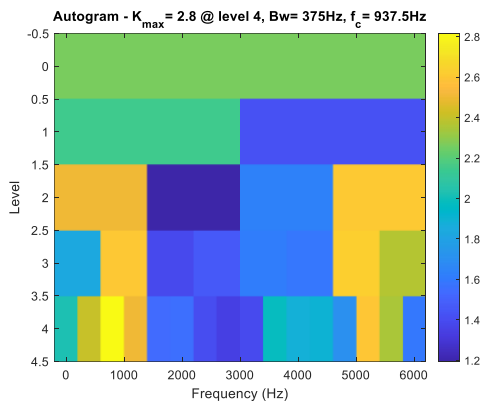


Fig 84. Autogram

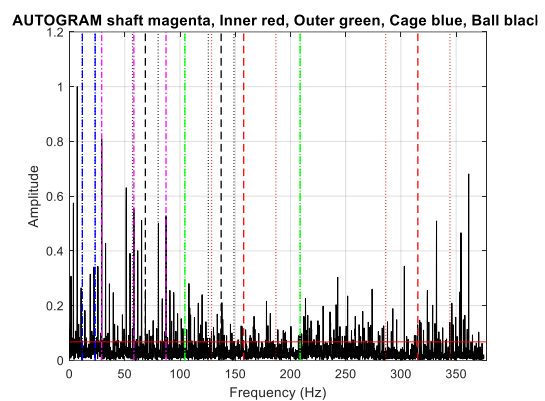


Fig 85. Autogram, Normalized SES

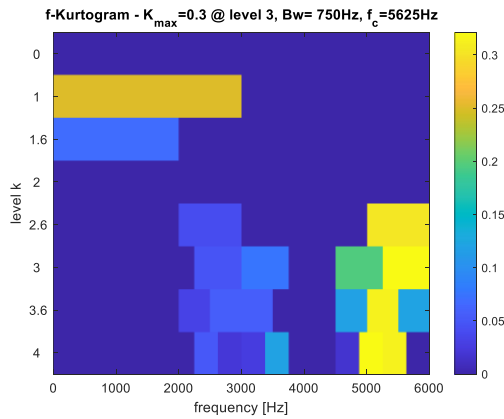


Fig 86. FastKurtogram

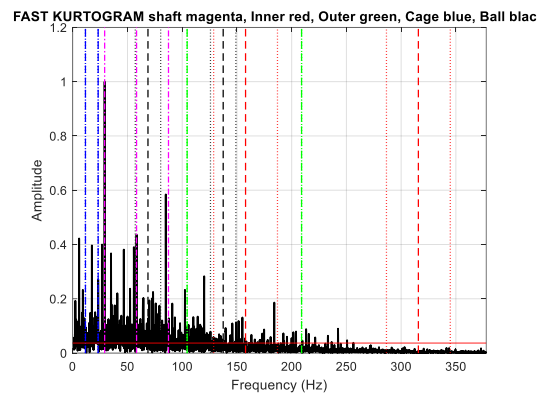


Fig 87. FastKurtogram, Normalized SES

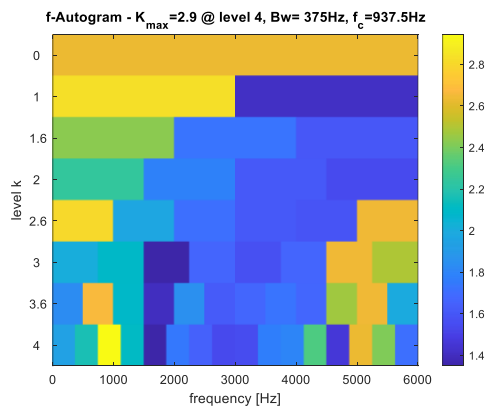


Fig 88. FastAutogram

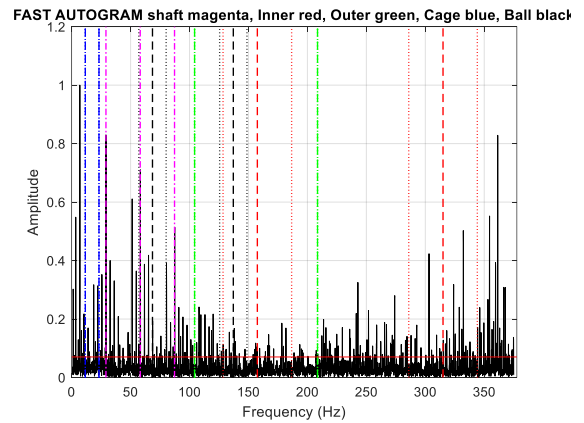


Fig 89. FastAutogram, Normalized SES

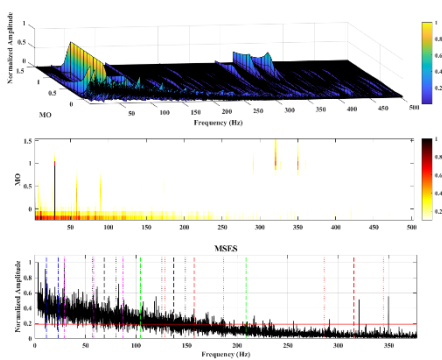


Fig 90. SAM, Normalized MSES

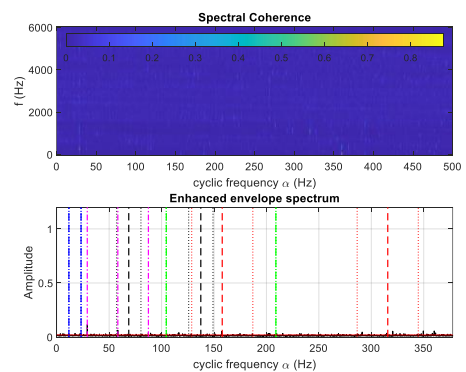


Fig 91. SC, Normalized EES

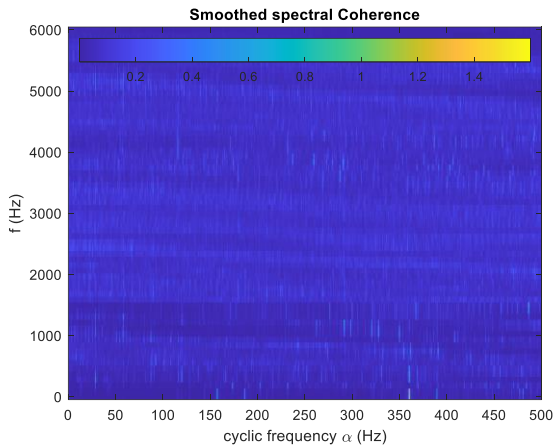


Fig 92. Smoothed SC

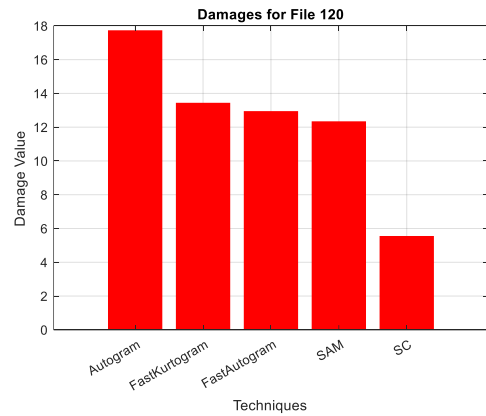


Fig 93. Damage value for file 120FE

In the analysis of the 120FE data file, it was concluded that no damage is present. Using the quantification method outlined in Section 3.3.1, the approach yielded a damage value of 17.7376, which, although slightly higher than other techniques, suggests this method may have greater sensitivity in detecting even minor anomalies. The error analysis in Section 3.3.2 produced an error value of 0.6942, highlighting the method's accuracy in this case. This relatively low error indicates an alignment with expected non-damage frequencies, confirming that no significant damage patterns were detected, thus supporting the conclusion of no damage in the system.

B_014 (187FE) (medium fault)

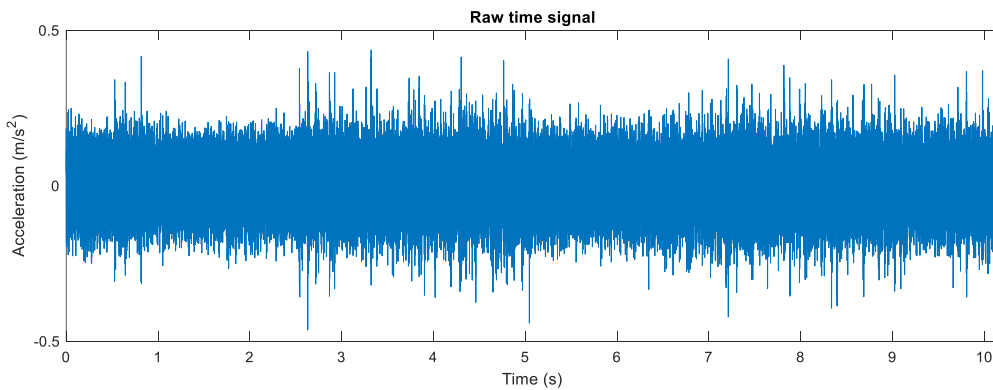


Fig 94. Raw Signal

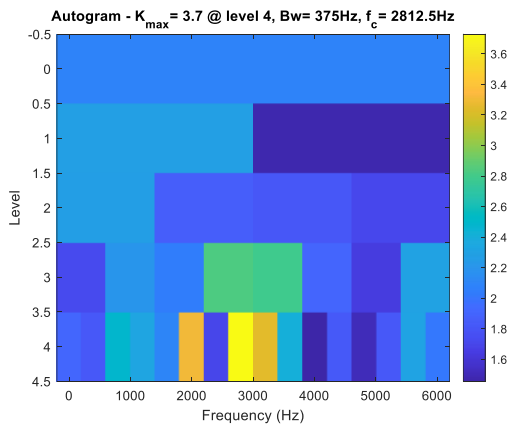


Fig 95. Autogram

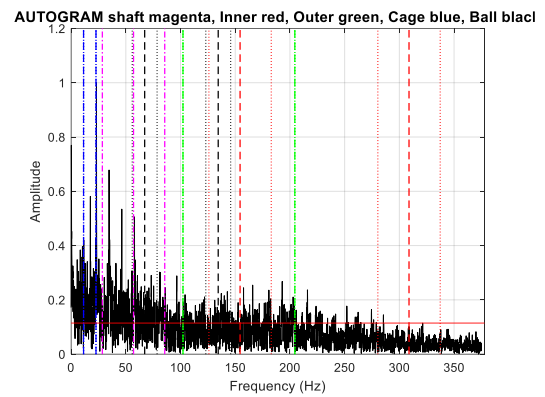


Fig 96. Autogram, Normalized SES

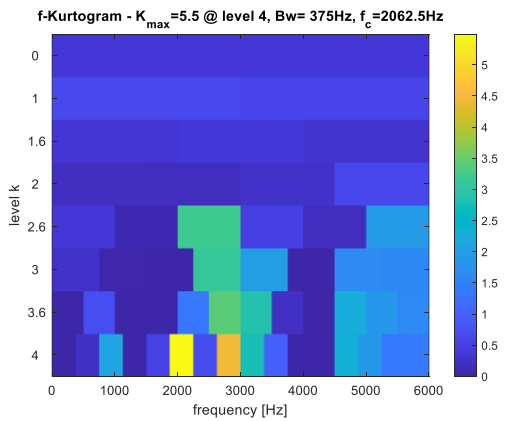


Fig 97. FastKurtogram

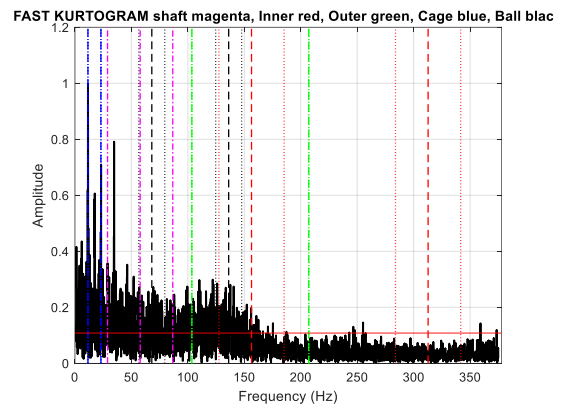


Fig 98. FastKurtogram, Normalized SES

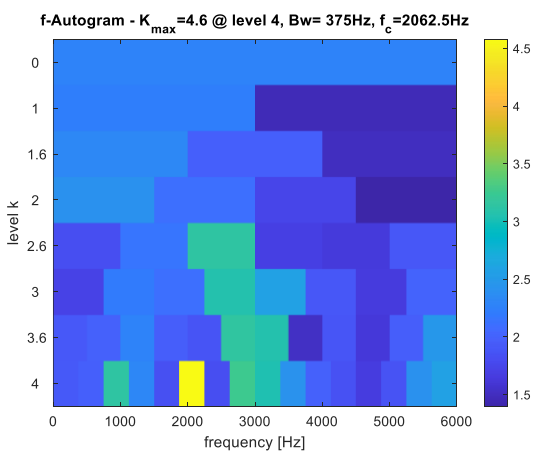


Fig 99. FastAutogram

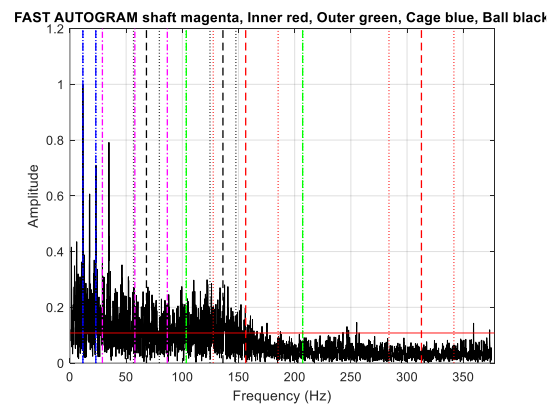


Fig 100. FastAutogram, Normalized SES

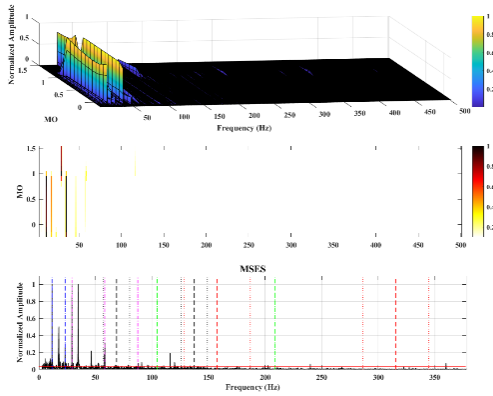


Fig 101. SAM, Normalized MSES

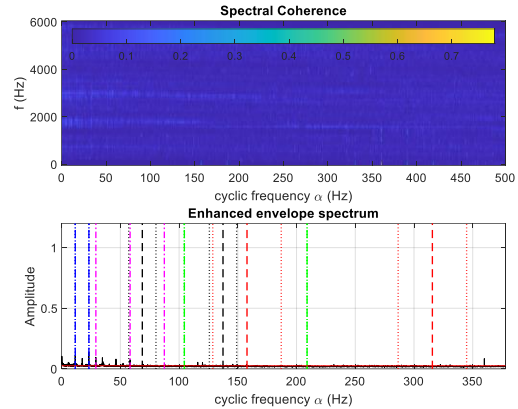


Fig 102. SC, Normalized EES

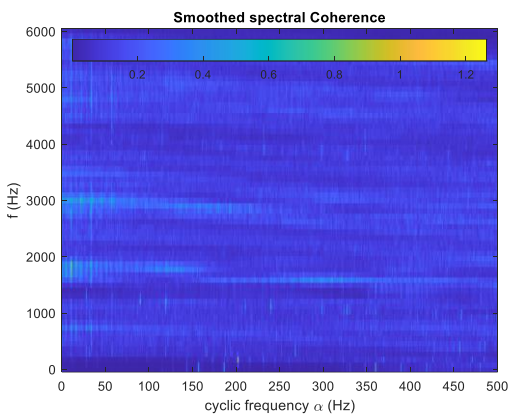


Fig 103. Smoothed SC

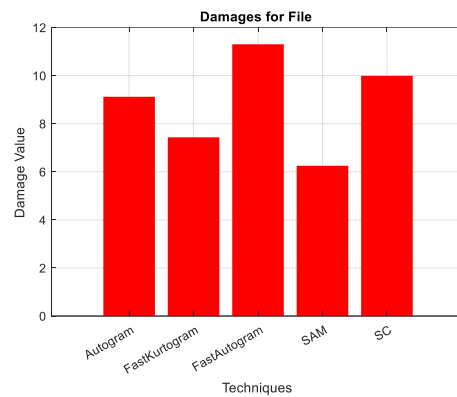


Fig 104. Damage value for file 187FE

In the analysis of the 187FE data file, it was concluded that no damage is present. Using the quantification method outlined in Section 3.3.1, the FastAutogram approach yielded a damage value of 11.3045, which, although slightly higher than other techniques, suggests this method may have greater sensitivity in detecting even minor anomalies. The error analysis in Section 3.3.2 produced an error value of 0.2227, highlighting the method's accuracy in this case. This relatively low error indicates an alignment with expected non-damage frequencies, confirming that no significant damage patterns were detected, thus supporting the conclusion of no damage in the system.

The initial analysis, focused solely on the Ball, detected no significant damage. However, upon further investigation using advanced diagnostic techniques, additional peaks were identified, specifically in the Cage, highlighted in blue. These findings suggest the presence of potential damage in the Cage component, which was not apparent during the initial review.

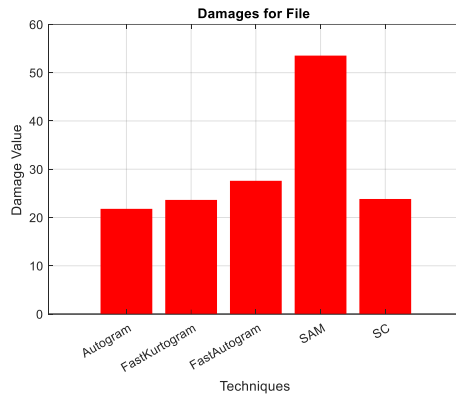


Fig 105. Damage value for file 187FE

Fig. 105 visually confirms the distinction between the damage assessments for the Ball and Cage. The advanced techniques revealed a damage value of 53.5390 for the Cage, with an associated error value of 0.7291. This reinforces the importance of comprehensive analysis involving both components to ensure accurate detection and diagnosis.

B_021 (224FE) (high fault)

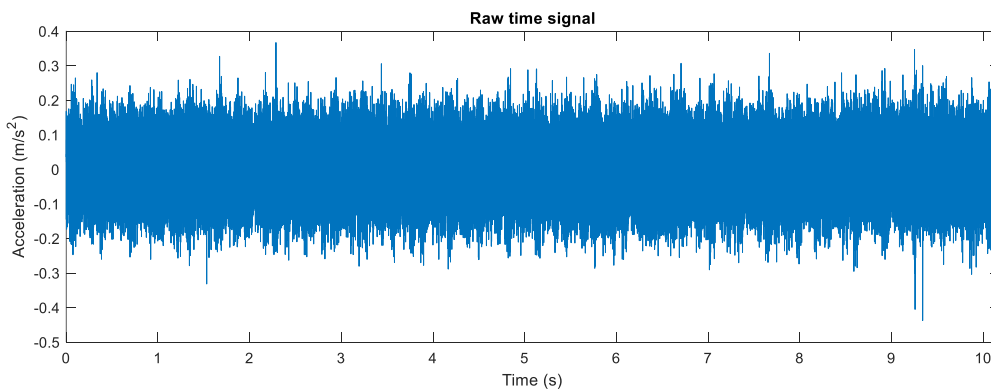


Fig 106. Raw Signal

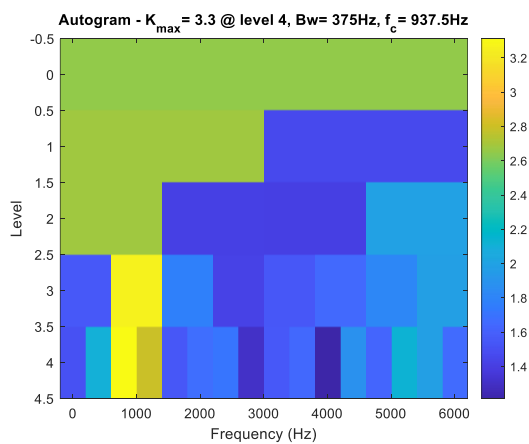


Fig 107. Autogram

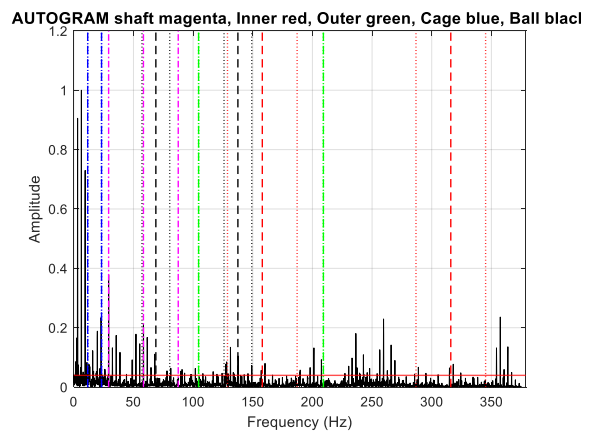


Fig 108. Autogram, Normalized SES

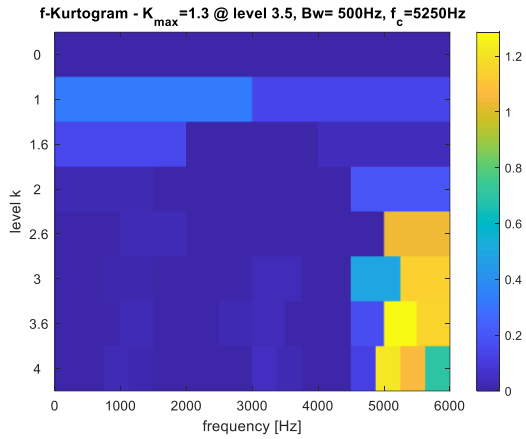


Fig 109. FastKurtogram

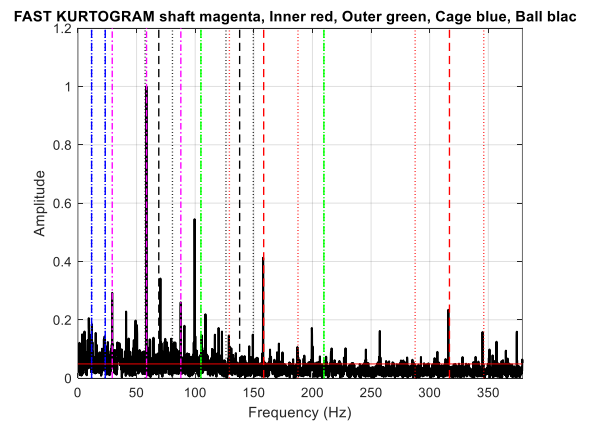


Fig 110. FastKurtogram, Normalized SES

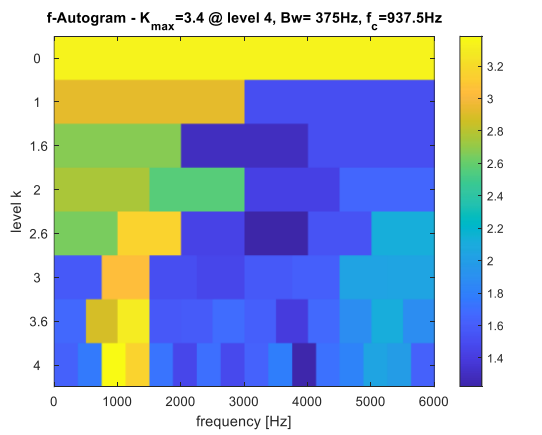


Fig 111. FastAutogram

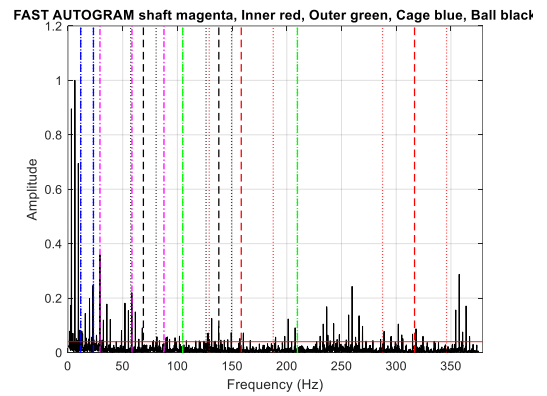


Fig 112. FastAutogram, Normalized SES

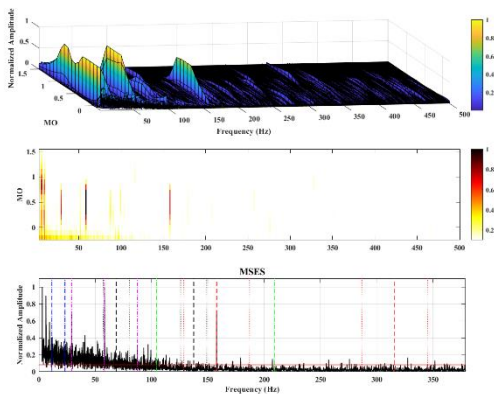


Fig 113. SAM, Normalized MSES

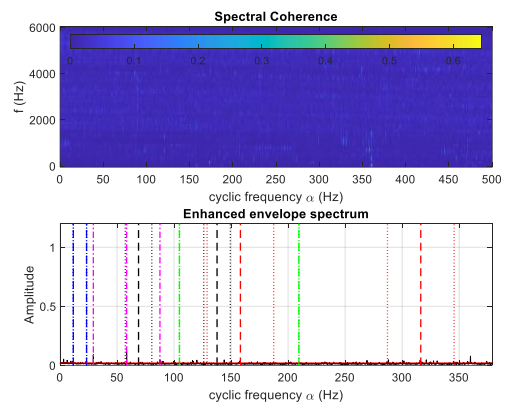


Fig 114. SC, Normalized EES

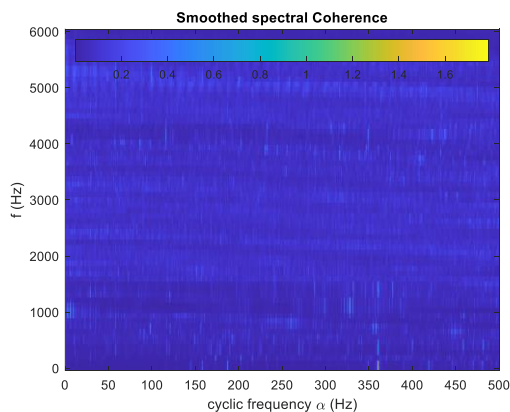


Fig 115. Smoothed SC

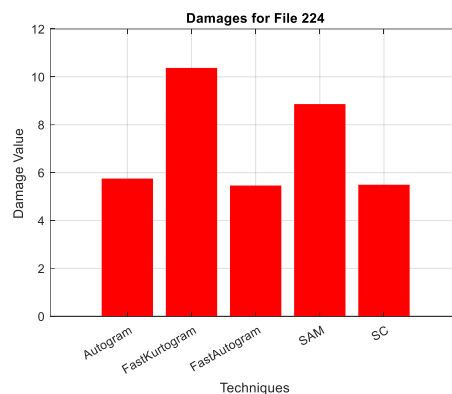


Fig 116. Damage value for file 224FE

In the analysis of the 224FE data file, it was concluded that no damage is present. Using the quantification method outlined in Section 3.3.1, the approach yielded a damage value of 10.3737, which, although slightly higher than other techniques, suggests this method may have greater sensitivity in detecting even minor anomalies. The error analysis in Section 3.3.2 produced an error value of 0.2364, highlighting the method's accuracy in this case. This relatively low error indicates an alignment with expected non-damage frequencies, confirming that no significant damage patterns were detected, thus supporting the conclusion of no damage in the system.

3.4 Summary of Comparison

In summary, the comparison of varying fault diameters (small: 0.007 inches, medium: 0.014 inches, and high: 0.021 inches) confirms a direct correlation between defect size and the severity of bearing performance issues. The analysis in section 3.3 highlights that as fault diameter increases, there is a significant rise in vibration and noise levels, indicating greater instability across all defect types (Inner Race, Outer Race, Cage, and Ball) under a 2 HP load. This clear relationship between fault size and operational impact emphasizes the need for effective monitoring to manage potential degradation in bearing performance.

Furthermore, the study supports the efficacy of advanced processing techniques described in section 1.4 for accurate fault detection. These methods allow for the identification of fault presence through maximum peaks in spectral analysis, while low or minimum peak spectra indicate an absence of damage, validating the condition of the bearing. This reliable differentiation between healthy and damaged states underscores the importance of spectral analysis in preventive maintenance.

In conclusion, the combination of fault diameter analysis and advanced spectral processing techniques is crucial for proactive maintenance, enhancing the overall reliability and lifespan of bearings. By enabling early detection of faults, these techniques help prevent unexpected breakdowns and ensure stable operation across various conditions, contributing to the sustainable and efficient performance of rolling element bearings.

Here, there are some special cases to be known,

Case 1: Electrical noise

This case highlights a scenario where the signal, recorded from the fan end (FE), is significantly corrupted by electrical noise across each diagnostic technique. The presence of this noise introduces repetitive transients in the time waveform, which can mimic fault signatures or obscure real fault signals.

In the data file for 187FE, despite the presence of transients, no actual bearing damage is present. However, peaks are still visible in the frequency spectrum for the cage component, which is highlighted in blue. This suggests that the observed peaks may be an artifact of electrical noise rather than a true indication of a bearing fault. When comparing these results to the benchmark study discussed in section 3.2.3, the fault diagnosis result for this case falls under the categories N1 or N2 (not diagnosable) according to benchmark method 3. This categorization reflects the inability to reliably diagnose any bearing fault due to the overwhelming influence of noise and the absence of distinct fault-related features in the signal.

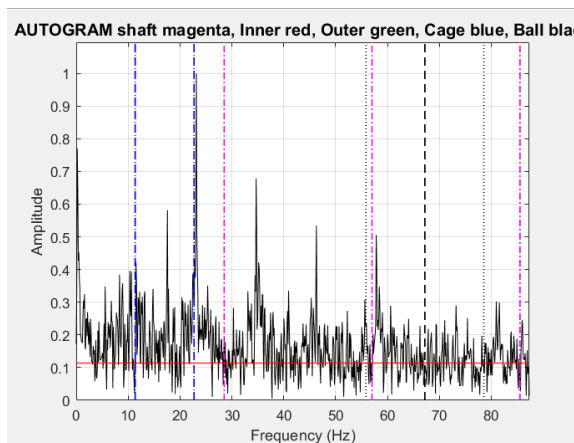


Fig 117. Autogram, Normalized SES

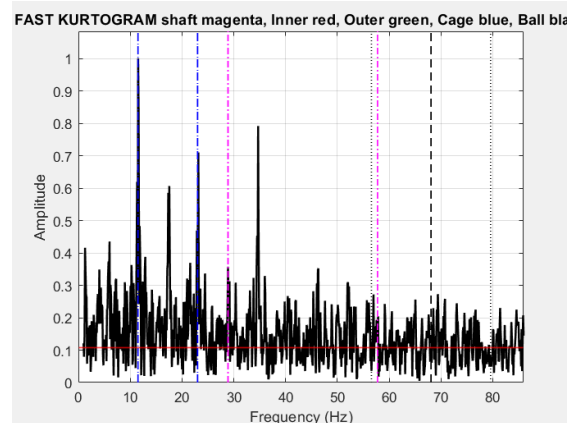


Fig 118. FastKurtogram, Normalized SES

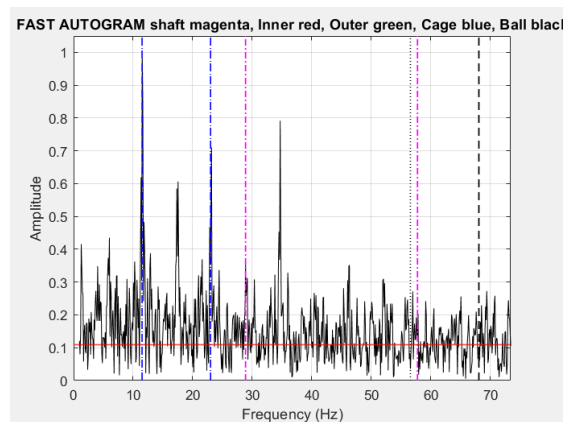


Fig 119. FastAutogram, Normalized SES

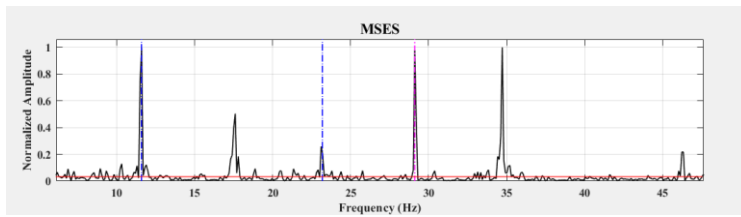


Fig 120. SAM, Normalized MSES

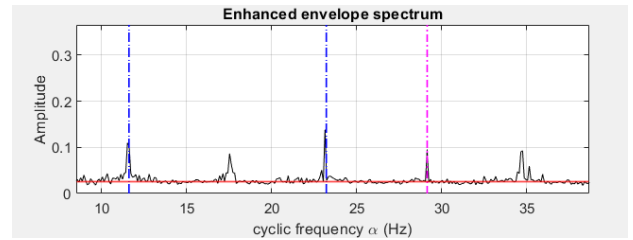


Fig 121. SC, Normalized EES

Case 2: Impulsive noise

In the case of data File 275DE indicates a damage in inner ring measured in the fan-end, the signal exhibits non-stationary characteristics, which means that its statistical properties change over time. This non-stationarity often emphasizes impulses in the signal, making it challenging to analyze using conventional steady-state diagnostic techniques. However, these impulses can sometimes be indicative of underlying faults, especially in rotating machinery like bearings.

Diagnosability with Benchmark Methods:

Method 1 & Method 2: The fault in 275DE is partially diagnosable, as indicated by the P1 category under both methods. This category implies that while some fault-related features (such as discrete spectral components) are visible, they may not be prominent or dominant in the spectrum, requiring careful interpretation.

Method 3: In contrast, Method 3 does not identify a fault in this case. This result underscores the limitations of Method 3 in handling non-stationary signals where fault indicators might be present only intermittently or in weaker forms that this method cannot detect.

Autogram and Maximum Kurtosis:

The Autogram analysis (a tool used for enhanced fault detection by emphasizing impulsive components) shows the highest kurtosis value of 5.008 at level 4, node 4. Kurtosis is a statistical measure of the "peakedness" of the data, with higher values often indicating the presence of transient, impulse-like features, which are characteristic of bearing faults. The maximum kurtosis achieved in this case confirms that the signal contains impulsive events likely related to a defect.

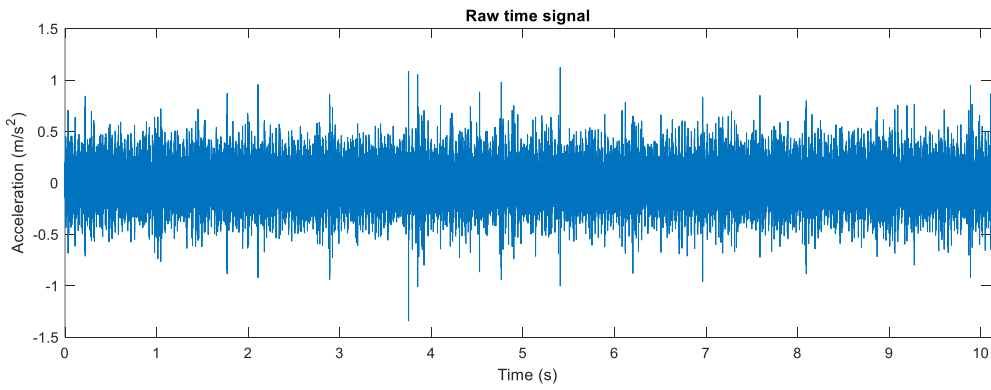


Fig 122. Raw Signal

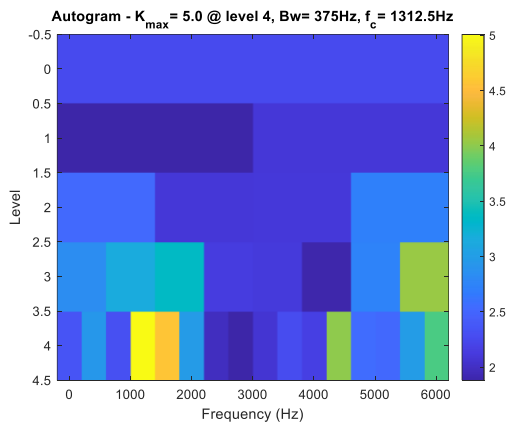


Fig 123. Autogram

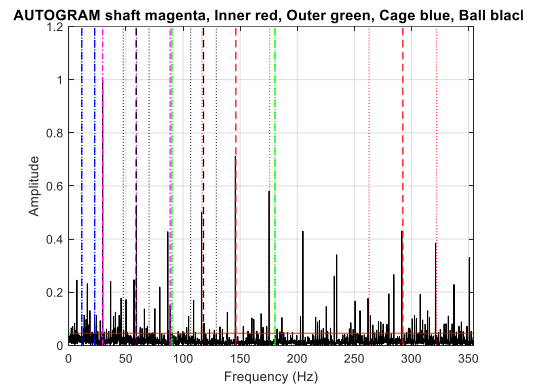


Fig 124. Autogram, Normalized SES

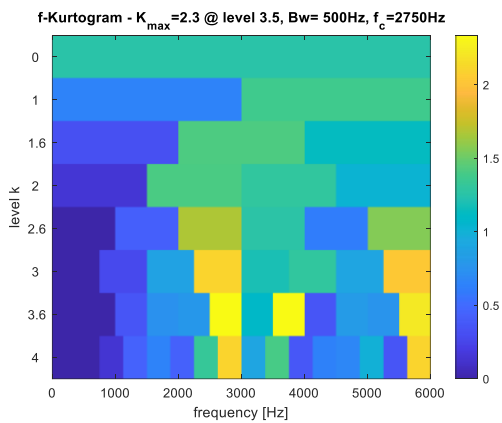


Fig 125. FastKurtogram

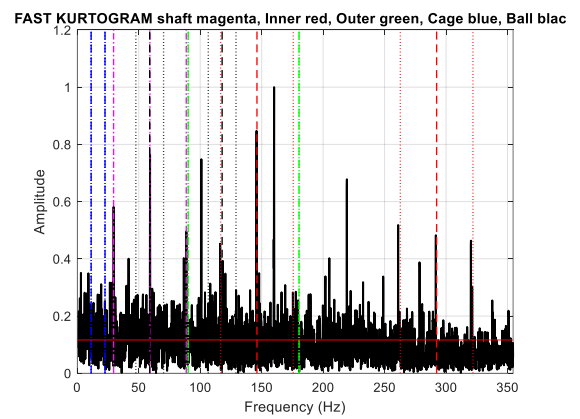


Fig 126. FastKurtogram, Normalized SES

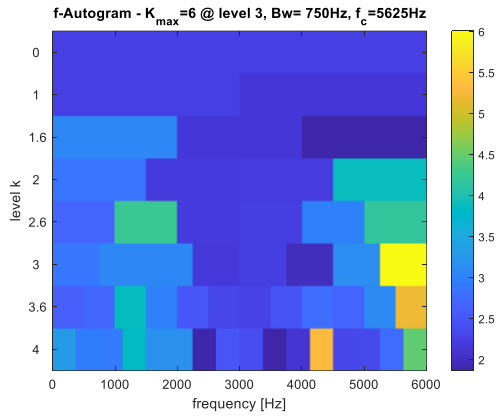


Fig 127. FastAutogram

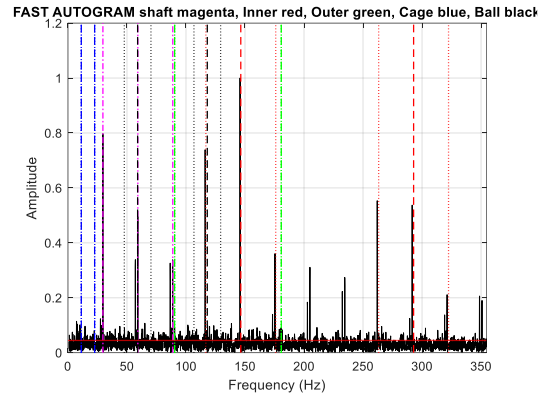


Fig 128. FastAutogram, Normalized SES

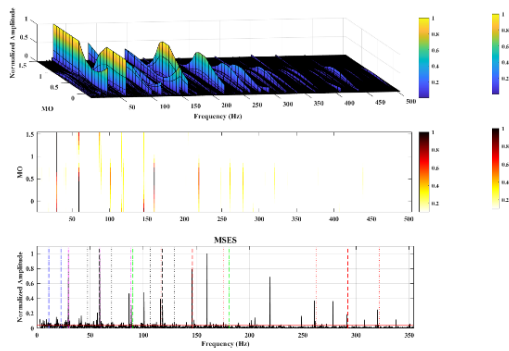


Fig 129. SAM, Normalized MSES

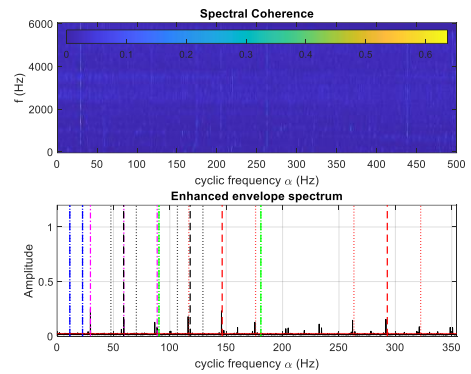


Fig 130. SC, Normalized EES

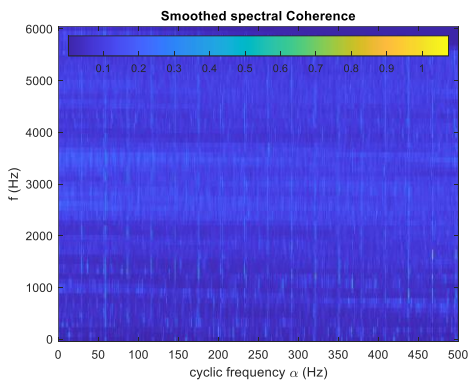


Fig 131. Smoothed SC

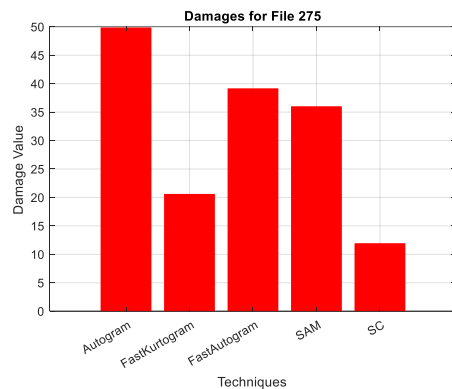


Fig 132. Damage value for file 275DE

The Autogram technique stands out by yielding a damage value of 49.8796, which is notably higher compared to other diagnostic methods. Additionally, the error value of 0.6546 confirms the condition is partially diagnosable, aligning with the findings described earlier in Case 2.

4. Results and Discussions

4.1 Data records

From the benchmark dataset of bearing data center for bearing diagnostics, it has the information for nearly 161 data sets in a .mat file. The data sets are grouped into four categories such as 12K Drive-end fault, 48K Drive-end fault, and 12K fan end fault as mentioned in section 3.1 and faulty bearing location. Each group contains the data sets for inner and outer race faults and rolling element faults. Meanwhile, outer race faults are classified into three categories corresponding to the fault position relative to the load zone: ‘centred’ (fault in the 6.00 o’clock position), ‘orthogonal’ (3.00 o’clock) and ‘opposite’ (12.00 o’clock).

4.2 Characterisation of all data sets

To effectively evaluate the performance of bearing diagnostic algorithms, it is essential to classify the available data sets based on their diagnosability and fault characteristics. This classification not only ensures a rigorous testing framework but also highlights the strengths and limitations of the algorithms under varying diagnostic challenges. The categorization scheme described below serves as a guide for interpreting diagnostic results across different scenarios, ranging from easily diagnosable faults to cases where identifying faults is highly challenging or nearly impossible.

Categories of Diagnosis Outcomes

The data sets are divided into three primary categories: Y (Yes), P (Partial), and N (No). Each category reflects the level of diagnostic success and the characteristics of the data. These are further subdivided to provide more granular insights into the fault diagnostic capabilities.

1. Y Category: Clearly Diagnosable Data

Data sets in this category represent cases where faults are identifiable with relative ease, using both traditional and advanced diagnostic methods.

- **Y1: Classic Characteristics**
 - **Diagnosis Success:** Yes
 - **Description:** The data exhibit classic fault signatures, which are evident in both the time and frequency domains. Examples include:
 - Clear periodic impacts in the time-domain waveform.
 - Well-defined fault frequencies in the spectrum (e.g., ball pass frequency).
 - **Use Case:** Useful for benchmarking algorithms under ideal conditions.

- **Y2: Non-Classic Characteristics**

- **Diagnosis Success:** Yes
- **Description:** The data contain fault characteristics, but they deviate from classic patterns. This could include:
 - Weak or distorted fault signals in the time domain.
 - Frequency components with unusual amplitudes or harmonics.
- **Use Case:** Tests the robustness of algorithms in handling variations from ideal fault patterns.

2. P Category: Partially Diagnosable Data

The P category includes data sets where faults can be partially identified, but with some ambiguity or weaker signals. These data sets are more challenging and serve as a critical test for the effectiveness of advanced algorithms.

- **P1: Probable Diagnosis**

- **Diagnosis Success:** Partial
- **Description:** The envelope spectrum shows discrete components at expected fault frequencies, but these components are not dominant.
 - Fault peaks may be overshadowed by noise or other signals.
- **Use Case:** Evaluates the algorithm's ability to distinguish weak fault signals from background noise.

- **P2: Potential Diagnosis**

- **Diagnosis Success:** Partial
- **Description:** The envelope spectrum displays smeared or broadened components, roughly aligning with the expected fault frequencies.
 - Fault patterns are less distinct and may require advanced techniques for interpretation.
- **Use Case:** Tests the capability of the algorithm to identify subtle fault indicators.

3. N Category: Non-Diagnosable Data

Data sets in the N category are either too noisy or contain non-relevant patterns, making fault diagnosis extremely difficult or impossible.

- **N1: Non-Diagnosable with Other Identifiable Issues**
 - **Diagnosis Success:** No
 - **Description:** The data do not reveal any signs of the specified bearing fault, but other mechanical issues (e.g., shaft misalignment, looseness) are evident.
 - Such conditions may present as sideband frequencies or harmonics.
 - **Use Case:** Assesses whether algorithms can differentiate between different fault types.
- **N2: Non-Diagnosable Resembling Noise**
 - **Diagnosis Success:** No
 - **Description:** The data appear indistinguishable from noise, with little to no discernible fault features.
 - The only possible indicators might be weak shaft harmonics.
 - **Use Case:** Tests the algorithm's limits in extremely adverse conditions.

Detailed Evaluation Parameters

To ensure comprehensive testing, algorithms are evaluated using the following performance metrics:

1. **Fault Detection Accuracy:** Measures the correctness of fault identification across different data sets.
2. **Sensitivity:** Determines the algorithm's ability to detect even weak fault signals, especially in P and N categories.
3. **Computational Efficiency:** Assesses how quickly and efficiently the algorithm processes data, critical for real-time applications.
4. **Robustness:** Evaluates performance consistency under varying conditions, such as noise, load variations, and speed changes.

Table 1. Categorisation of Diagnosis Outcomes

Diagnosis category	Diagnosis success	Explanation
Y1	Yes	Data is clearly diagnosable and shows classic fault characteristics in both time and frequency domains.
Y2	Yes	Data is diagnosable but shows non-classic fault characteristics in either or both time and frequency domains.
P1	Partial	Data is probably diagnosable; the envelope spectrum contains discrete components at expected fault frequencies, though they are not dominant.
P2	Partial	Data is potentially diagnosable; the envelope spectrum contains smeared components that roughly align with expected fault frequencies.
N1	No	Data is not diagnosable for the specified bearing fault but indicates other issues (e.g., looseness).
N2	No	Data is not diagnosable, resembling noise, with only shaft harmonics potentially observable in the envelope spectrum.

This categorization framework provides a structured approach to evaluating the effectiveness of diagnostic algorithms, particularly under challenging conditions. By comparing performance across Y, P, and N data sets, this study aims to identify algorithms capable of delivering reliable and comprehensive fault diagnostics for rolling bearing systems.

4.3 Summary of Results

The data sets in these extreme categories are listed in Tables 2 and 3 respectively which exhibits a classical symptoms Y1 diagnosis and N1 & N2 diagnosis found to be a undiagnosable method.

Data sets in Table 2, provides the information about clear fault indicators that could assist in understanding and quantifying spall (surface wear or chipping) size, which is often an indicator of fault severity. These data sets, with their well-defined fault characteristics, could serve as valid, high-quality training sets for machine learning models designed for fault diagnosis, enhancing model accuracy and reliability.

Table 2. Y1 diagnosis

Fault type					
	IR	Ball	OR centred	OR orthogonal	OR opposite
Drive-end 12 kHz data	107FE, 171FE, 209DE, 209DE, 210DE 211DE, 211FE, 212DE	-	132FE 236FE	144DE, 144BA, 145DE, 145FE, 145BA, 146DE, 146FE, 146BA, 147DE, 147FE, 147BA	156DE, 156FE, 159DE, 160DE
Drive-end 48 kHz data	213, 215FE	-	135 136 137 138	148, 149, 150, 151	161DE, 162, 163DE,163FE,164
Fan-end 12 kHz data	278DE, 278FE, 279DE, 280DE, 280BA, 281DE, 274FE, 275FE, 276FE, 276BA, 277FE, 277BA, 271DE, 271FE, 271BA, 272DE, 272BA, 273DE, 273FE, 273BA	-	313DE, 313FE, 315DE	310DE, 310FE, 309DE, 311DE, 311FE, 312FE, 317DE, 317FE, 317BA	-

Furthermore, the undiagnosable records listed in Table 3 might provide a robust test for any newly proposed diagnostic algorithms.

Table 3. N1 or N2 diagnosis

Fault type					
	IR	Ball	OR centred	OR orthogonal	OR opposite
Drive-end 12 kHz data	3001, 3002, 3003, 3004	118, 119, 120DE, 120FE, 120BA, 121BA, 187FE, 224DE, 224FE, 224BA, 225DE, 225FE	197FE, 197BA, 198FE, 198BA 199FE, 200	-	-
Drive-end 48 kHz data	174	122, 123, 124, 125, 192, 228DE, 229DE	202FE, 204FE	-	-
Fan-end 12 kHz data	-	282FE, 285FE, 290DE, 290FE, 292FE, 293DE	-	298BA	302, 305FE, 306, 307

4.4 Verification of Algorithms with Politecnico test rig

The test was conducted at the DIRG Lab in the Department of Mechanical and Aerospace Engineering at Politecnico di Torino [7]. The experiment focused on evaluating high-speed aeronautical bearings under varying conditions, including changes in rotational speed, radial load, and damage levels. An accelerometer was strategically positioned on the shaft to capture precise vibration data. These datasets can serve as benchmarks for comparing and analyzing the performance of diagnostic algorithms for rolling bearings.

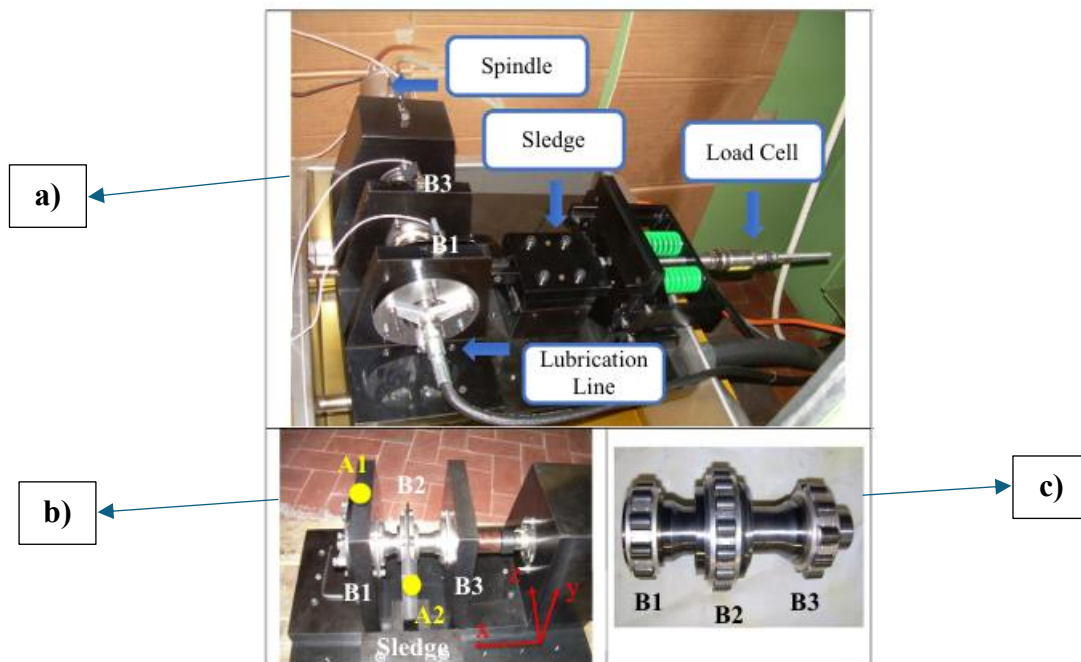


Fig 133. The test rig a) general view of the test rig; b) positions of the two accelerometers and the reference system; c) the shaft with its three roller bearings

4.4.1 Description of the tests

In this paper, two different experimental sessions are seen:

1. Session 1: Measurements of acceleration were taken for bearings with various damage levels, operating under different rotational speeds and radial loads.
2. Session 2: The behavior of a single damaged bearing was monitored during an extended test lasting approximately 330 hours, performed at a constant speed and load.

Variable speed and load

The bearing in position B1 (Fig. 1a) was simply designed for easy removal from its support allowing for the evaluation of system responses when bearings with various types and degrees of damage were installed.

Localized faults on the bearing components were introduced using a Rockwell tool, creating conical indentations either on the inner ring or on a single roller (cases 1A to 6A). The

approximate diameters of these circular indentations were measured as 150 mm, 250 mm, and 450 mm.

Each bearing, from 0A to 6A, was subjected to the same testing procedure:

- A brief run at the minimum speed (100 Hz) with no load to ensure correct mounting.
- Application of static loads, starting at 1000 N, then increasing to 1400 N and finally 1800 N.
- Incremental increases in shaft speed from 0 Hz to 500 Hz, in steps of 100 Hz.
- Measurement of acceleration at each steady shaft speed.

Table 4. List of the defects of the various bearings mounted in position B1

Name	Defect	Dimension (μm)
0A	NO DEFECT	-
1A	Diameter of an indentation on the inner ring	450
2A	Diameter of an indentation on the inner ring	250
3A	Diameter of an indentation on the inner ring	150
4A	Diameter of an indentation on a roller	450
5A	Diameter of an indentation on a roller	250
6A	Diameter of an indentation on a roller	150

About filename:

C: root of the file name, common to all files.

n: integer value from 0 to 6, indicating the kind of the defect, e.g. 0A, 1A, ...,6A (Table4).

fff: integer value from 100 to 500, indicating the nominal speed of the shaft (Hz).

vvv: integer value corresponding to the voltage of the load cell (mV), indicating the applied load.

m: integer value, indicating if the measurement has been repeated ($m = 2$) or not ($m = 1$)

.mat Matlab file extension.

For example, C4A_100_702_1.mat contains the first registration of acceleration signal produced by bearing 4A (defect on a roller), at the nominal rotational speed of 100 Hz (i.e. 6000 rpm), under a load of about 1407 N which corresponds to an output of the load cell of 702 mV (sensitivity 0.499 mV/N).

Each file contains a matrix with the same name of the file (apart from the .m extension) with 512,000 rows (time samples) and 6 columns (one for each channel).

4.4.2 Experimental results

The diagnostic algorithms were verified using data from the Politecnico test rig. The analysis focused on defects located on the inner ring and roller, evaluated under constant speed (100 Hz) conditions with varying load scenarios: no load, minimum load, and maximum load.

Inner ring: (C1A - Maximum defect)

According to Table 4, the C1A defect is categorized under the "Maximum Defect" classification of Inner ring. In the subsequent sections, we will examine the results obtained under varying load conditions and analyze their implications.

No load (C1A_100_000_2)

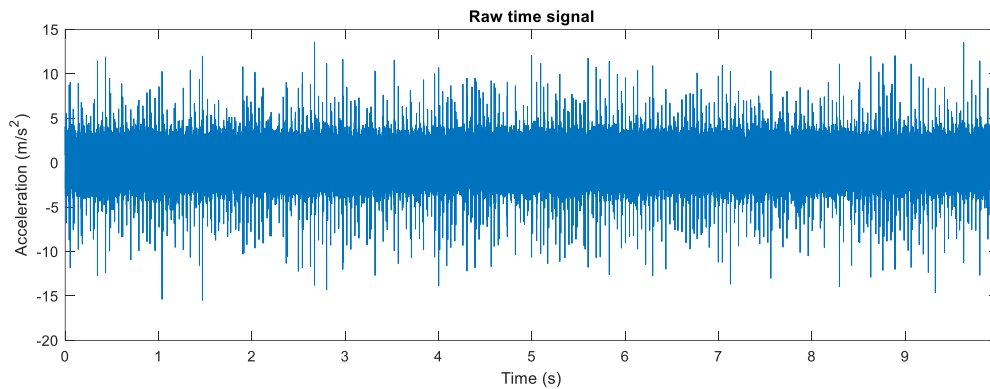


Fig 134. Raw Signal

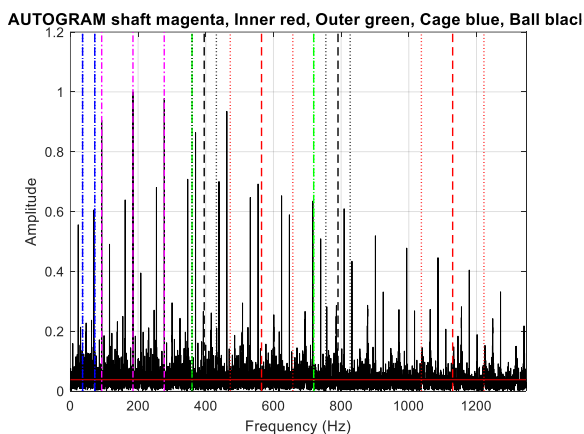


Fig 135. Autogram, Normalized SES

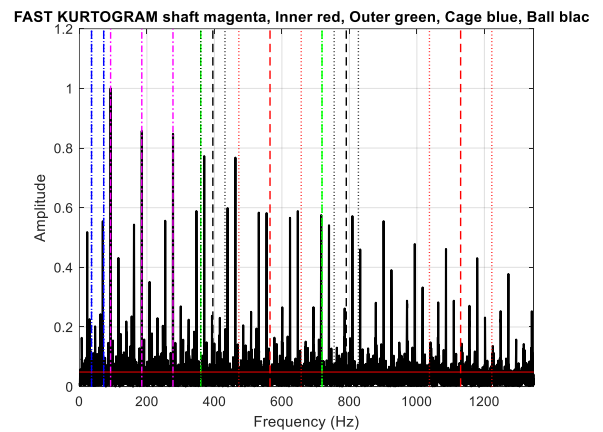


Fig 136. FastKurtogram, Normalized SES

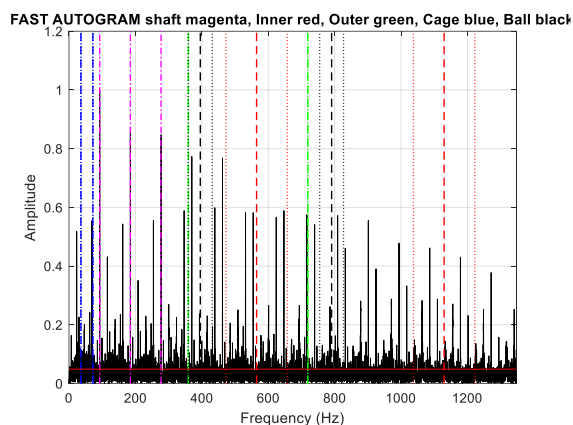


Fig 137. FastAutogram, Normalized SES

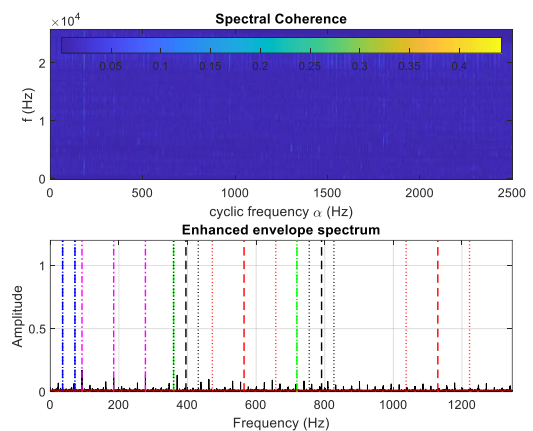


Fig 138. SC, Normalized EES

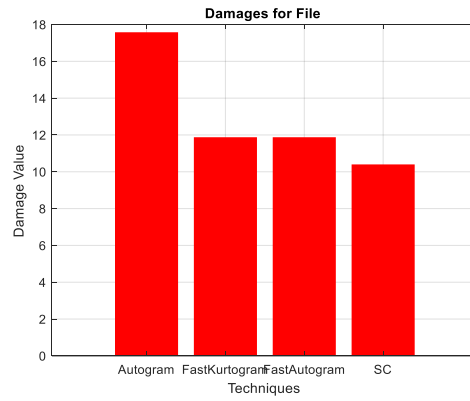


Fig 139. Damage value for C1A_100_000_2

Medium load (C1A_100_502_2)

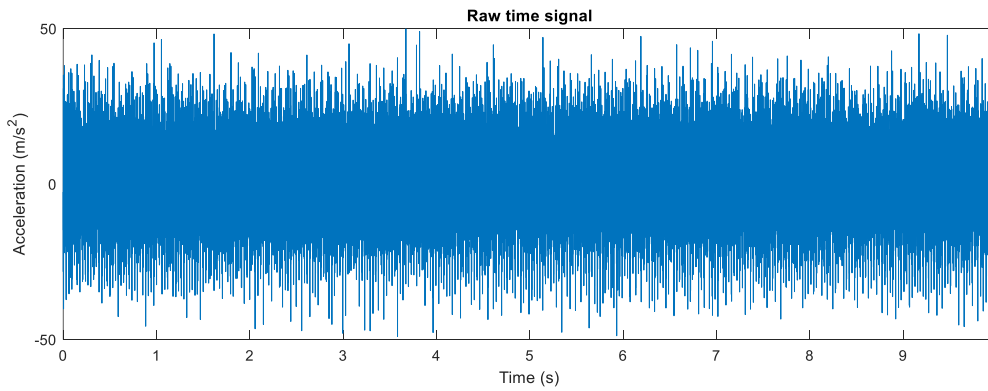


Fig 140. Raw Signal

AUTOGRAM shaft magenta, Inner red, Outer green, Cage blue, Ball black

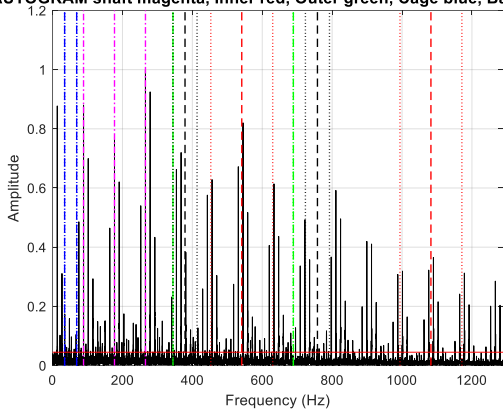


Fig 141. Autogram, Normalized SES

FAST KURTOGRAM shaft magenta, Inner red, Outer green, Cage blue, Ball black

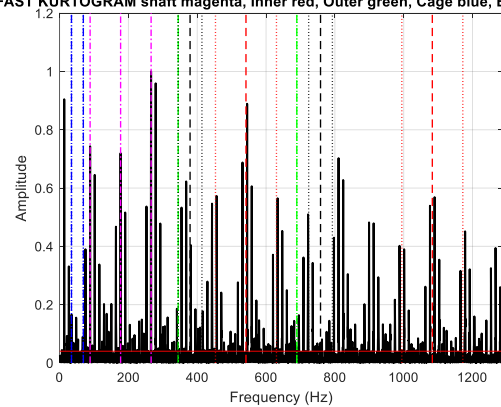


Fig 142. FastKurtogram, Normalized SES

FAST AUTOGRAM shaft magenta, Inner red, Outer green, Cage blue, Ball black

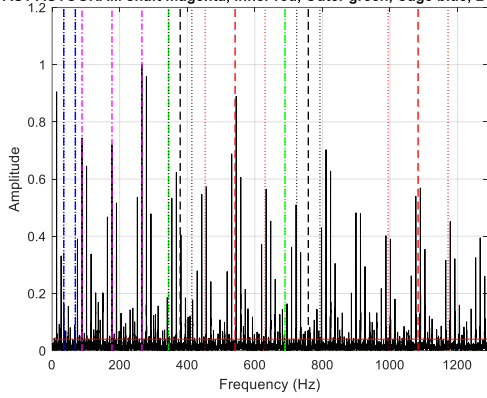


Fig 143. FastAutogram, Normalized SES

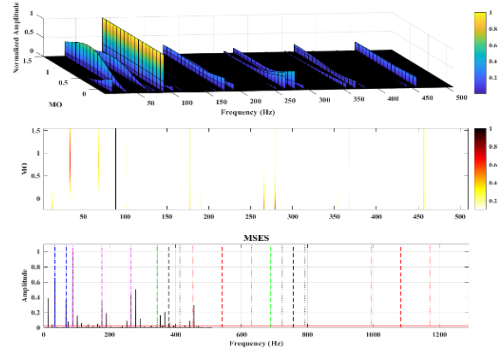


Fig 144. SAM, Normalized MSES

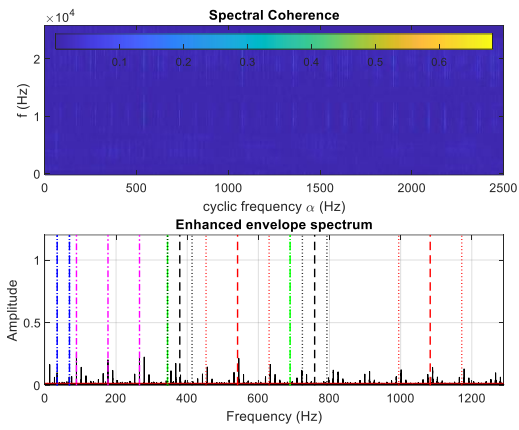


Fig 145. SC, Normalized EES

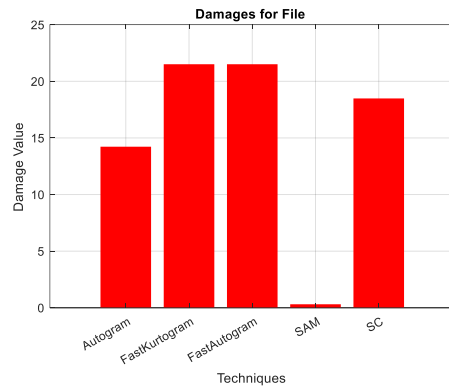


Fig 146. Damage value for C1A_100_502_2

Maximum load (C1A_100_898_2)

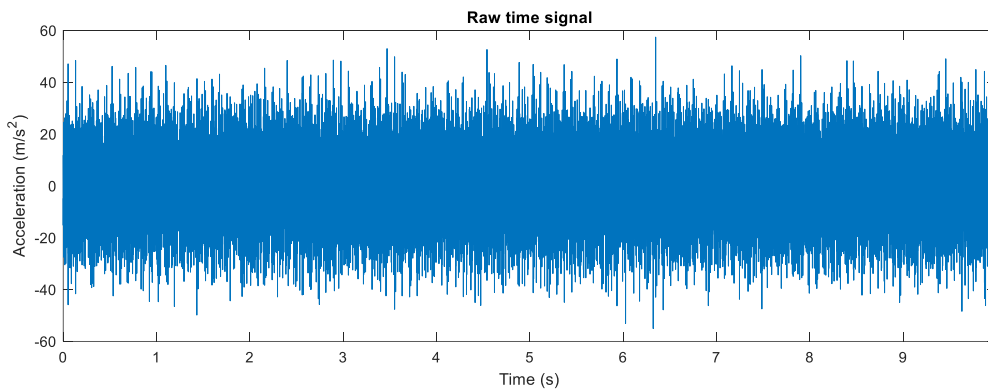


Fig 147. Raw Signal

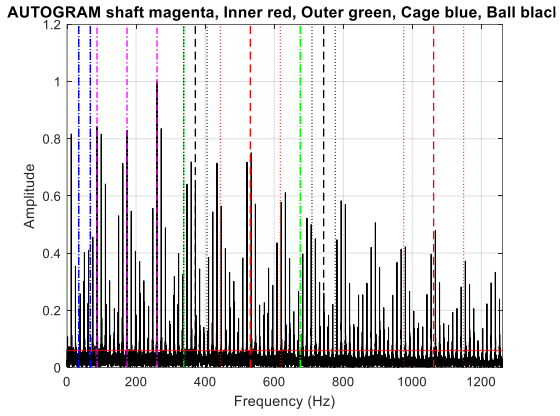


Fig 148. Autogram, Normalized SES

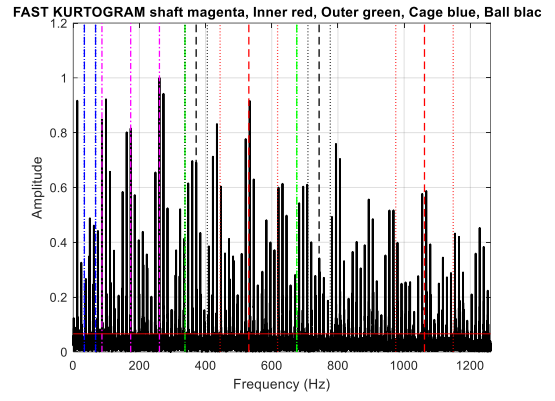


Fig 149. FastKurtogram, Normalized SES

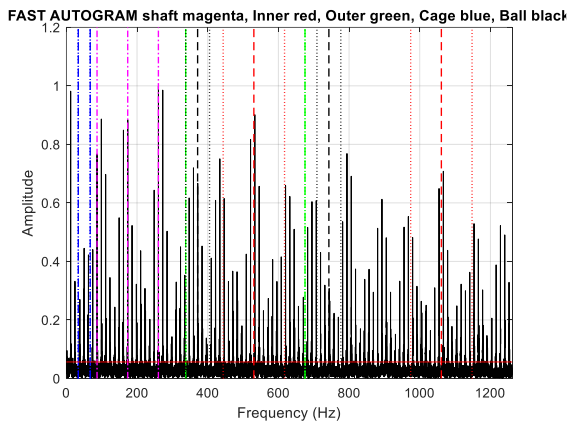


Fig 149. FastAutogram, Normalized SES

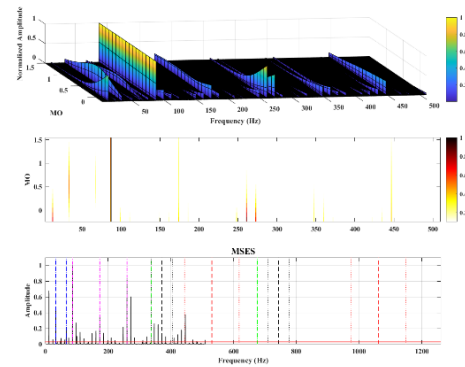


Fig 150. SAM, Normalized MSES

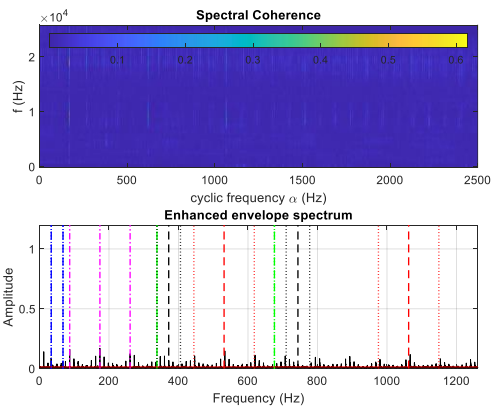


Fig 151. SC, Normalized EES

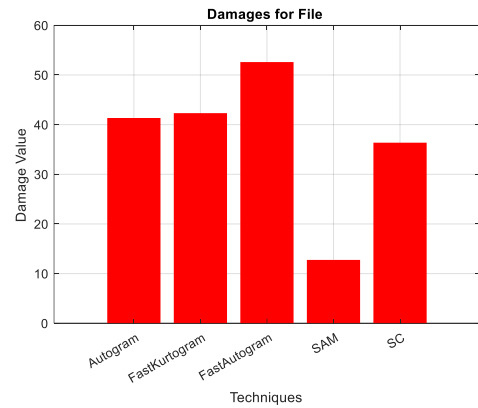


Fig 152. Damage value for C1A_100_898_2

Inner ring: (C3A - Minimum defect)

According to Table 4, the C3A defect is categorized under the "Minimum Defect" classification of Inner ring. In the subsequent sections, we will examine the results obtained under varying load conditions and analyze their implications.

No load (C3A_100_000_1)

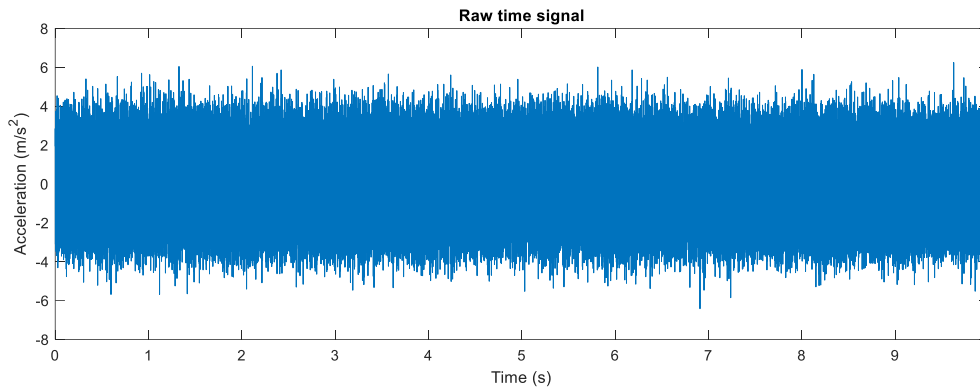


Fig 153. Raw Signal

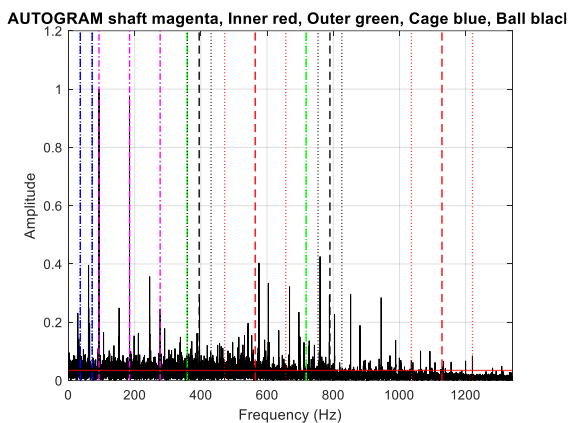


Fig 154. Autogram, Normalized SES

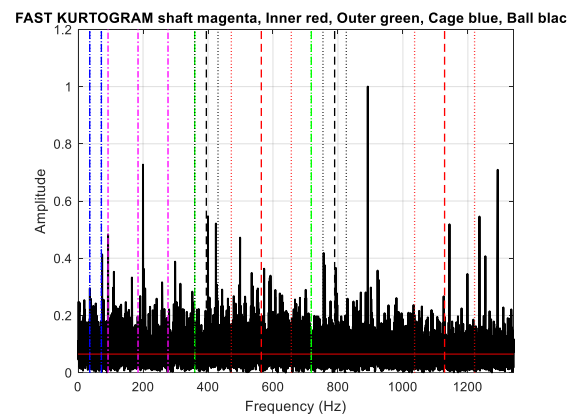


Fig 155. FastKurtogram, Normalized SES

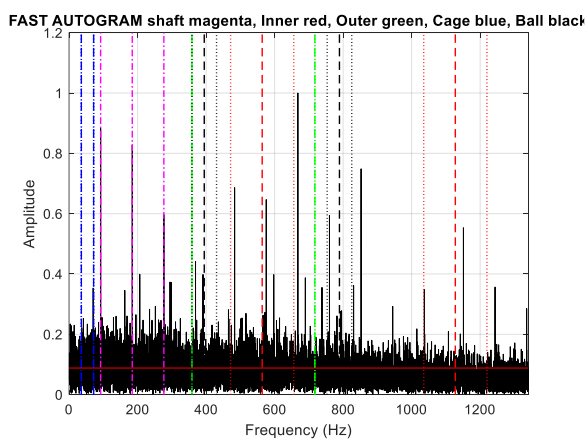


Fig 156. FastAutogram, Normalized SES

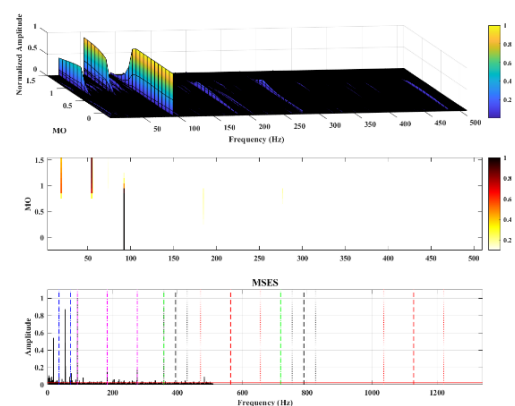


Fig 157. SAM, Normalized MSES

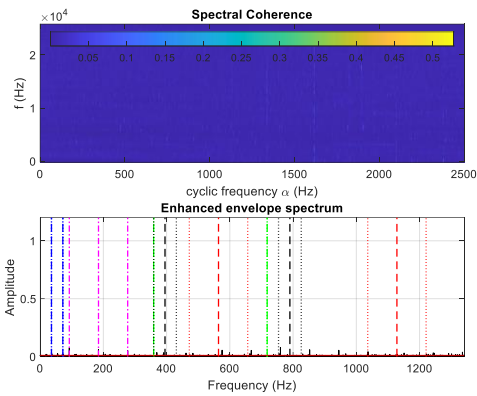


Fig 158. SC, Normalized EES

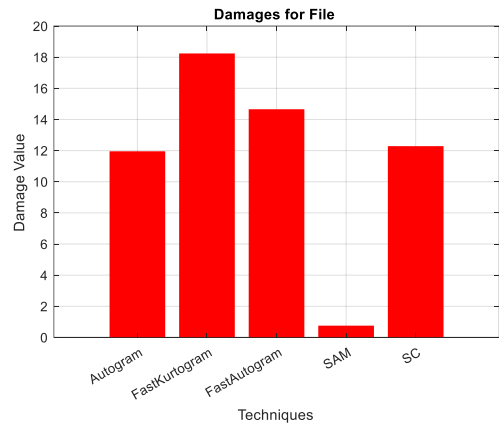


Fig 159. Damage value for C3A_100_000_1

Medium load (C3A_100_505_1)

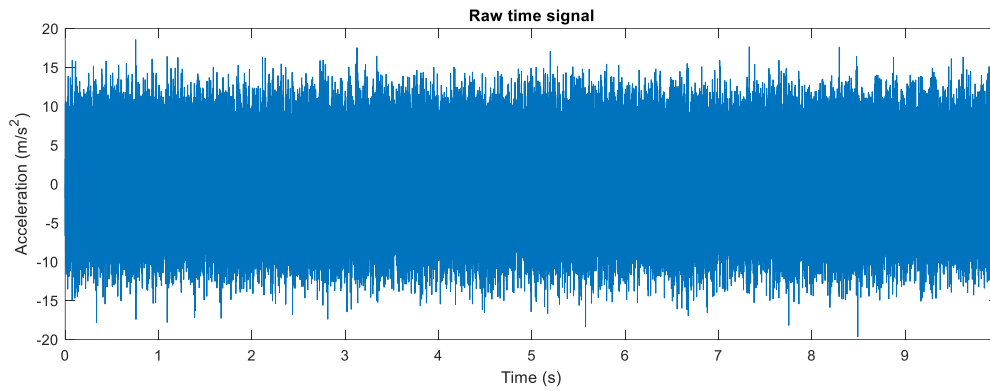


Fig 160. Raw Signal

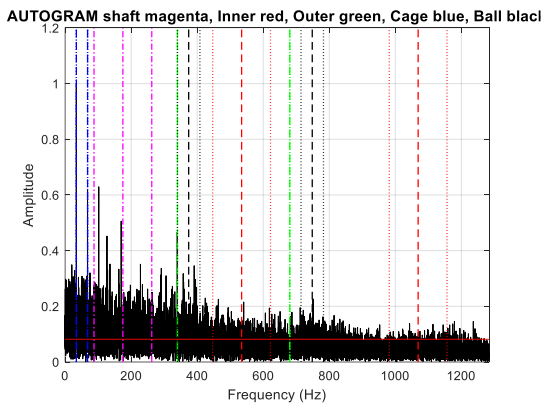


Fig 161. Autogram, Normalized SES

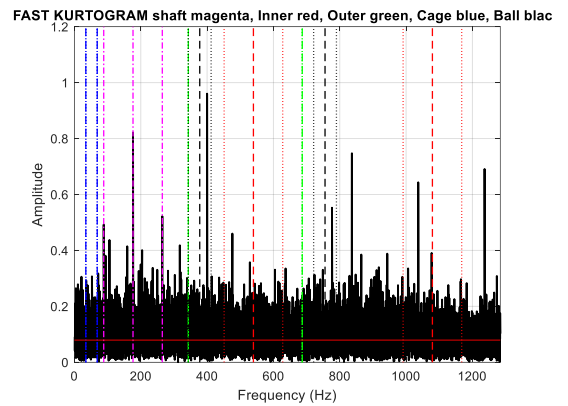


Fig 162. FastKurtogram, Normalized SES

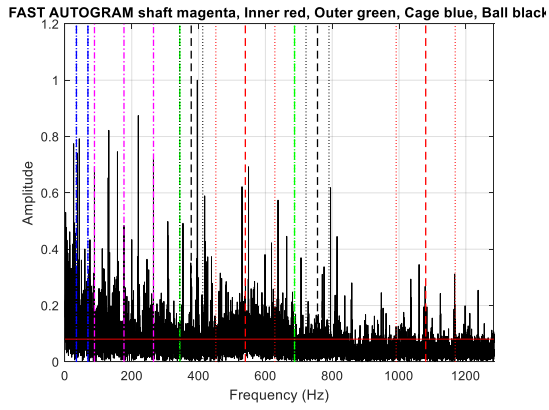


Fig 163. FastAutogram, Normalized SES

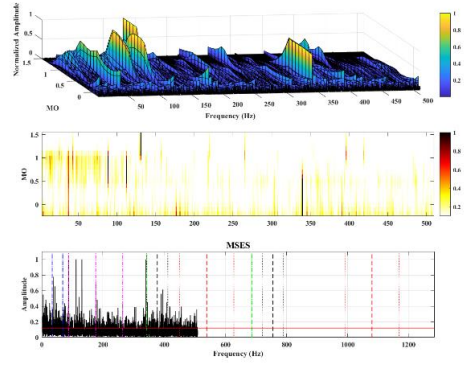


Fig 164. SAM, Normalized MSES

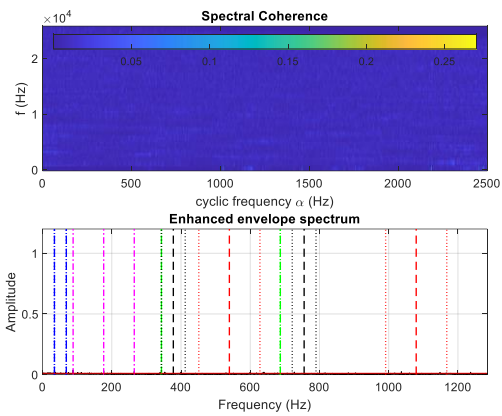


Fig 165. SC, Normalized EES

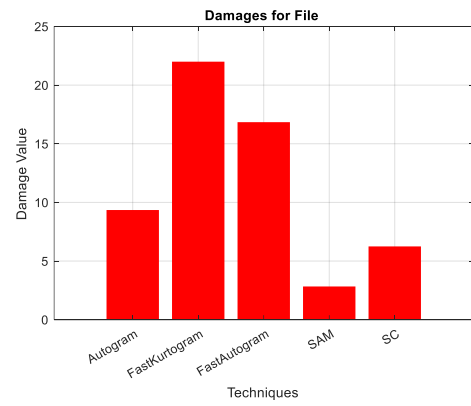


Fig 166. Damage value for C3A_100_505_1

Maximum load (C3A_100_906_1)

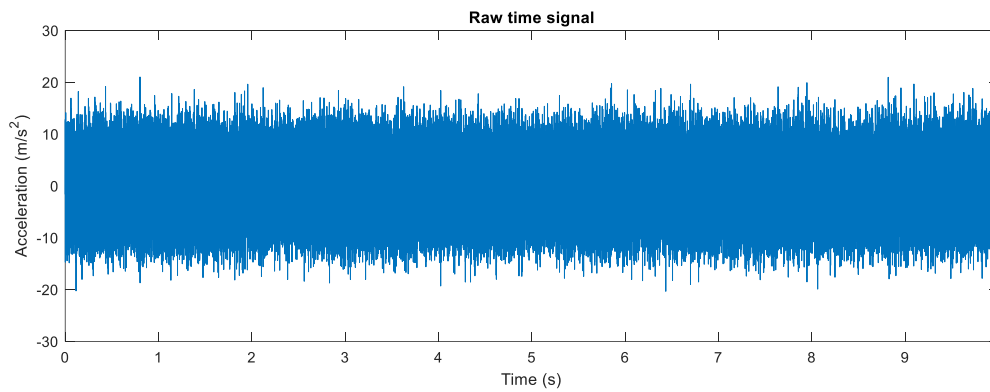


Fig 167. Raw Signal

AUTOGRAM shaft magenta, Inner red, Outer green, Cage blue, Ball black

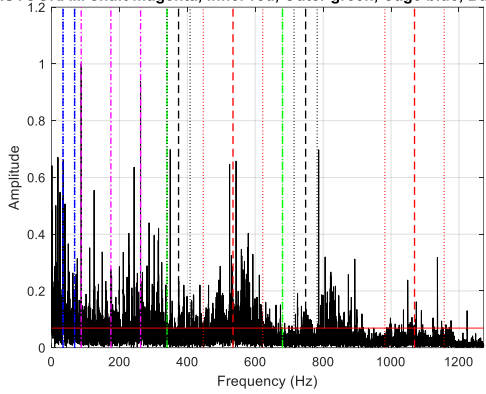


Fig 168. Autogram, Normalized SES

FAST KURTOGRAM shaft magenta, Inner red, Outer green, Cage blue, Ball black

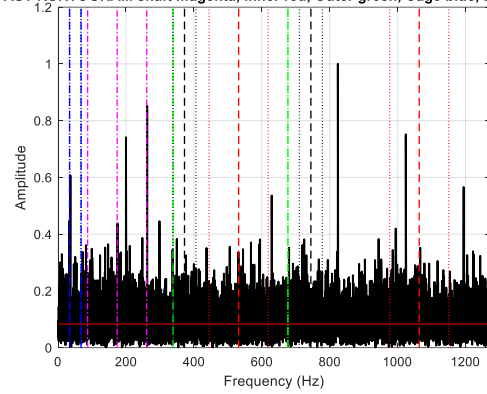


Fig 169. FastKurtogram, Normalized SES

FAST AUTOGRAM shaft magenta, Inner red, Outer green, Cage blue, Ball black

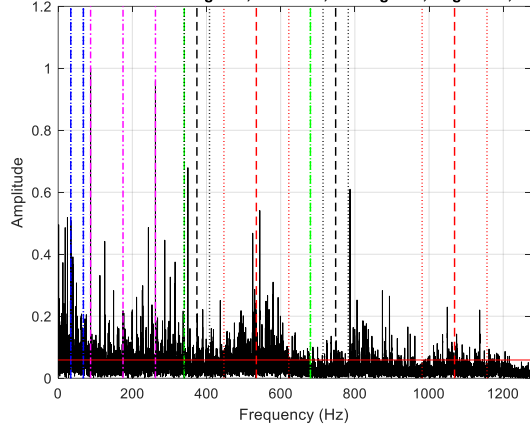


Fig 170. FastAutogram, Normalized SES

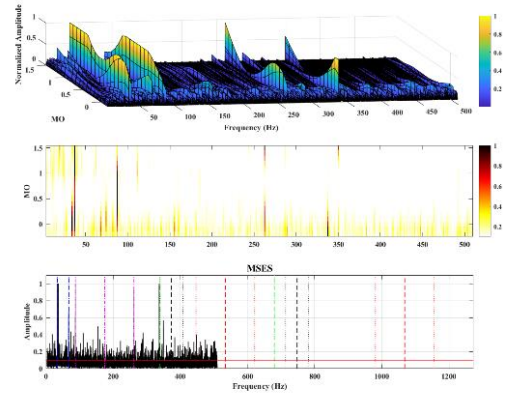


Fig 171. SAM, Normalized MSES

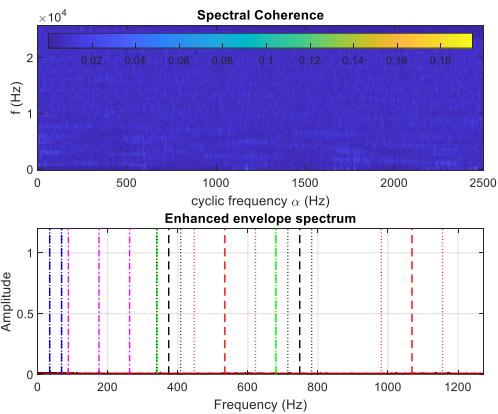


Fig 172. SC, Normalized EES

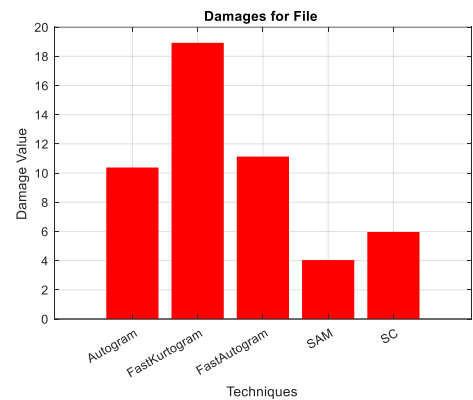


Fig 173. Damage value for C3A_100_906_1

Roller: (C4A - Maximum defect)

According to Table 4, the C4A defect is categorized under the "Maximum Defect" classification of Roller. In the subsequent sections, we will examine the results obtained under varying load conditions and analyze their implications.

No load (C4A_100_000_1)

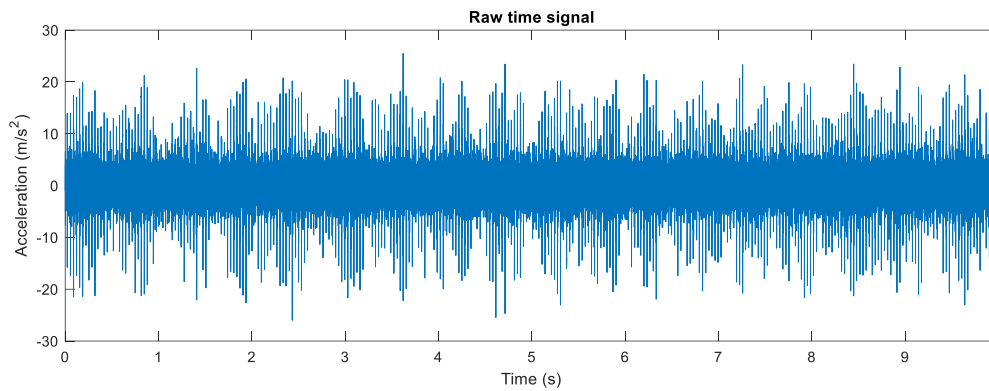


Fig 174. Raw Signal

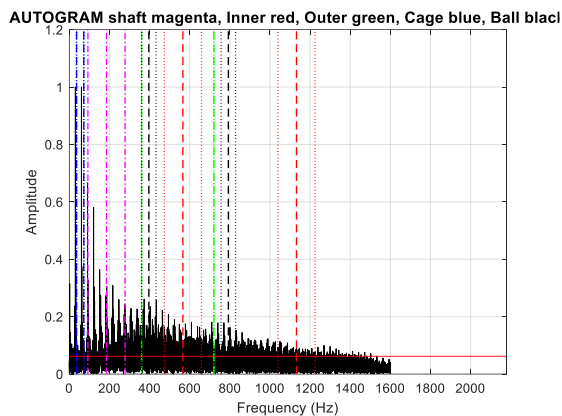


Fig 175. Autogram, Normalized SES

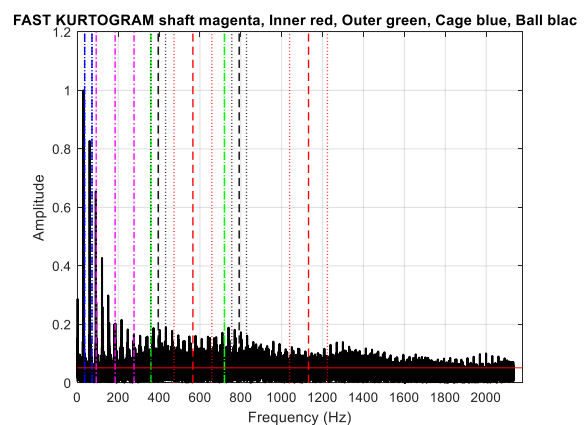


Fig 176. FastKurtogram, Normalized SES

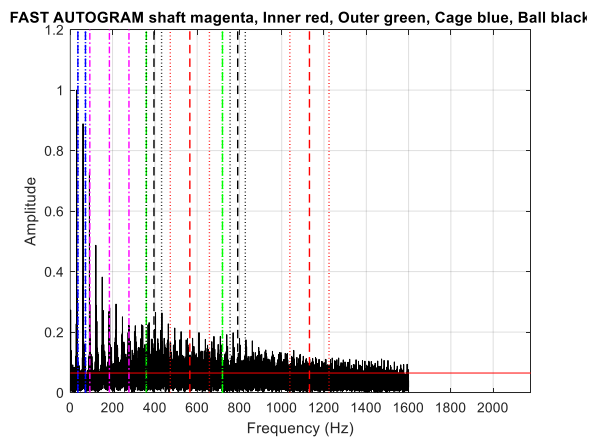


Fig 177. FastAutogram, Normalized SES

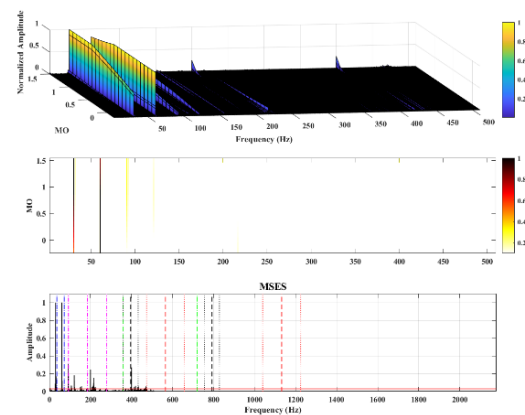


Fig 178. SAM, Normalized MSES

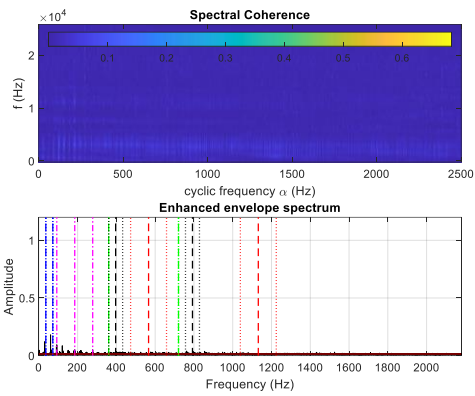


Fig 179. SC, Normalized EES

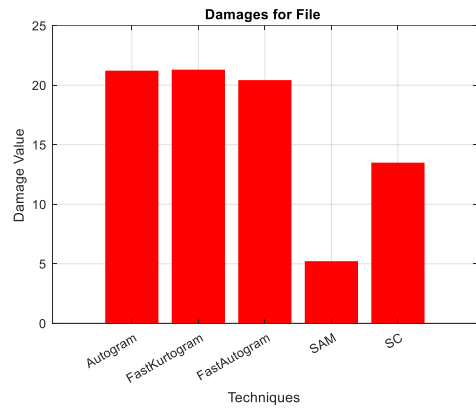


Fig 180. Damage value for C4A_100_000_1

Medium load (C4A_100_496_1)

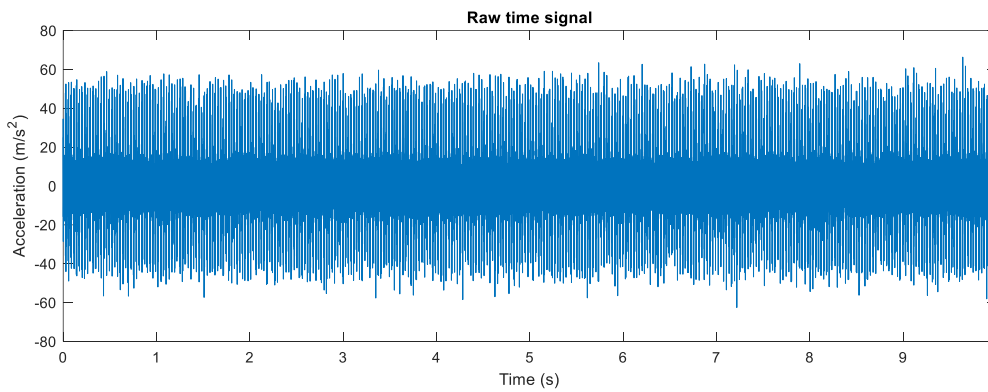


Fig 181. Raw Signal

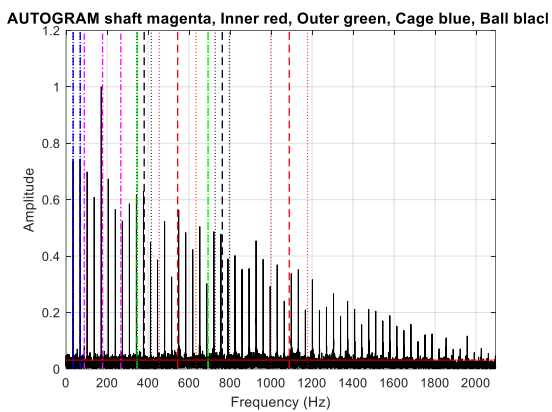


Fig 182. Autogram, Normalized SES

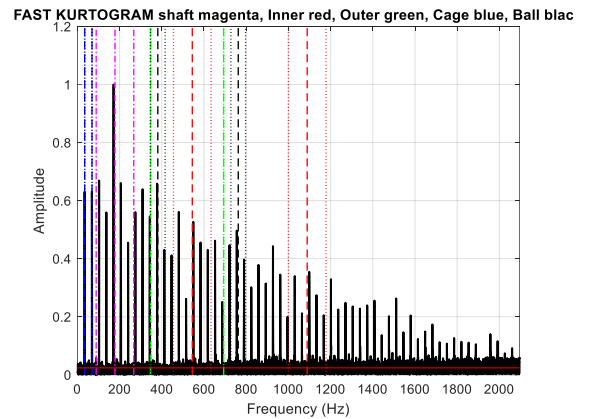


Fig 183. FastKurtogram, Normalized SES

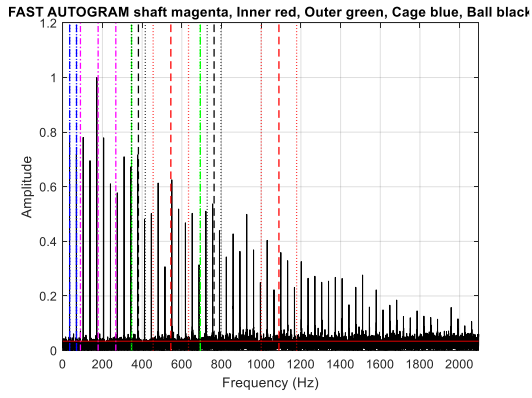


Fig 184. FastAutogram, Normalized SES

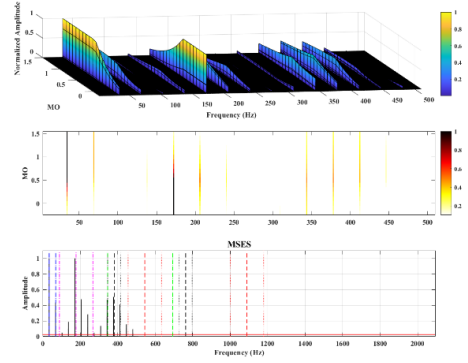


Fig 185. SAM, Normalized MSES

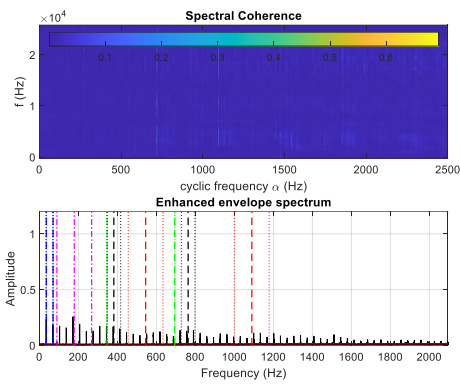


Fig 186. SC, Normalized EES

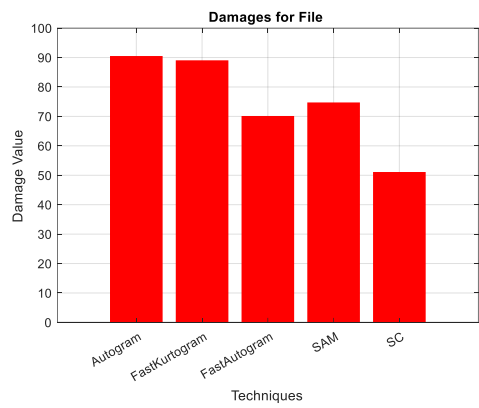


Fig 187. Damage value for C4A_100_496_1

Maximum load (C4A_100_895_1)

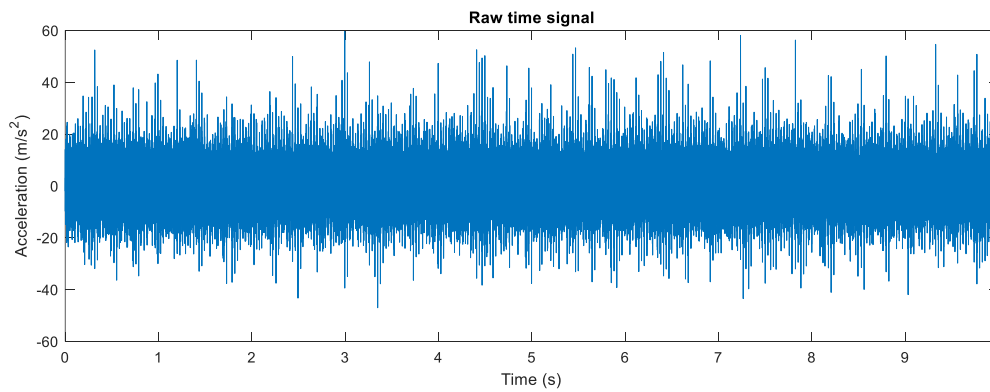


Fig 188. Raw Signal

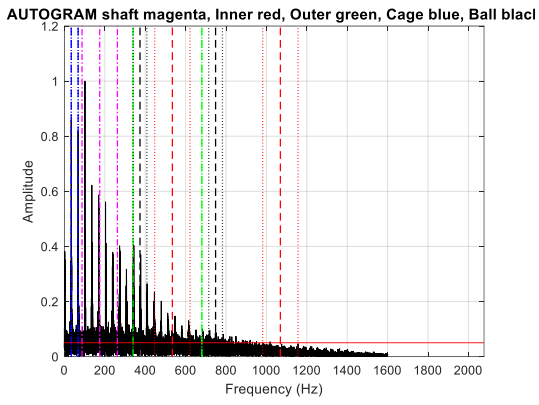


Fig 189. Autogram, Normalized SES

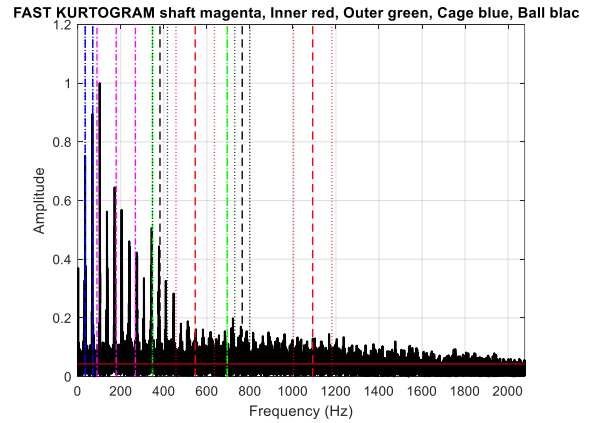


Fig 190. FastKurtogram, Normalized SES

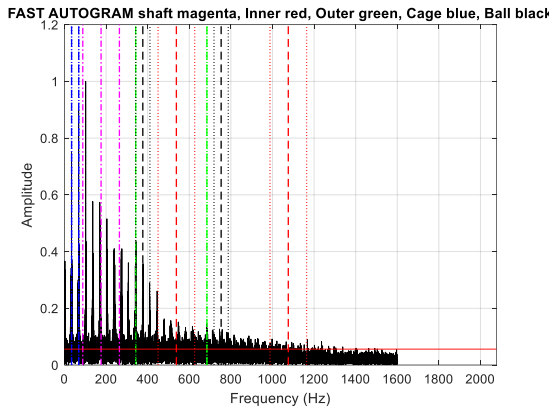


Fig 191. FastAutogram, Normalized SES

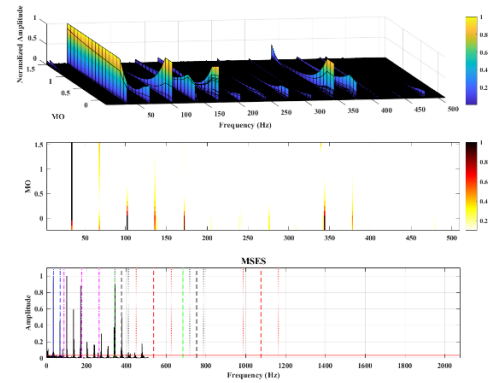


Fig 192. SAM, Normalized MSES

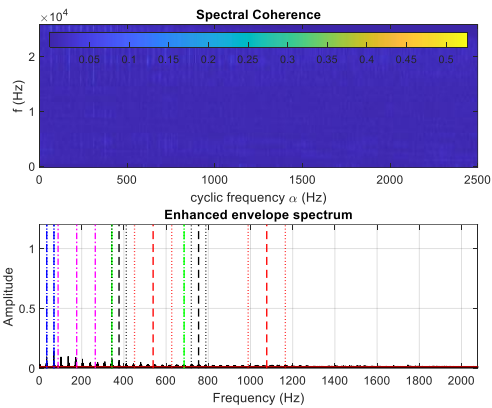


Fig 193. SC, Normalized EES

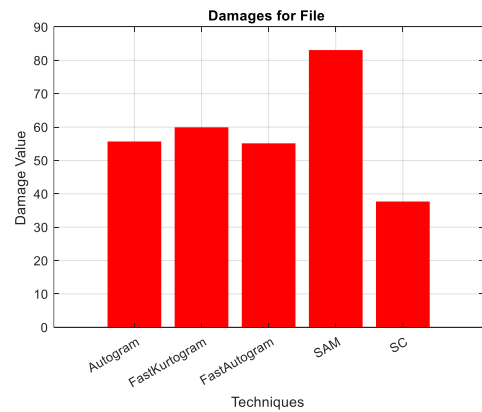


Fig 194. Damage value for C4A_100_895_1

4.5 Conclusion

This thesis research is mainly focused on a comprehensive comparison of damage detection applied to rolling bearing elements using algorithms. The various types of defects are inner race, outer race, cage, and ball faults under different fault sizes and signal conditions. With the diagnostic algorithms, both the strengths and limitations of these methods has been highlighted, especially in challenging cases involving noise, non-stationarity, and complex fault patterns.

The key findings from the comparative analysis indicate that:

1. **Fault Size Matters:** The severity of bearing faults increases with fault size, leading to more prominent diagnostic features such as higher vibration and distinct spectral peaks. Algorithms that rely on amplitude thresholds and frequency domain analysis generally performed well in identifying larger faults, while smaller faults were sometimes missed or misinterpreted.
2. **Noise and Non-Stationarity:** Signals corrupted with noise or showing non-stationary characteristics posed significant challenges to conventional diagnostic methods. In cases where electrical noise or repetitive transients were present, algorithms struggled to distinguish between true fault indicators and noise artifacts. Non-stationary signals, in particular, required advanced processing techniques to reveal intermittent fault-related impulses.
3. **Autogram and Fast Kurtogram:**
 - The **Autogram** analysis, with its high kurtosis values in fault cases, demonstrated a strong ability to highlight impulsive characteristics, making it particularly useful for detecting transient, non-stationary fault signatures.
 - A significant advantage of the **Fast Kurtogram (FK)** over Autogram lies in its computational efficiency. Unlike Autogram, FK utilizes Multirate filtering, which speeds up the analysis process by efficiently managing different frequency bands through down-sampling. This approach significantly reduces the computational load, as it allows FK to focus only on the essential frequency components associated with bearing faults, bypassing unnecessary processing of irrelevant bands.
4. **Advanced Signal Processing:** Techniques like cepstrum pre-whitening and envelope analysis (as used in Method 2) showed promise in mitigating the masking effects of noise and non-stationary artifacts. Additionally, kurtosis-based measures provided valuable insights in cases with impulsive fault characteristics, proving to be a useful complementary tool in diagnosing subtle or transient faults.

Overall Implications:

This comparative study underscores the importance of selecting appropriate algorithms based on the nature of the signal and fault type. While traditional methods may work well under controlled conditions, real-world applications often involve noise, variable load conditions, and non-stationary signals, which require more advanced and adaptive diagnostic tools.

For future research, it needs to be refined for diagnostic algorithms to handle the complexities of real-world bearing conditions more effectively. Specifically, algorithms that integrate signal processing techniques to handle noise and non-stationarity, such as cepstrum pre-whitening, and that leverage metrics like kurtosis for impulsive signal detection, could significantly enhance diagnostic accuracy and reliability.

In conclusion, while current diagnostic algorithms offer valuable insights into bearing health, the challenges observed in non-stationary and noise-corrupted data suggest that further advancements are needed. Developing algorithms that can adapt to complex signal environments will be crucial for achieving accurate, reliable, and early detection of bearing faults, thereby improving maintenance strategies and enhancing the operational life of machinery in diverse industrial settings.

References

- [1] Robert B. Randall, Jérôme Antoni, Rolling element bearing diagnostics—A tutorial, *Mechanical Systems and Signal Processing*, Volume 25, Issue 2, February 2011, Pages 485-520.
- [2] P.D. McFadden, J.D. Smith, Model for the vibration produced by a single point defect in a rolling element bearing, *Journal of Sound and Vibration*, Volume 96, Issue 1, 8 September 1984, Pages 69-82.
- [3] Jérôme Antoni, Fast computation of the Kurtogram for the detection of transient faults, *Mechanical Systems and Signal Processing*, Volume 21, Issue 1, January 2007, Pages 108-124.
- [4] Alessandro Fasana, Ali Moshrefzadeh, The Autogram: An effective approach for selecting the optimal demodulation band in rolling element bearings diagnosis, *Mechanical Systems and Signal Processing*, Volume 105, 15 May 2018, Pages 294-318.
- [5] Alessandro Paolo Daga, Alessandro Fasana, Luigi Garibaldi, Stefano Marchesiello, Ali Moshrefzadeh, Fast Computation of the Autogram for the detection of transient faults.
- [6] Wade A. Smith, Robert B. Randall, Rolling element bearing diagnostics using the Case Western Reserve University data: A benchmark study, *Mechanical Systems, and Signal Processing*, Volumes 64–65, December 2015, Pages 100-131.
- [7] Alessandro Paolo Daga, Alessandro Fasana, Stefano Marchesiello, Luigi Garibaldi, The Politecnico di Torino rolling bearing test rig: Description and analysis of open access data, *Mechanical Systems, and Signal Processing*, Volume 120, 1 April 2019, Pages 252-273.
- [8] Sandeep Sambhaji Udmale, Sangram S Patil, Vikas M. Phalle, Sanjay Kumar Singh, A bearing vibration data analysis based on spectral kurtosis and ConvNet.
- [9] Jérôme Antoni, Cyclic spectral analysis in practice, *Mechanical Systems and Signal Processing*, Volume 21, Issue 2, February 2007, Pages 597-630.
- [10] W. Gardner, Measurement of spectral correlation, *IEEE Transactions on Acoustics, Speech, and Signal Processing* (Volume: 34, Issue: 5, October 1986), Pages 1111 - 1123.
- [11] P. Borghesani, The envelope-based cyclic periodogram, *Mechanical Systems and Signal Processing*, Volumes 58–59, June 2015, Pages 245-270.

- [12] Jérôme Antoni, Cyclostationarity by examples, *Mechanical Systems and Signal Processing*, Volume 23, Issue 4, May 2009, Pages 987-1036.
- [13] Jérôme Antoni, Ge Xin, N. Hamzaoui, Fast computation of the spectral correlation, *Mechanical Systems and Signal Processing*, 92 (2017), Pages 248–277.
- [14] Robert B. Randall, A history of cepstrum analysis and its application to mechanical problems, *Mechanical Systems and Signal Processing*, Volume 97, December 2017, Pages 3-19.
- [15] Robert B. Randall, Nader Sawalhi, A New Method for Separating Discrete Components from a Signal, *SOUND & VIBRATION/MAY* 2011.
- [16] P. Borghesani, P. Pennacchi, R.B. Randall, N. Sawalhi, R. Ricci, Application of cepstrum pre-whitening for the diagnosis of bearing faults under variable speed conditions, *Mechanical Systems and Signal Processing*, Volume 36, Issue 2, April 2013, Pages 370-384.
- [17] D. HO, R.B. RANDALL, OPTIMISATION OF BEARING DIAGNOSTIC TECHNIQUES USING SIMULATED AND ACTUAL BEARING FAULT SIGNALS, *Mechanical Systems and Signal Processing*, Volume 14, Issue 5, September 2000, Pages 763-788.
- [18] P. Borghesani, Md. Rifat Shahriar, Cyclostationary analysis with logarithmic variance stabilization, *Mechanical Systems and Signal Processing* 70-71(6), September 2015.
- [19] Xinghui Zhang, Lei Xiao, A New Improved Kurtogram and Its Application to Bearing Fault Diagnosis.
- [20] S. J. Lacey, An Overview of Bearing Vibration Analysis.
- [21] Antonio Afonso Roque, Tiago A N Silva, João Manuel Ferreira Calado, J. C. Q. Dias, An approach to fault diagnosis of rolling bearings.
- [22] Alonso-González Miguel, Díaz Vicente García, Pérez Benjamin López, G-Bustelo B. Cristina Pelayo, Anzola John Petearson, Bearing Fault Diagnosis With Envelope Analysis and Machine Learning Approaches Using CWRU Dataset, *IEEE Access*, vol. 11, pp. 57796-57805.
- [23] M. A. Eissa, F. R. Gooma, K. M. Khader, BEARING'S EARLY FAULT DETECTION USING VIBRATION ANALYSIS.

- [24] Bartosz Jakubek, Michał Jakubowicz, Wojciech Smulek, Comparison of Rolling Bearings' Diagnosing Methods – Procedures of Damage Introduction, *Vibrations in Physical Systems* 2018, 29, 2018011.
- [25] Yong Ren, Wei Li, Bo Zhang, Zhencai Zhu, Fang Jiang, Fault Diagnosis of Rolling Bearings Based on Improved Kurtogram in Varying Speed Conditions, *Applied Sciences* 9(6):1157.
- [26] R.K. Upadhyay, L.A. Kumaraswamidhas, Md. Sikandar Azam, Rolling element bearing failure analysis: A case study, Volume 1, Issue 1, January 2013, Pages 15-17.
- [27] Alessandro Fasana, Luigi Garibaldi, Ali Moshrefzadeh, Using Unbiased Autocorrelation to Enhance Kurtogram and Envelope Analysis Results for Rolling Element Bearing Diagnostics.
- [28] Peter Sulka, Alzbeta Sapietova, Vladimir Dekys, Ondrej Stalmach, Vibration analysis and comparison of the damaged and undamaged rolling ball bearing, *Transportation Research Procedia*, Volume 40, 2019, Pages 511-518.
- [29] Ravindra A. Tarle, Nilesh K. Kharate, Shyam P. Mogal, Vibration Analysis of Ball Bearing.
- [30] Konstantinos Kamaras, Anastasios Garantziotis, Ilias Dimitrakopoulos, Vibration Analysis of Rolling Element Bearings (Air Conditioning Motor Case Study).
- [31] H. Saruhan, S. Sandemir, A. Çiçek, I. Uygur, Vibration Analysis of Rolling Element Bearings Defects, *Journal of Applied Research and Technology*, Volume 12, Issue 3, June 2014, Pages 384-395.
- [32] A Khadersab, S Shivakumar Dr., Vibration Analysis Techniques for Rotating Machinery and its effect on Bearing Faults, *Procedia Manufacturing*, Volume 20, 2018, Pages 247-252.
- [33] Ahmed. H. Osman, Ahmed Salman, Khaled M. Fawzy, Vibration Signature of Roller Bearing's Faults, *European Scientific Journal* April 2019 edition Vol.15, No.12 ISSN: 1857 – 7881 (Print) e - ISSN 1857- 7431.
- [34] D. Dyer, R. Stewart, Detection of Rolling Element Bearing Damage by Statistical Vibration Analysis, *Journal of Mechanical Design*, Published 1 April 1978.

- [35] Jérôme Antoni, R.B. Randall, The spectral kurtosis: Application to the vibratory surveillance and diagnostics of rotating machines, *Mechanical Systems and Signal Processing* 20(2), Pages 308-331.
- [36] R.B. RANDALL, J. ANTONI, S. CHOBSAARD, THE RELATIONSHIP BETWEEN SPECTRAL CORRELATION AND ENVELOPE ANALYSIS IN THE DIAGNOSTICS OF BEARING FAULTS AND OTHER CYCLOSTATIONARY MACHINE SIGNALS, *Mechanical Systems and Signal Processing*, Volume 15, Issue 5, September 2001, Pages 945-962.
- [37] R.S. Roberts, W.A. Brown, H.H. Loomis, Computationally efficient algorithms for cyclic spectral analysis, *IEEE Signal Processing Magazine* (Volume: 8, Issue: 2, April 1991), Pages: 38 - 49.
- [38] W.A. Gardner, Exploitation of spectral redundancy in cyclostationary signals, *IEEE Signal Processing Magazine* (Volume: 8, Issue: 2, April 1991), Pages: 14 - 36.
- [39] W.A. Brown, H.H. Loomis, Digital implementations of spectral correlation analyzers, *IEEE Transactions on Signal Processing* (Volume: 41, Issue: 2, February 1993), Pages: 703 - 720.
- [40] Alan Hase, Hiroshi Mishina, Fundamental Study on Early Detection of Seizure in Journal Bearing by Using Acoustic Emission Technique, November 2015 *Wear* 346, DOI:10.1016/j.wear.2015.11.012.
- [41] Case Western Reserve University Bearing Data Center Website, <https://engineering.case.edu/bearingdatacenter/welcome>.
- [42] Wade A. Smith, Robert B. Randall, Rolling element bearing diagnostics using the Case Western Reserve University data: a benchmark study, *School of Mechanical and Manufacturing Engineering, Mechanical Systems and Signal Processing* (May 2015), DOI: 10.1016/j.ymsp.2015.04.021.
- [43] N. Sawalhi, R.B. Randall, Signal Pre-whitening using Cepstrum Editing (Liftering) to Enhance Fault Detection in Rolling Element Bearings, *COMADEM*, Stavanger, Norway, 2011.
- [44] N. Sawalhi, *Diagnostics, Prognostics and Fault Simulation For Rolling Element Bearings*, PhD Thesis, The University of New South Wales, 2007.

- [45] J. Antoni, R.B. Randall, Unsupervised noise cancellation for vibration signals: part II—a novel frequency-domain algorithm, *Mechanical Systems and Signal Processing*, 18 (2004) 103-117.
- [46] Lian Cheng Su, Yan E Shi, Xiao Li Li, Yan Liao Zhang, Fault Diagnosis of Bearing Based on the Ultrasonic Signal, *Advanced Materials Research* 422:122-126, December 2011.
- [47] Benjamin Paul Clarke, Development of Ultrasonic Techniques for Rolling Element Bearing Monitoring, The University of Sheffield, Department of Mechanical Engineering, January 2022.
- [48] Jeremy Lineham, Ultrasonic probes for inspecting bearings, *World Pumps*, Volume 2008, Issue 503, August 2008, Pages 34-36.
- [49] NDT Resource Center, IOWA State University, Center for Non-destructive Evaluation, Ultrasonic Testing, <https://www.nde-ed.org/NDETechniques/Ultrasonics/index.xhtml>.
- [50] Jabid Quiroga Mendez, Omar Ardila Sanchez, Gustavo Andres Martinez Gordillo, Ultrasonic-based monitoring of tapered roller bearings in frequency and time domains, School of Mechanical Engineering. Industrial University of Santander, Ingeniare. Chilean engineering journal, *Ingeniare. Rev. chil. ing.* vol.25 no.2 Arica jun. 2017.
- [51] Wontae KIM, Jinju SEO, Dongpyp HONG, Infrared Thermographic Inspection of Ball Bearing; Condition Monitoring for Defects under Dynamic Loading Stages, 18th World Conference on Non-destructive Testing, 16-20 April 2012, Durban, South Africa.
- [52] Sebastian Roldan, David Sanchez-Londono, Giacomo Barbieri, Thermographic Indicators for the State Assessment of Rolling Bearings, Department of Mechanical Engineering, IFAC-Papers Online Volume 54, Issue 1, 2021, Pages 1218-1223.
- [53] Zuhua Jiang, Kun Zhang, Ling Xiang, Gang Yu, Yonggang Xu, A time-frequency spectral amplitude modulation method and its applications in rolling bearing fault diagnosis, *Mechanical Systems and Signal Processing*, Volume 185, 15 February 2023, 109832.
- [54] Ali Moshrefzadeh, Alessandro Fasana, Jérôme Antoni, The spectral amplitude modulation: A nonlinear filtering process for diagnosis of rolling element bearings, *Mechanical Systems and Signal Processing* 132 (2019) 253–276.